

# Proteomic Profiling of the *mdx* Animal Model for Duchenne Muscular Dystrophy

Submitted to National University of Ireland Maynooth for the degree of  
Doctor of Philosophy



NUI MAYNOOTH

Ollscoil na hÉireann Má Nuad

Steven Carberry, B. Sc

**Head of Department**

Professor Paul Maynough,  
Department of Biology,  
NUIM Maynooth,  
Co. Kildare.

**Supervisor**

Professor Kay Ohlendieck,  
Department of Biology,  
NUIM Maynooth,  
Co. Kildare.

## Publications

**Carberry, S.**, M. Zweyer, D. Swandulla, and K. Ohlendieck. 2014. Comparative proteomic analysis of the contractile-protein-depleted fraction from normal versus dystrophic skeletal muscle. *Anal Biochem* 446: 108-115.

**Carberry, S.**, M. Zweyer, D. Swandulla, and K. Ohlendieck. 2013. Application of Fluorescence Two-Dimensional Difference In-Gel Electrophoresis as a Proteomic Biomarker Discovery Tool in Muscular Dystrophy Research. *BIOLOGY* 2: 1438-1464.

**Carberry, S.**, H. Brinkmeier, Y. Zhang, C. K. Winkler, and K. Ohlendieck. 2013. Comparative proteomic profiling of *soleus*, *extensor digitorum longus*, *flexor digitorum brevis* and *interosseus* muscle from the *mdx* mouse model of Duchenne muscular dystrophy. *Int J Mol Med* 32: 544–556.

Holland, A., **S. Carberry**, and K. Ohlendieck. 2013. Proteomics of the dystrophin-glycoprotein complex and dystrophinopathy. *Curr. Protein Pep Sci* 14 (8): 680-97.

**Carberry, S.**, M. Zweyer, D. Swandulla, K. Ohlendieck. 2012. Proteomics reveals drastic increase of extracellular matrix proteins collagen and dermatopontin in the aged *mdx* diaphragm model of Duchenne muscular dystrophy. *Int J Mol Med* 30: 229-234.

**Carberry, S.**, M. Zweyer, D. Swandulla, and K. Ohlendieck. 2012. Profiling of age-related changes in the *tibialis anterior* muscle proteome of the *mdx* mouse model of dystrophinopathy. *J. Biomed Biotechnol* 2012: 691641.

**Carberry, S.**, and K. Ohlendieck. Gel electrophoresis-based proteomics of senescent tissues. *Methods Mol Biol.* 2013; 1048:229-46.

Lewis, C., **S. Carberry**, and K. Ohlendieck. 2009. Proteomic profiling of x-linked muscular dystrophy. *J Muscle Res Cell Motil* 30(7-8): 267-9.

## **Presentations:**

### **Poster presentations**

Comparative proteomic profiling of *soleus*, *extensor digitorum longus*, *flexor digitorum brevis* and *interosseus* muscle from the *mdx* mouse model of Duchenne muscular dystrophy. Carberry, S., H. Brinkmeier, Y. Zhang, C. K. Winkler, and K. Ohlendieck. European Proteomics association 2013, Saint Malo, France.

Comparative proteomic profiling of *soleus*, *extensor digitorum longus*, *flexor digitorum brevis* and *interosseus* muscle from the *mdx* mouse model of Duchenne muscular dystrophy. Carberry, S., H. Brinkmeier, Y. Zhang, C. K. Winkler, and K. Ohlendieck. EMBO life sciences conference 2013, Amsterdam, Netherlands.

Proteomics reveals drastic increase of extracellular matrix proteins collagen and dermatopontin in aged *mdx* diaphragm muscle. Carberry, S., M. Zweyer, D. Swandulla, and K. Ohlendieck. Biology Research Day 2012, NUI Maynooth.

### **Research Presentations**

Establishment of a protein biomarker signature for x-linked muscular dystrophy: Identificant of novel integral muscle proteins by mass spectrometry-based proteomics. 2012-14. Muscular Dystrophy Ireland, MDI.

### **Departmental Seminars**

Proteomic profiling of x-linked muscular dystrophy. 2011-13. National University of Ireland, Maynooth.

# Table of contents

## **1. Introduction**

1.1 Muscle Biology.....	1
1.2 Skeletal muscle structure.....	1
1.3 Sliding filament and lever-arm theory.....	1
1.4 Skeletal muscle excitation-contraction coupling.....	4
1.5 Skeletal muscle fibers.....	6
1.6 Dystrophin and its Isoforms.....	7
1.7 Dystrophinopathies.....	11
1.8 Dystroglycan complex.....	14
1.9 Dystrophic <i>mdx</i> animal model.....	16
1.10 Proteomics.....	17
1.10.1 Sample preparation.....	18
1.10.2 2-D gel electrophoresis.....	19
1.10.3 Protein visualisation.....	19
1.10.4 Protein identification.....	22
1.10.5 Mass Spectrometry.....	22
1.11 Aims of proposed project.....	22

## **2. Materials and methods**

2.1 Materials.....	24
2.1.1 Equipment.....	24
2.1.2 Reagent solutions.....	24
2.1.3 1-D and 2-D electrophoresis.....	25
2.1.4 Protein Staining.....	25
2.1.5 Mass Spectrometry.....	25
2.1.6 Western blotting.....	26

## 2.2 Methods

2.2.1 Dystrophic <i>mdx</i> animal model.....	28
2.2.2 Preparation of crude skeletal muscle extracts.....	28
2.2.3 1-D Gel Electrophoresis.....	29
2.2.4 2-D Gel Electrophoresis.....	29
2.2.5 Protein Staining.....	30
2.2.5.1 Collodial Coomassie Staining.....	30
2.2.5.2 RuBPs Stain Preparation.....	31
2.2.5.3 RuBPs Staining.....	31
2.2.6 Fluorescence difference in-gel electrophoretic analysis.....	32
2.2.7 Protein visualization and data analysis.....	32
2.2.8 In-gel digestion of proteins for Mass spectrometric identification.....	33
2.2.9 Mass spectrometric identification of skeletal muscle proteins.....	33
2.2.10 Immunoblot analysis.....	34
2.2.11 Statistical Analysis.....	35

## 3. Proteomic profiling of age-related changes in the *tibialis anterior* muscle proteome of the *mdx* mouse model of dystrophinopathy

3.1 Introduction.....	36
3.1.1 Duchenne muscular dystrophy and <i>tibialis anterior</i> skeletal muscle.....	36
3.1.2 Experimental design.....	37
3.2 Results.....	37
3.2.1 Comparative proteomic analysis of <i>mdx tibialis anterior</i> muscle .....	37
3.2.2 RuBPs analysis of landmark proteins in normal <i>tibialis anterior</i> muscle.....	38
3.2.3 Proteomic analysis of dystrophic <i>tibialis anterior</i> muscle during aging.....	42
3.2.4 RuBPs analysis of dystrophic <i>tibialis anterior</i> muscle.....	44
3.2.5 Immunoblot analysis of dystrophic <i>tibialis anterior</i> muscle .....	47
3.3 Discussion.....	51
3.3.1 Proteomic expression changes of <i>tibialis anterior</i> analysis.....	51

3.3.2 Elevated metabolic enzymes in <i>mdx</i> tissue.....	52
3.3.3 Perturbed stress response in <i>mdx</i> tissue... ..	52
3.3.4 Altered glycolytic and oxidative enzymes in <i>mdx</i> tissue .....	53
3.3.5 Other proteins.....	53
3.4 Conclusions.....	54

#### **4. Proteomic profiling of age-related changes in severely dystrophic Diaphragm muscle proteome of the *mdx* mouse model of dystrophinopathy**

4.1 Introduction.....	55
4.1.1 Duchenne muscular dystrophy and Diaphragm skeletal muscle... ..	55
4.1.2 Experimental design.....	56
4.2 Results.....	57
4.2.1 Comparative proteomic analysis of <i>mdx</i> diaphragm muscle... ..	57
4.2.2 Proteomic analysis of dystrophic diaphragm muscle during aging.....	57
4.2.3 RuBPs analysis of dystrophic diaphragm muscle.....	60
4.2.4 Comparative proteomic analysis of <i>mdx</i> versus wild-type diaphragm muscle.....	63
4.2.5 DIGE analysis of dystrophic Diaphragm muscle.....	66
4.2.6 Immunoblot analysis of of altered proteins in aged <i>mdx</i> diaphragm muscle .....	76
4.3 Discussion... ..	86
4.3.1 Proteomic expression changes of diaphragm analysis during aging.....	86
4.3.2 Increased extracellular matrix proteins in aging <i>mdx</i> tissue.....	87
4.3.3 Perturbed stress response and cytoskeletal disruption in aging <i>mdx</i> tissue in aging <i>mdx</i> tissue.....	88
4.3.4 Other proteins.....	88
4.3.5 Proteomic expression changes of aged diaphragm analysis .....	88
4.3.6 Increased extracellular matrix proteins in aged <i>mdx</i> tissue.....	89
4.3.7 Perturbed stress response in aged <i>mdx</i> tissue.....	89
4.3.8 Increased expression of Iron handling proteins in aged <i>mdx</i> tissue .....	90
4.3.9 Reduced mitochondrial enzymes in aged <i>mdx</i> tissue.....	90
4.3.10 Other proteins.....	91

4.3.11 Predicted interaction patterns of altered proteins in aged <i>mdx</i> diaphragm muscle.....	91
4.4 Conclusions.....	94

**5. Comparative proteomic profiling of *soleus*, *extensor digitorum longus*, *flexor digitorum brevis* and *interosseus* muscle from the *mdx* mouse model of Duchenne muscular dystrophy**

5.1 Introduction.....	95
5.1.1 Duchenne muscular dystrophy and skeletal muscle subtypes.....	95
5.1.2 Experimental design.....	96
5.2 Results.....	97
5.2.1 Comparative proteomic analysis of <i>mdx</i> versus normal muscle.....	97
5.2.2 Proteomic analysis of dystrophic skeletal muscle subtypes.....	97
5.2.3 RuBPs analysis of dystrophic <i>soleus</i> muscle.....	100
5.2.4 RuBPs analysis of dystrophic EDL muscle.....	104
5.2.5 RuBPs analysis of dystrophic FDB muscle.....	108
5.2.6 RuBPs analysis of dystrophic INT muscle.....	112
5.2.7 Immunoblot analysis of dystrophic skeletal muscle subtypes.....	115
5.2.8 Histological profiling of skeletal muscle tissue from <i>mdx</i> mice.....	125
5.3 Discussion.....	127
5.3.1 Moderate expression changes of RuBPs labelled skeletal muscle proteins.....	128
5.4 Conclusions.....	131

**6. Comparative proteomic analysis of the contractile protein-depleted fraction of the *mdx* mouse model of dystrophinopathy**

6.1 Introduction.....	133
6.1.1 Duchenne muscular dystrophy and hind limb skeletal muscles.....	133
6.1.2 Experimental design.....	134
6.2 Results.....	134
6.2.1 Comparative proteomic analysis of <i>mdx</i> hind limb skeletal muscle.....	134

6.2.2 RuBPs analysis of landmark proteins in total extract of normal hind limb skeletal muscle.....	135
6.2.3 DIGE analysis of landmark proteins in the contractile protein-depleted fraction from mouse skeletal muscle.....	141
6.2.4 Proteomic analysis of dystrophic skeletal muscle.....	147
6.2.5 DIGE analysis of dystrophic muscle proteins.....	149
6.2.6 Immunoblot analysis of dystrophic hind limb muscle.....	152
6.3 Discussion.....	161
6.3.1 Proteomic expression changes of skeletal muscle analysis.....	163
6.3.2 Increased expression of Iron handling proteins.....	164
6.3.3 Perturbed stress response in <i>mdx</i> tissue.....	165
6.3.4 Other protein.....	165
6.4 Conclusions.....	166
<b>7. General Discussion.....</b>	<b>168</b>
<b>Bibliography.....</b>	<b>179</b>

## List of figures

Figure 1-1 Skeletal muscle structure.....	2
Figure 1-2 Cross-bridge sliding filament theory.....	3
Figure 1-3 Voltage-gated action potential.....	5
Figure 1-4 Genomic organisation of the dystrophin gene.....	8
Figure 1-5 Dystrophin and Utrophin domain structures.....	10
Figure 1-6 Overview of neuromuscular disorders with primary defects in components of the dystrophin-glycoprotein complex.....	13
Figure 1-7 Synopsis of the structure of the DAGC form skeletal muscle and its role in the molecular pathogenesis of X-linked muscular dystrophy.....	15
Figure 1-8 Overview of the main approaches used in fluorescence difference in-gel electrophoresis (DIGE) gel-based proteomics.....	21

Figure 3-1 Landmark 2D gel of normal mouse <i>tibialis anterior</i> muscle .....	39
Figure 3-2 Two-dimensional gel electrophoretic analysis of aging <i>mdx</i> mouse <i>tibialis anterior</i> muscle.....	43
Figure 3-3 Fluorescence two-dimensional gel electrophoretic analysis of <i>mdx tibialis anterior</i> muscle.....	45
Figure 3-4 Immunoblotting analysis of dystrophin-associated glycoprotein $\beta$ -dystroglycan.....	48
Figure 3-5 Immunoblotting analysis of carbonic anhydrase enzyme .....	49
Figure 3-6 Immunoblotting analysis of the small heat shock protein 27.....	50
Figure 4-1 Two-dimensional gel electrophoretic analysis of aging <i>mdx</i> mouse diaphragm muscle .....	59
Figure 4-2 Fluorescence gel electrophoretic analysis of aged <i>mdx</i> mouse diaphragm muscle.....	61
Figure 4-3 Shown is the 2-D DIGE analysis of dystrophic <i>mdx</i> versus normal diaphragm skeletal muscle.....	64
Figure 4-4 Overview of the standard 2D-DIGE image analysis process used in muscle proteomics .....	65
Figure 4-5 Fluorescence 2D-DIGE master gel of aged <i>mdx</i> diaphragm muscle.....	68
Figure 4-6 Protein interaction map of <i>mdx</i> diaphragm muscle proteins.....	75
Figure 4-7A Immunoblotting analysis of extracellular matrix protein collagen.....	77
Figure 4-7B Immunoblotting analysis of unchanged extracellular matrix laminin.....	78
Figure 4-7C Immunoblotting analysis of of dystrophin-associated glycoprotein $\beta$ -dystroglycan.....	79
Figure 4-7D Immunoblotting analysis of small heat shock protein $\alpha$ HSP .....	80
Figure 4-7E Immunoblotting analysis of large heat shock protein 70.....	81
Figure 4-7F Immunoblotting analysis of prohibitin protein.....	82
Figure 4-7G Immunoblotting analysis of calcium-binding protein parvalbumin.....	83
Figure 4-7H Immunoblotting analysis of the luminal calcium-binding protein calsequestrin.....	84
Figure 4-7I Immunoblotting analysis of mitochondrial enzyme ATP synthase.....	85

Figure 4-8 Overview of the molecular function of altered diaphragm-associated proteins...	93
Figure 5-1 Overview of two-dimensional gel electrophoretic analysis of the <i>mdx</i> mice skeletal muscles for x-linked muscular dystrophy .....	99
Figure 5-2 Fluorescence two-dimensional gel electrophoretic analysis of <i>mdx soleus</i> muscle.....	101
Figure 5-3 Fluorescence two-dimensional gel electrophoretic analysis of <i>mdx extensor digitorum longus</i> muscle.....	105
Figure 5-4 Fluorescence two-dimensional gel electrophoretic analysis of <i>mdx flexor digitorum brevis</i> muscle .....	109
Figure 5-5 Fluorescence two-dimensional gel electrophoretic analysis of <i>mdx interosseus</i> muscle.....	113
Figure 5-6A Immunoblotting analysis of the extracellular matrix protein laminin in normal versus <i>mdx</i> skeletal muscle subtypes.....	116
Figure 5-6B Immunoblotting analysis of myoglobin in <i>soleus</i> muscle.....	117
Figure 5-6C Immunoblotting analysis of extracellular matrix protein collagen in <i>soleus</i> muscle.....	118
Figure 5-6D Immunoblotting analysis of $\alpha$ -actinin-3 in <i>extensor digitorum longus</i> muscle.....	119
Figure 5-6E Immunoblotting analysis of phosphoglycerate kinase in <i>extensor digitorum longus</i> muscle.....	120
Figure 5-6F Immunoblotting analysis of calcium-binding protein parvalbumin in <i>flexor digitorum brevis</i> muscle.....	121
Figure 5-6G Immunoblotting analysis of serpin 1d in <i>flexor digitorum brevis</i> muscle.....	122
Figure 5-6H Immunoblotting analysis of calcium-binding protein parvalbumin in <i>interosseus</i> muscle .....	123
Figure 5-6I Immunoblotting analysis of $\alpha$ B-crystallin in <i>interosseus</i> muscle.....	124
Figure 5-7 Histological profiling of skeletal muscles from <i>mdx</i> mice.....	126
Figure 6-1 landmark 2D gel of total mouse skeletal muscle extracts.....	137
Figure 6-2 landmark 2D gel of the subcellular mouse muscle fraction.....	142

Figure 6-3 Fluorescence 2D-DIGE analytical gel of normal versus <i>mdx</i> skeletal muscle fraction.....	148
Figure 6-4 Fluorescence 2D-DIGE master gel of the subcellular mouse muscle fraction.....	150
Figure 6-5A Immunoblotting analysis of unchanged MLC2... ..	153
Figure 6-5B Immunoblotting analysis of equally loaded extracellular matrix protein laminin.....	154
Figure 6-5C Immunoblotting analysis of dystrophin-associated glycoprotein $\beta$ -dystroglycan.....	155
Figure 6-5D Immunoblotting analysis of extracellular matrix protein collagen.....	156
Figure 6-5E Immunoblotting analysis of iron transporter protein transferrin.....	157
Figure 6-5F Immunoblotting analysis of large heat shock protein 70.....	158
Figure 6-5G Immunoblotting analysis of unchanged calcium-binding protein parvalbumin.....	159
Figure 6-5H Immunoblotting analysis of iron storage protein ferritin.....	160
Figure 6-6 Differential centrifugation of muscle homogenates to obtain a contractile protein-depleted fraction for comparative subproteomic analysis.....	162
Figure 7-1 MS-based proteomic profiling of the <i>mdx</i> mouse model of Duchenne muscular dystrophy... ..	170
Figure 7.2 Proteomic survey of the <i>mdx</i> animal model for Duchenne muscular dystrophy.....	174

## List of tables

Table 2.1 Antibodies.....	27
Table 3.1 List of unchanged landmark 2D protein spots from normal mouse <i>tibialis anterior</i> muscle.....	40
Table 3.2 List of identified muscle proteins with a significant change of abundance in aging <i>mdx tibialis anterior</i> muscle.....	46
Table 4.1 List of identified muscle proteins with a significant change of abundance in aging <i>mdx</i> diaphragm muscle.....	62
Table 4.2 List of identified proteins from 2D-DIGE analyses that exhibit a drastic change	

in abundance in the aged <i>mdx</i> diaphragm.....	69
Table 5.1 List of muscle-associated proteins with changes in abundance in the <i>soleus</i> muscle from <i>mdx</i> mice.....	102
Table 5.2 List of muscle-associated proteins with changes in abundance in the <i>extensor digitorum longus</i> muscle from <i>mdx</i> mice.....	106
Table 5.3 List of muscle-associated proteins with changes in abundance in the <i>flexor digitorum brevis</i> muscle from <i>mdx</i> mice.....	110
Table 5.4 List of muscle-associated proteins with changes in abundance in the <i>interosseus</i> muscle from <i>mdx</i> mice.....	114
Table 6.1 Mass spectrometry list of 2D-landmark proteins from crude tissue extracts.....	138
Table 6.2 Mass spectrometry list of 2D-landmark proteins from the subcellular fraction.....	143
Table 6.3 List of changed proteins in the subcellular fraction from <i>mdx</i> muscle as verified by fluorescent 2D-DIGE analysis .....	151

## **Acknowledgements**

Firstly, I would like to thank Prof. Kay Ohlendieck for giving me the opportunity to pursue a PhD in his laboratory and for all his guidance and support throughout my studies.

Thank you to all members of the Muscle Biology laboratory past and present. I would especially like to thank Caroline Lewis for getting me settled in the lab and showing me the ropes, Lisa for all the chats and teaching me about the countryside and Ashling for the lifts from DCU when the Typhoon decided to act up.

To all the Biology Department staff at NUI Maynooth who keep the department running, Prof. Sean Doyle for guidance throughout my undergrad and Michelle for help with the most random things.

To the college for the John Hume scholarship which enabled me to carry out my studies, as well as the Ulysses and Endeavour research award for giving me the opportunity to travel and study aboard as part of my PhD.

To Joe and Muscular Dystrophy Ireland for all their support and to all the families I have met over the years at the AGMs or at the CRC, who remind me of the importance of the research.

To all my friends for postponing their social life's so I wouldn't feel left out and for stop saying "so when yeah finished?" and "sure college closes during the summer!".

I would especially like to thank my family, my parents Tony and Ann for their constant support throughout my education from late nights in the lab to surprise trips to Belfast to catch ferries. You both have always been there for me whenever I have needed encouragement or an ear, to listen to a random science rant. Thank you for all your support and I dedicate this work to you.

PhD is time consuming, so looking forward to catching up on the latest youtube cat videos.

## Declaration

This thesis has not been submitted in whole or in part to this or any other university for any degree, and is the original work of the author except where stated.

Signed \_\_\_\_\_

Date \_\_\_\_\_

## Abbreviations

1D	One-dimensional
2D	Two-dimensional
2D-GE	Two-dimensional gel electrophoresis
Ab	Antibody
AB	Abcam
ACh	Acetylcholine
AChR	Acetylcholine receptor
ADP	Adenosine diphosphate
AK1	Adenylate kinase
AMC	Actin membrane cytoskeleton
AT	Amino terminal
ATP	Adenosine triphosphate
BIO	Affinity Bioreagents
BMD	Becker muscular dystrophy
Ca <sup>2+</sup>	Calcium
CBB	Coomassie brilliant blue
CHAPS	3-[3-chloramidopropyl- Dimethylammonio-1-propane sulfonate]
Ck	Chicken
CMD	Congenital muscular dystrophy
CR	Cysteine-rich
CSQ	Calsequestrin
CT	Carboxyl terminal
cvHSP	Cardiovascular heat shock protein
CYT	Cytosol
DAGC	Dystrophin-associated glycoprotein complex
DG	Dystroglycan
DGC	Dystrophin-glycoprotein complex
DHPR	Dihydropyridine receptor

DIA	Diaphragm
DIGE	Difference in-gel electrophoresis
DMD	Duchenne muscular dystrophy
DMF	Dimethylformamide
DTT	Dithiothreitol
DYB	Dystrobrevin
ECL	Enhanced chemiluminescence
ECM	Extracellular matrix
EDL	Extensor Digitorum Longus
EOM	Extraocular muscle
ES	Extracellular space
ESI	Electrospray ionization
FABP	Fatty acid binding-protein
FDB	Flexor digitorum brevis
fmol	Femtomole
<i>g</i>	<i>g</i> force
GAPDH	Glyceraldehyde 3-phosphate
GRMD	Golden retriever muscular dystrophy
h	Hours
HCl	Hydrochloric acid
HPLC	High performance liquid
HRP	Horse radish peroxidase
Hsp	Heat shock protein
ID	Identification
IDH	Isocitrate dehydrogenase
IEF	Isoelectric focusing
IF	Intermediate filament
INT	Interosseus
IPG	Immobilized pH gradient
K <sup>+</sup>	Potassium ions
kDa	Kilodaltons

LAM	Laminin
LC-MS	Liquid chromatography mass spectrometry
LGMD	Limb-girdle muscular dystrophy
M	Molar
m/z	Mass/charge
MDX	Murine X chromosome linked
MHC	Myosin heavy chain
min	Minute
ml	Milliliter
MLC	Myosin light chain
mM	Millimolar
mRNA	Messenger ribonucleic acid
MS	Mass spectrometry
Ms	Mouse
MW	Molecular Weight
µg	Microgram
µL	Microlitre
µM	Micromolar
Na <sup>+</sup>	Sodium Ions
NADH	Nicotinamide adenine dinucleotide
NC	Novocastra
ng	Nanogram
NL	Non linear
PAGE	Polyacrylamide gel electrophoresis
PBS	Phosphate buffered saline
pI	Isoelectric point
PTM	Post-translational modifications
Rb	Rabbit
RuBPs	Ruthenium (II) tris-bathophenanthroline disulfonate
RyR1	Ryanodine receptor
SAR	Sarcalumenin

SC	Santa Cruz
SDS	Sodium dodecyl sulphate
SERCA	Sarcoplasmic endoplasmic reticulum calcium ATPase
SG	Sarcoglycan
SGC	Sigma Chemicals
SGN	Stressgen
SL	Sarcolemma
SOL	Soleus
SR	Sarcoplasmic reticulum
SS	Sarcospan
SYN	Syntrophin
TA	Tibialis anterior
TEMED	Tetramethylethylenediamine
TGF- $\beta$	Transforming growth factor beta
Tn	Troponin
TnC	Troponin C
TnI	Troponin I
TnT	Troponin T
TRAMP	Tyrosine-rich matrix protein
T-tubules	Transverse tubules
V	Volts
W	Watts
WB	Western blotting
WGA	Wheat germ agglutinin
WT	Wild-type
XLDCM	X-linked dilated cardiomyopathy
$\alpha$ -DG	alpha-Dystroglycan
$\beta$ -DG	beta-Dystroglycan

## **Abstract**

Duchenne Muscular Dystrophy is a lethal childhood disorder which results in progressive muscle weakness and wasting due to genetic abnormalities in the dystrophin gene. While the primary abnormality lies with the loss of the crucial membrane cytoskeletal protein dystrophin and the reduction of its associated glycoprotein complex, secondary alterations in cellular signalling, ion homeostasis regulation and metabolic pathways lead to fiber degeneration and subsequent fibrosis. These changes result in loss of ambulation and sufferers being wheelchair bound in early adulthood. Severe diaphragm and cardiac complications in later life tend to be fatal. The aim of this project was to create a detailed proteomic profile of differentially affected dystrophic tissues using the *mdx* mouse model; from severely dystrophic diaphragm; moderately affected hind limb to naturally protected *interosseus* muscle were used to investigate the pathogenesis of the disease.

Proteomic analysis of the muscle subtypes indicated that skeletal muscles are differentially affected by the absence of dystrophin protein. Naturally protected *interosseus* exhibited very little histological and proteomic changes. In contrast to the moderately affected *mdx* hind limb muscles, the dystrophic diaphragm exhibits severe symptoms of skeletal muscle fiber degeneration that more closely resembles that of the neuromuscular pathology exhibited in Duchenne patients than any other muscle. Novel molecular insights into dystrophic changes suggest increased cellular stress, impaired calcium buffering, cytostructural alterations and disturbances of mitochondrial metabolism in dystrophin-deficient muscle tissue.

Thus, the absence of the dystrophin isoform Dp427 and resulting reduction in dystrophin-associated glycoproteins in the dystrophic sarcolemma seems to trigger a variety of secondary abnormalities in muscular dystrophy. This work has successfully established a detailed biomarker signature that maybe used to evaluate new treatments, improve understanding of the pathobiochemical process and supports the use of *mdx* mouse as a suitable model for Duchenne muscular dystrophy.

# 1 Introduction

## 1.1 Muscle Biology

Muscle tissue can be divided into four distinct types: skeletal muscle, smooth muscle, cardiac muscle and myoepithelial cells, all differing in location and function. In this thesis, we examined multiple subtypes of skeletal muscle from the diaphragm, *interosseus* and *flexor digitorum brevis* muscle to hind limb muscles such as *tibialis anterior*, *extensor digitorum longus* and *soleus* muscle of the murine animal model.

## 1.2 Skeletal muscle structure

A muscle is comprised of many skeletal muscle fibers. A muscle fiber consists of bundles of myofibrils that are arranged longitudinally along the axis of each muscle fibers. Thus results in the striated muscle pattern of skeletal muscle, a myofibril contain sarcomeres (see Figure 1-1). The sarcomere structure consists of two main filaments, a thick and a thin filament.

## 1.3 Sliding filament and lever-arm theory

Skeletal muscle contraction involves the two types of filaments. Thick filaments are made up of myosin (and myosin heads) found in the centre of the sarcomeres. Thin filaments are made up of actin, tropomyosin and troponin (Tn) and surround each thick filament. It is this alignment that gives muscle cells its striated pattern. Calcium in the cytosol released from the sarcoplasmic reticulum (SR) binds to Troponin C (TnC) (see Figure 1-2) leading to a conformational change of the Troponin complex. In the presence of ATP this allows a myosin head on the thick filaments to bind with actin initiating a cross-bridge (Holmes, 1997; Huxley, 2000; Huxley, 2004).

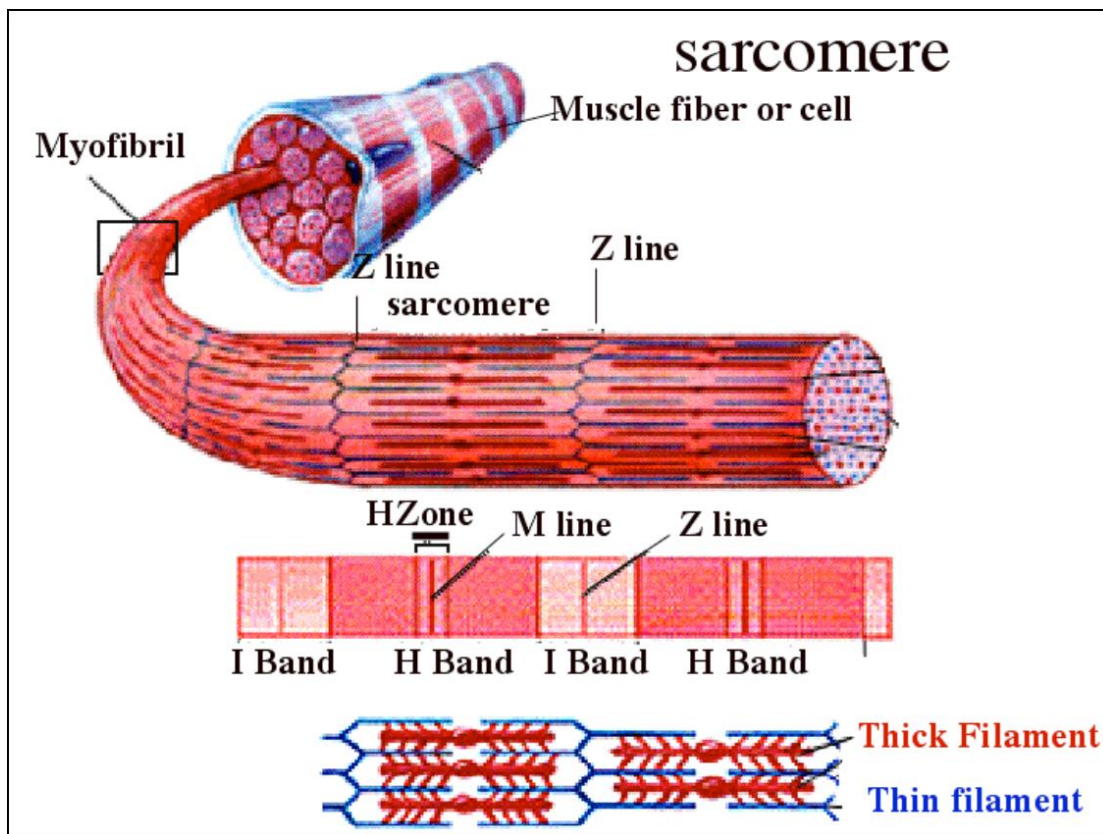


**Figure 1-1 Skeletal muscle structure**

Contractile elements comprise the repeating sarcomeres, which arrange to form the myofibrils. The thick filaments of the H band consist of intertwined myosin chains enclosed by the thin actin filaments. (image from ucl.ac.uk)

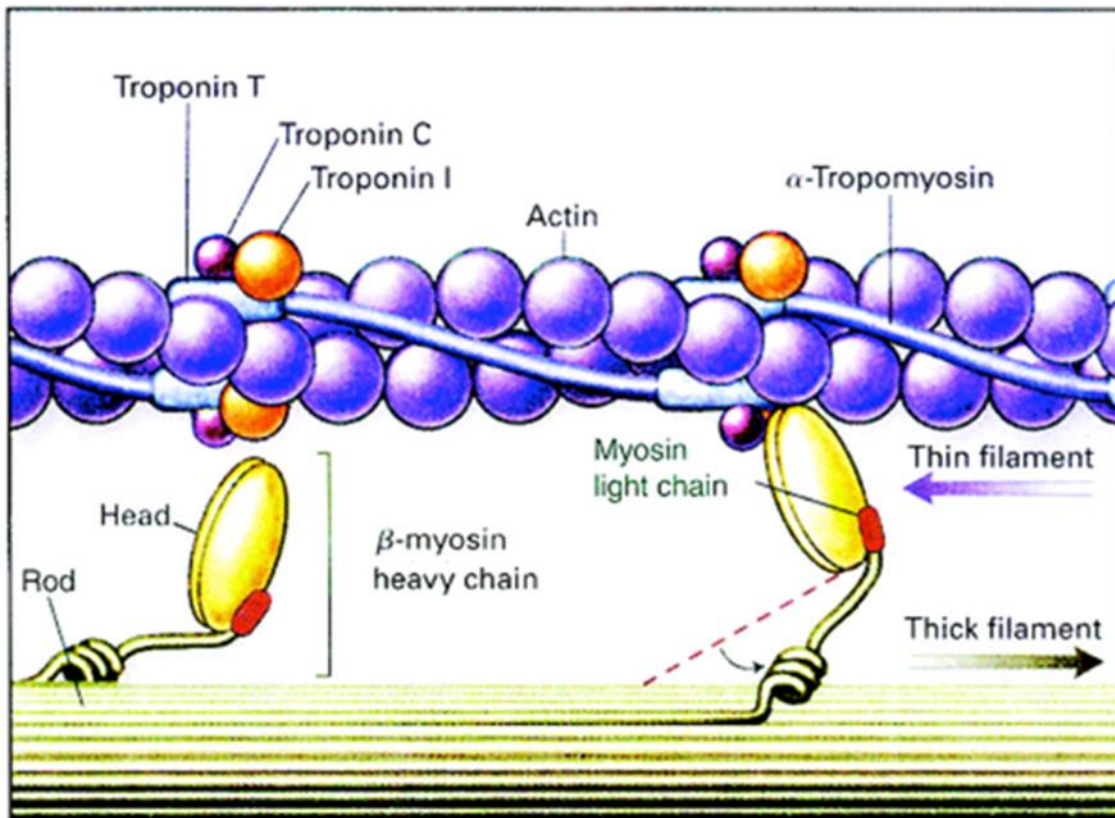


**Figure 1-2 Cross-bridge sliding filament theory**

A conformational change happens to tropomyosin after the binding of calcium to troponin C. An actin binding site becomes exposed and the myosin head forms a cross-bridge. Allowing the thin filaments to slide over the thick filament and result in muscle shortening. (image from edoc.hu-berlin.de)

ATP is broken down and myosin head released and continues to the next actin along the thin filaments causing the sarcomere to shorten. This cycle of muscle fiber shortening is maintained by the interaction of multiple myosin head and actin cross-bridges (while calcium is present). The filaments, thin and thick are not altered in length but the H zone and I band which are shortened and the level of shortening is proportional with the degree of contraction (Reedy, 2000).

#### 1.4 Skeletal muscle excitation-contraction coupling

Before skeletal muscle can contract an electrical signal must travel from the motor center of the brain along the spinal cord. When an electrical signal meets a motor neuron that ends beside a muscle fiber it enters the neuromuscular junction. The electrical signal is then converted into a chemical signal at this junction in the form of acetylcholine (ACh) (see Figure 1-3) which can then cross the synapse to the muscle fiber. In the muscle membrane ACh binds to and activates post-synaptic acetylcholine receptors (AChR) causing localised depolarisation (Farley and Miles, 1977). The activation of the voltage dependent channels results in sodium channels opening causing sodium ions ( $\text{Na}^+$ ) to flux out to the cytosol and potassium ions to enter into the sarcoplasm. Depolarisation of the sarcolemma results in an action potential and enters down into the transverse tubules (T-tubules) (Cooke, 1986).

Depolarization of the T-tubules activates the alpha-1 subunit of dihydropyridine receptor (DHPR). A conformational change in the protein allows its II - III loop domain to physically interact with the ryanodine receptor (RyR1) on the SR (Tanabe et al., 1990). The interaction with RyR1 allows calcium channels to open causing a flux of  $\text{Ca}^{2+}$  into the cytoplasm of the cells (Meissner and Lu, 1995). The increase in cytosolic  $\text{Ca}^{2+}$  results in the conformational change in the troponin complex, no longer inhibiting the interaction of the myosin head with actin (Cooke, 1986).

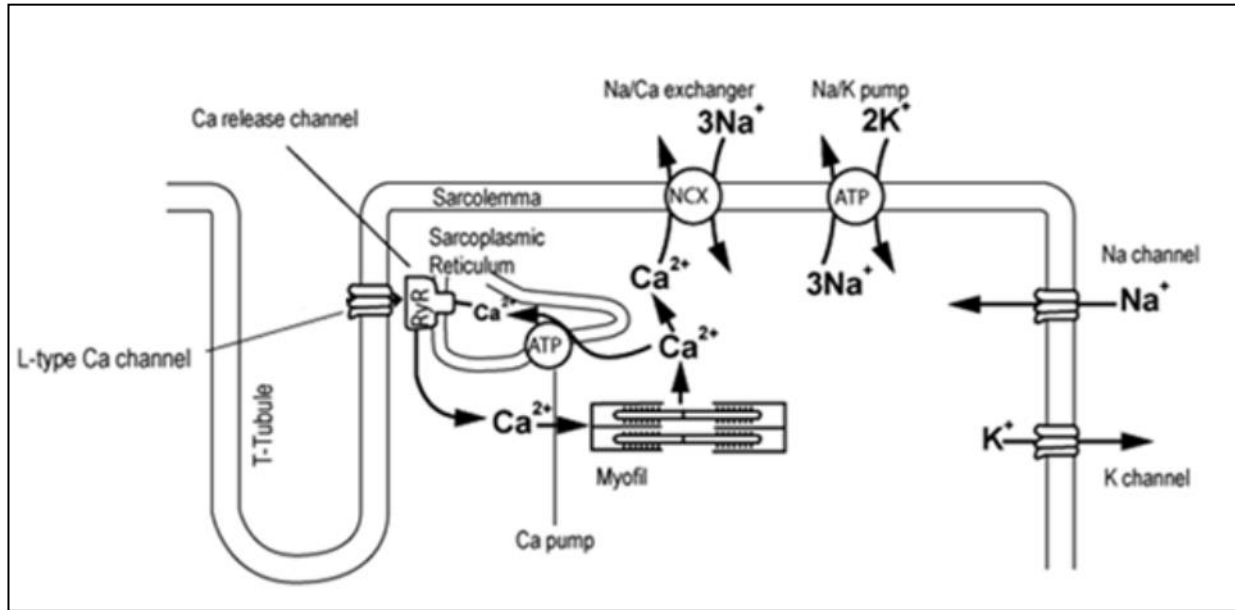


**Figure 1-3 Voltage-gated action potential**

An impulse activates voltage-gated ion channels along the sarcolemma and into T-tubules. The activated dihydropyridine receptor also known as the L-type calcium channel interacts with the ryanodine receptor (RyR1) of the sarcoplasmic reticulum. Storage bodies release calcium within the sarcoplasmic reticulum, which result in interactions with contractile elements of the myofibril. (image from [www.sim-bio.org](http://www.sim-bio.org))

## 1.5 Skeletal Muscle Fibers

Skeletal muscle is an extremely heterogeneous tissue composed of a large variety of functionally diverse fiber types and subtypes. The properties of individual muscles largely depend on the combination of the individual properties of their different fiber types and their proportions. Traditionally, fiber types were classified depending on their varying color, type I fibers red (slow-twitch) due to the high levels of myoglobin and type II fibers white (fast-twitch). These fiber types can be further subdivided into type IIA or type IIB whereby the fast-twitch fibers were more aerobic using oxidative metabolism or anaerobic using glycolytic metabolism, respectively. Thus, muscle fibers can be classified by their contractile and metabolic properties. There are a number of methods employed to classify muscle fibers, histochemical staining for myofibrillar ATPase activity, immunohistochemical staining for myosin heavy chain (MHC) type identification and biochemical identification of metabolic enzymes (Pette and Staron 2000).

Muscle fibers are dynamic structures capable of change under certain conditions for example, altered neuromuscular activity, mechanical loading or unloading, changes in hormonal profiles, systemic diseases or during aging. Fiber transitions generally follow a pattern of either fast-to-slow or slow-to-fast. These MHC isoform transitions are linked to energy cost for force and also differences in the ATP phosphorylation in fast and slow muscle fibers production (Bottinelli et al., 1994; Conjard et al., 1998). During sarcopenia the degenerative loss of skeletal muscle mass and strength associated with aging there is a decrease in type II fibers with fast-to-slow transitions and glycolytic-to-oxidative shifts in aging muscle.

## 1.6 Dystrophin and its Isoforms

It has been over 20 years since the discovery of the genetic defect causing DMD. The DMD gene is a huge 2.5 Mb gene that encodes for the dystrophin protein (see Figure 1-4). The massive gene accounts for 1.5% of the X chromosome and also represents 0.1% the total human genome (Wells, 2006). Dystrophin is a member of the spectrin family of very large actin binding proteins (Menhart, 2006).

The dystrophin gene has 7 different promoters controlling transcription. Three full-length dystrophin isoforms that are transcribed by these promoters include Dp427-B, Dp427-M and Dp427-P in the brain, skeletal muscle and Purkinje cells respectively, differing in the amino terminal end sequence (Boyce et al., 1991; Gorecki et al., 1992; Yaffe et al., 1992).

Shorter isoforms of dystrophin protein are produced by four internal promoters. These transcribe Dp260 a 260kDa retina isoform, Dp140 a 140kDa brain/kidney isoform, Dp116 a 116Da Schwann cell isoform and Dp71 a 71kDa truncated general isoform. Each of these isoforms have an unique amino terminal end and some lack the actin binding domain found in full-length dystrophin (Byers et al., 1993; D'Souza et al., 1995; Lidov et al., 1995). Thus, these shorter isoforms function differently compared to that of Dp427 in skeletal/cardiac muscle and nervous system.

Also a number of dystrophin-related proteins exist, 94kDa  $\alpha$ -dystrobrevin in muscle, 61kDa  $\beta$ -dystrobrevin in muscle and brain (Rentschler et al., 1999), 395kDa full length utrophin Up395 in the brain and at neuromuscular junction, 116kDa Up116 in the brain and 62kDa N-utrophin in glioma cells.

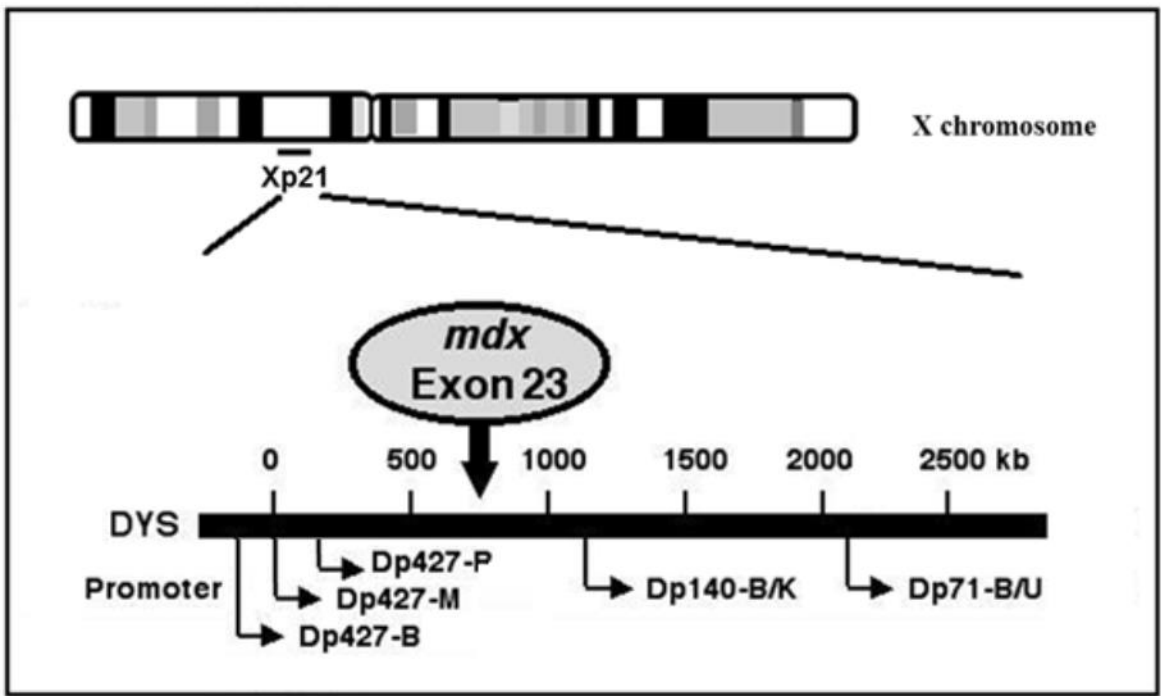


**Figure 1-4 Genomic organisation of the dystrophin gene**

Figure 1-4 represents the Genomic organisation of the dystrophin gene which is located in Xp21. The 79 exons of the dystrophin gene are represented by the black line. The 79 exons are distributed over about 2.5 million bases. The arrows indicate the various promoters like are brain (B), muscle (M), and Purkinje (P) promoters are indicated by the arrows. The point mutation in exon 23 results in the absence of Dp427 in mdx mice (image modified from Culligan et al., 2001).

Full-length dystrophin is comprised of four major domains, three of which are homologous to domains present in several actin binding cytoskeletal proteins (Koenig et al., 1988). Dystrophin has four domains: (i) N-terminal “actin binding” domain with 2 calponin homology units, (ii) a central “rod domain” consisting of 24 spectrin-like repeats and four hinge regions which provide a flexible characteristic, (iii) a cysteine-rich domain which is vital for binding the integral glycoprotein  $\beta$ -dystroglycan and  $\alpha$ -dystrobrevin, and (Rentschler et al., 1999) (iv) a carboxyl terminal domain, a unique sequence that binds dystrophin-associated proteins dystrobrevin and syntrophin through its coiled-coil protein-binding motifs (seen in Figure 1-5). Both the cysteine-rich domain and C terminus are found in all the dystrophin isoforms (Tinsley et al., 1992). Genetic deletions or nonsense mutations that block translation resulting in x-linked muscular dystrophy occur in distinct regions in these domains, more frequently in the N-terminal area of the rod domain.

Dystrophin is localised to the cytoplasmic face of the sarcolemma (Zubrzycka-Gaarn et al., 1988) and mainly within a cytoskeletal lattice termed costameres, (Campbell, 1995) where dystrophin interacts through its actin binding domain and cysteine-rich domain interacts linking the extracellular dystroglycan complex via  $\beta$ -dystroglycan. Without the support of dystrophin, these glycoproteins are quickly lost and thus weaken the linkage between the actin membrane cytoskeleton and the extracellular matrix. The plasmalemma in turn becomes more susceptible to contraction-induced micro-rupturing. Repair mechanisms seem to introduce  $\text{Ca}^{2+}$ -leak channels in the sarcolemma, which result in pathophysiologically elevated  $\text{Ca}^{2+}$ -levels in the dystrophic cytosol (Alderton and Steinhardt 2000). Elevated proteolytic activity triggers then various direct and indirect negative effects on ion handling, energy metabolism and the structural integrity of dystrophic muscle. Chronic alterations of key pathways and important cellular mechanisms cause severe tissue wasting and muscle weakness, eventually leading to end-stage contractile failure. Suggesting that dystrophin stabilises the sarcolemma against mechanical forces experienced during muscle contraction.

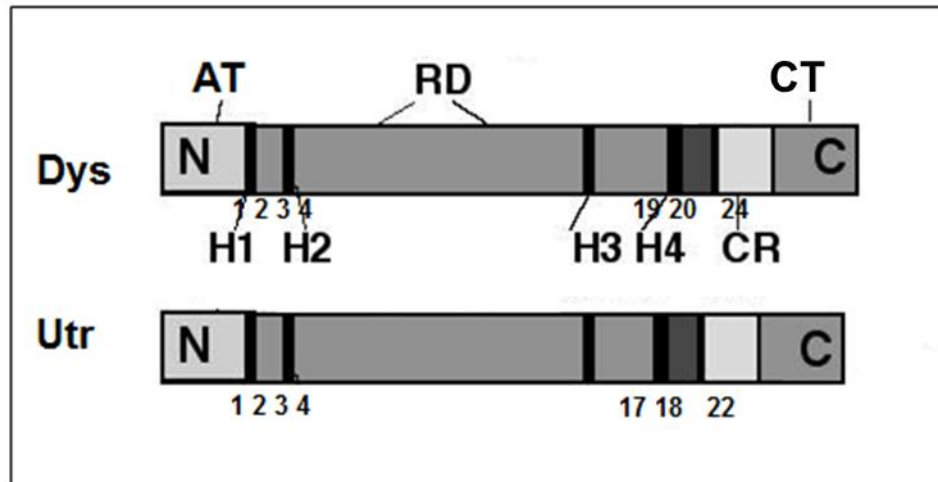


**Figure 1-5 Dystrophin and Utrophin domain structures**

Shown is a comparative representation of the domain regions of murine dystrophin and utrophin. Utrophin structure lacks the rod domain modules which correspond to the helical repeats 15-19 in dystrophin. However, the structures both contain an amino terminal (AT) domain, the four hinge regions (H1-H4) comprising the rod domain (RD) of up to 24 helical repeats, the cysteine-rich (CR) domain and finally the carboxyl terminal (CT) domain (image modified from Culligan et al., 2001).

## 1.7 Dystrophinopathies

Changes in dystrophin and various dystrophin-associated proteins result in a number of muscular dystrophies, the effects of which can be seen across multiple muscle types. The most common form of muscular dystrophy is Duchenne Muscular dystrophy (DMD) (Dellefave and McNally, 2007). DMD is named after Guillaume Benjamin Amand Duchenne a French neurologist and was first reported in 1836 (Conte and Gioja, 1836) and later described in 1852 by Meryon. DMD is a lethal disorder of childhood believed to affect 1 in every 3500 live male births. A recent epidemiology study of DMD reported the incidence ranged from 10.71 to 27.78 per 100,000 (Mah et al., 2014). DMD is inherited as an X-linked recessive condition only affects males, with women being carriers.

The reading frame of the dystrophin transcript is changed due to the mutations in the dystrophin gene, resulting in a premature stop codon (Dellefave and McNally, 2007). Positional cloning was used to identify the DMD defect. Patients with DMD can have different types of mutations. Approximately 65% of patients have intragenic out-of-frame deletions and approximately 10% have duplications of one or more of the dystrophin gene's exons. The remaining DMD patients have point mutations or smaller gene rearrangements (Kinali et al., 2007). The absence of the dystrophin protein is the molecular basis for DMD (Rando, 2006). Dystrophin links the cytoskeleton to the extracellular matrix (see Figure 1-6). Reduction or absence of dystrophin protein compromises this link and leads to muscle fiber degeneration (Kinali et al., 2007). Thus DMD is considered a neuromuscular disorder of the membrane cytoskeleton.

In DMD symptomatic muscle disease onset occurs between three and five years of age. The most frequent presenting symptoms are an abnormal gait or motor delays. Affected boys may present difficulty in getting up from the ground (Gower's sign), running and may have frequent falls, due to severe impairment of lower extremities (Dellefave and McNally, 2007). Proximal weakness affects the lower extremities before the upper extremities (Yiu and Kornberg, 2008). The weakness is accompanied by muscle pseudohypertrophy, the

enlargement of the muscle tissue, typically calf muscles, caused by infiltration of connective tissue and adipose into the degenerating muscle. The progression of muscle weakness generally leads to DMD patients being wheelchair bound by the age of 12. The leading cause of death in individuals is respiratory insufficiency between the late teens or early 20s. Respiratory complications account for approximately 80% of deaths, while 20% succumb to dilated cardiomyopathy (DCM) (Kinali et al., 2007).

It depends on the type of mutation, whether a patient shows DMD or its more benign counter-part Becker muscular dystrophy (BMD) phenotype. DMD results from a severe reduction or absence of dystrophin, whereas BMD is associated with expression of a partly functional dystrophin protein. BMD is more variable phenotypically with a later onset of severe symptoms and normally follows a less progressive form of fiber degeneration than DMD (Monaco et al., 1988). An abnormality in DMD gene, which results in the promoter on the 5' end that transcribes for the cardiac specific dystrophin protein, causes X-linked dilated cardiomyopathy (XLDCM). This form of dystrophinopathy shows little skeletal muscle disease progression however is fatal leading to cardiac failure in early 20s (Towbin et al., 1993).

Absence of dystrophin-associated proteins can lead to other muscular dystrophies. Certain limb-girdle muscular dystrophies (LGMD) result from loss of different sarcoglycan isoforms and are referred to as sarcoglycanopathies (Lim et al., 1995; Jung et al., 1996). These various muscular dystrophies are progressive diseases which affect shoulder and pelvic girdle muscles. Congenital muscular dystrophy (CMD) results from a deficiency in laminin protein which interacts with the dystrophin-glycoprotein complex (DGC). While not a progressive disease, CMD shows muscle weakness and can result in loss of ambulation (Minetti et al., 1996).

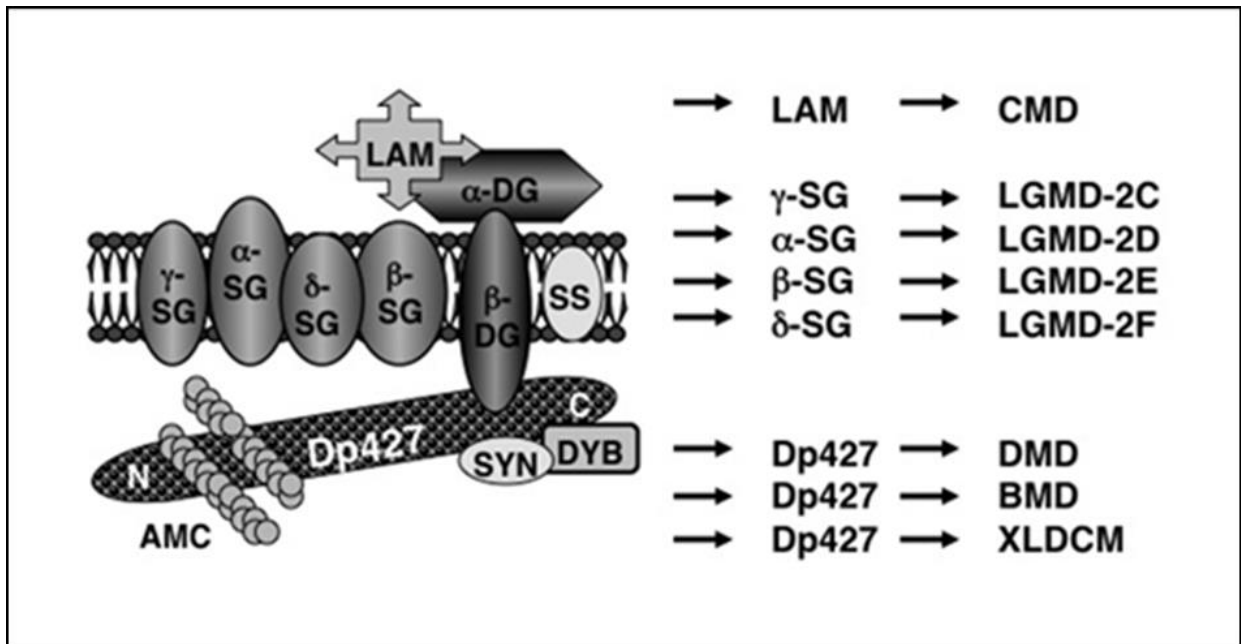


**Figure 1-6 Overview of neuromuscular disorders with primary defects in components of the dystrophin-glycoprotein complex**

Shown is a diagram representing the dystrophin-associated glycoprotein complex and a list of muscle proteins with a genetic abnormality in muscular disorders. Genetic changes in laminin (LAM),  $\gamma$ -sarcoglycan ( $\gamma$ -SG),  $\alpha$ -SG,  $\beta$ -SG or  $\delta$ -SG are linked with congenital muscular dystrophy (CMD) and limb-girdle muscular dystrophy (LGMD) subtypes 2C, 2D, 2E and 2F, respectively. Primary abnormalities in the Dp427 isoform of dystrophin located in the actin membrane cytoskeleton (AMC) result in severe Duchenne muscular dystrophy (DMD), milder Becker muscular dystrophy (BMD) as well as X-linked dilated cardiomyopathy (XLDCM).

## 1.8 Dystroglycan complex

The plant lectin germ agglutinin chromatography was important for the biochemical isolation of dystrophin and led to the dystrophin-associated glycoprotein complex (DAGC) identification (Campbell and Kahl, 1989). Lectin chromatography established that dystrophin was tightly associated to the glycoprotein complex at the muscle periphery. The dystrophin-associated proteins can be grouped into three main components (i) the sarcolemma, (ii) the membrane cytoskeleton and (iii) the extracellular matrix. The DAGC structural overview is shown in Figure 1-7.

The sarcolemma components of the dystrophin-associated proteins include (i) 50kDa sarcoglycan, 43kDa  $\beta$ -sarcoglycan, 35kDa  $\gamma$ -sarcoglycan, 35kDa  $\delta$ -sarcoglycan and (ii) 25kDa highly hydrophobic sarcospan protein (Crosbie et al., 1997; Lim and Campbell, 1998; Barresi et al., 2000) and 43kDa  $\beta$ -dystroglycan trans-sarcolemmal linker glycoprotein (Rentschler et al., 1999). The membrane cytoskeletal components include (i) 43kDa cortical actin, (ii) 94kDa  $\beta$ -dystrobrevin (Wagner et al., 1993) and (iii) 58, 59 and 60 kDa syntrophins comprised of a protein family, the  $\alpha$ ,  $\beta_1$  and  $\beta_2$  isoforms respectively (Adams et al., 1993; Ahn et al., 1994; Ahn et al., 1996; Piluso et al., 2000).

Many other proteins are indirectly linked to muscle Dp427 like the extracellular matrix component 156kDa  $\alpha$ -dystroglycan and ~400 kDa laminin (Ibraghimov-Beskrovnaya et al., 1992; Hohenester et al., 1999). In addition to the main components a large number of signalling proteins and ion channels are linked to the dystrophin network of proteins. In dystrophic muscle tissue the levels of many of these dystrophin-associated proteins are dramatically decreased at the sarcolemma. Interestingly it is the absence of Dp427 that leads to the disintegration of the DAGC and subsequent separation of actin membrane cytoskeleton and laminin with progression of the disorder.

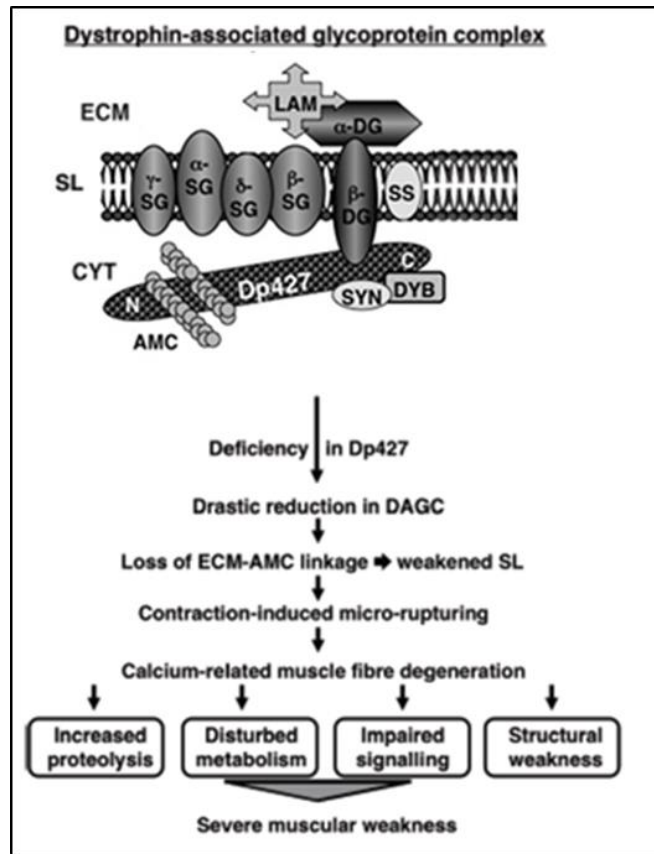


**Figure 1-7 Synopsis of the structure of the DAGC from skeletal muscle and its role in the molecular pathogenesis of X-linked muscular dystrophy**

Shown is a diagrammatic presentation of the supramolecular dystrophin-associated complex of the sarcolemma (SL) that connects the actin membrane cytoskeleton (AMC) of the cytosol (CYT) with the extracellular matrix (ECM) protein laminin (LAM). The Dp427 dystrophin isoform interacts with dystrobrevins (DYB), syntrophins (SYN) and the integral  $\beta$ -dystroglycan ( $\beta$ -DG) protein, which in turn binds directly to the extracellular laminin-binding protein  $\alpha$ -dystroglycan ( $\alpha$ -DG). Additional Dp427-associated proteins are shown as sarcospan (SS) and the sarcoglycans ( $\alpha$ -SG,  $\beta$ -SG,  $\gamma$ -SG and  $\delta$ -SG). Dystrophin-deficiency in muscle fibres from DMD patients and its dystrophic *mdx* animal model, result in a drastic decrease in the DAGC. Loss of the linkage between the ECM and AMC leads to the weakening of the SL membrane system, causing various cellular disturbances and finally severe muscular degeneration.

## 1.9 Dystrophic *mdx* animal model

In biochemical and biomedical research animal models play a crucial role for investigating molecular and cellular pathogenesis as well as preclinical evaluation of new treatment strategies for neuromuscular disorders they mimic (Vainzof et al., 2008). Ideally, an animal model for a genetic disorder should: (i) show similar primary defects and secondary downstream changes as seen in the equivalent human disease; (ii) closely resemble the pathogenesis of the human disorder in onset, progression and severity; (iii) develop majority of the multifactorial features seen in complex human pathologies; (iv) exhibit sufficient similarities to human physiology, metabolism and immune responses so that there no major differentiating influence of these biological factors on disease progression in animal models vs. patients; (v) be suitable for the facilitation of physiological and surgical procedures and for genetic manipulations; (vi) be easy to breed and house at a practical cost; and (vii) be large enough to yield adequate amounts of tissue samples for extended biological analyses (Guenet, 2011).

The murine X chromosome-linked (*mdx*) mouse animal model is an established model for the study of x-linked muscular dystrophies. The naturally occurring mouse model has a point mutation on exon 23 of the dystrophin gene. This results in the almost complete absence of the Dp427 protein isoform of the membrane cytoskeleton protein dystrophin. A single base pair change from cysteine to thymine on the exon creates a premature termination codon. This results in an 115kDa truncated protein product with limited function offering some of membrane stability but with over half the rod and terminal domain missing there is no interaction with the intracellular actin cytoskeleton. Four shorter isoforms of dystrophin are also expressed by *mdx* mouse in non-muscle tissues. These contain the C-terminal end and result in less severe pathologies of the dystrophy in these various tissues. This may account for the milder pathology observed in the *mdx* mouse compared with DMD patients (Sicinski et al., 1989).

The absence of dystrophin at the muscle sarcolemma causes many of the

pathological consequences observed in both *mdx* and human dystrophic muscle such as muscle damage shown by elevated creatine kinase levels in serum, an increased susceptibility to osmotic shock and vulnerability to contraction and stretch induced injury. Interestingly, the same primary abnormality appears to be subtype specific affecting *mdx* muscles differently. Form mildly affected extraocular (Porter et al., 1998) and *interosseus* muscle to moderately hind limb muscles and dystrophic diaphragm muscle with severe fiber degeneration.

While limb muscle of the *mdx* model is less severely affected than the human condition due to possible support of the truncated form of dystrophin and its non-muscle isoforms as well as homologous utrophin protein in the muscle (Blake et al., 2002; Deconinck et al., 1997; Rafael et al., 1999). Aged *mdx* muscle exhibit severe symptoms showing plasmalemma weakening, myofibre replacement by extensive connective tissue and exhausted structural and functional recovery of cells after injury. Proteomic profiling of senescent muscle is of particular interest to determine age related changes in dystrophin-deficient fibers, as the *mdx* senescent phenotype more closely resembles that of the human pathology (Lefaucheur et al., 1995).

## 1.10 Proteomics

Proteomics is the large-scale study of proteins expressed by a cell. The entire protein complement expressed by a cell is known as the proteome. It is important to note that the proteins produced in the cell do not fully match up with the translation of the nucleotide sequence. This is due to post-translational modification (PTM), when the proteome is subjected to environmental influences this process can be applied to adapt to changing situations (Anderson and Seilhamer, 1997). Classic proteomic techniques such as 1D and 2D polyacrylamide gel electrophoresis have been employed as standard methods to investigate the proteome. However, other recently developed in-gel techniques such as

DIGE and gel-free protein labelling methods have empowered proteomic quantitative analysis.

Thus, the rapid advancements in protein biochemical techniques and MS-based proteomics have allowed for the establishment of global protein expression patterns, molecular interactions and PTMs of muscle proteins in samples. In the case of sports physiology a recent study (Egan et al., 2011) employed a number of these novel tools following physical exercise and this is a successful example of applied proteomics and future exercise intervention in muscle and metabolic diseases can build on these kinds of studies. Regular exercise has been shown to be effective in the prevention of chronic diseases and increased knowledge of the molecular responses to exercise offers an important contrast for interpreting studies of disease and can highlight potential novel therapeutic targets (Burniston and Hoffman, 2011). Thus, proteomics is an important tool in profiling and characterising changes in protein expression in diseased organisms. Skeletal muscle proteomics is concerned with identification and cataloguing of the proteins constituents involved in voluntary contractile fibers in normal and disease muscle.

### 1.10.1 Sample preparation

This first step in proteomic study is solubilisation of the sample proteins. Denaturing buffers are used containing a pre-optimised and tailored combination of chemicals to both solubilise the maximum amount and variety of proteins depending on the sample. Usually consisting of chaotropic agents like urea to disrupt hydrogen and hydrophobic bonds (Rabilloud, 1998), reducing agents such as dithiothreitol DTT to break disulphide bridges and detergents such as CHAPS.

### 1.10.2 2-D gel electrophoresis

Two-dimensional electrophoresis is a powerful technique which allows for the separation and subsequent analysis of proteins in a sample. The technique separates proteins in two dimensions and was established by Klose, O'Farrell and many others by 1975. In the first dimension proteins are separated according to their pI by isoelectric focusing (IEF) using polyacrylamide gel strips with immobilised pH gradient (IPG). The protein sample must enter the gel strip before they are separated. This can be achieved through a number of methods; firstly rehydration buffer is used to rehydrate the IPG strips. With in-gel rehydration the protein sample is added to the rehydration buffer and enters the gel, or sample can be added post rehydration during IEF by cup/wick loading. When an electric field is applied, proteins travel along IPG strips till the protein has no net charge.

In the second dimension the focused strips are positioned running along the top of the polyacrylamide gels. An electric current is applied through the gels which move the proteins through the pores in the gel. The smaller proteins are capable of moving faster through the gel, therefore allowing the proteins to be separated based on their molecular weight. Gels are then fixed and stained to visualise the proteins.

### 1.10.3 Protein visualisation

There are a number of post separation visualisation methods. A method may be chosen a variety of reasons be it sensitivity, downstream processing or simply because it is cheap and convenient. Commonly used stains in proteomic studies are staining with anionic dyes. These include coomassie, silver and fluorescence staining. Coomassie brilliant blue (CBB) provides a low cost and mass spectrometry-compatible staining method. CBB binds to basic amino acids in a hydrophobic manner Neuhoff and colleagues (1985).

Silver staining while more sensitive than CBB, has a very limited dynamic range and is not reproducible thus, not suitable for quantitative analysis. Silver nitrate binds to proteins and then with the addition of formaldehyde the silver ions become reduced to metallic silver (Rabilloud et al., 1994). This method of staining is also mass spectrometry compatible however requires a destaining step to remove glutaraldehyde from the excised proteins.

Fluorescent compounds offer a better approach for protein detection with high sensitivity and large linear dynamic range but usually at more expense and require fluorescent scanners. Fluorescent detection of proteins can be performed in two ways. Firstly, post-electrophoretic fluorescent labelling such as Ruthenium (II) tris bathophenanthroline disulfonate (RuBPs) dye developed Rabilloud and co-workers is cost-efficient, simple, sensitive and mass spectrometry compatible.

Secondly, pre-electrophoretic protein staining such as difference in-gel electrophoresis (DIGE), where protein samples are fluorescently labelled with cyanine dyes (CyDyes) that react to proteins lysyl residues. CyDyes are the most sensitive dyes available capable of detecting nanogram of protein (Minden et al., 2009). CyDyes fluoresce at different wavelengths with Cy2 at 520 nanometres (nm), Cy3 at 550nm and Cy5 650nm. This allows for comparisons of samples to be analysed together on a single gel. Two protein samples are labelled with CyDyes, combined, separated, scanned and analysed with fluorescence software (see Figure 1-8).

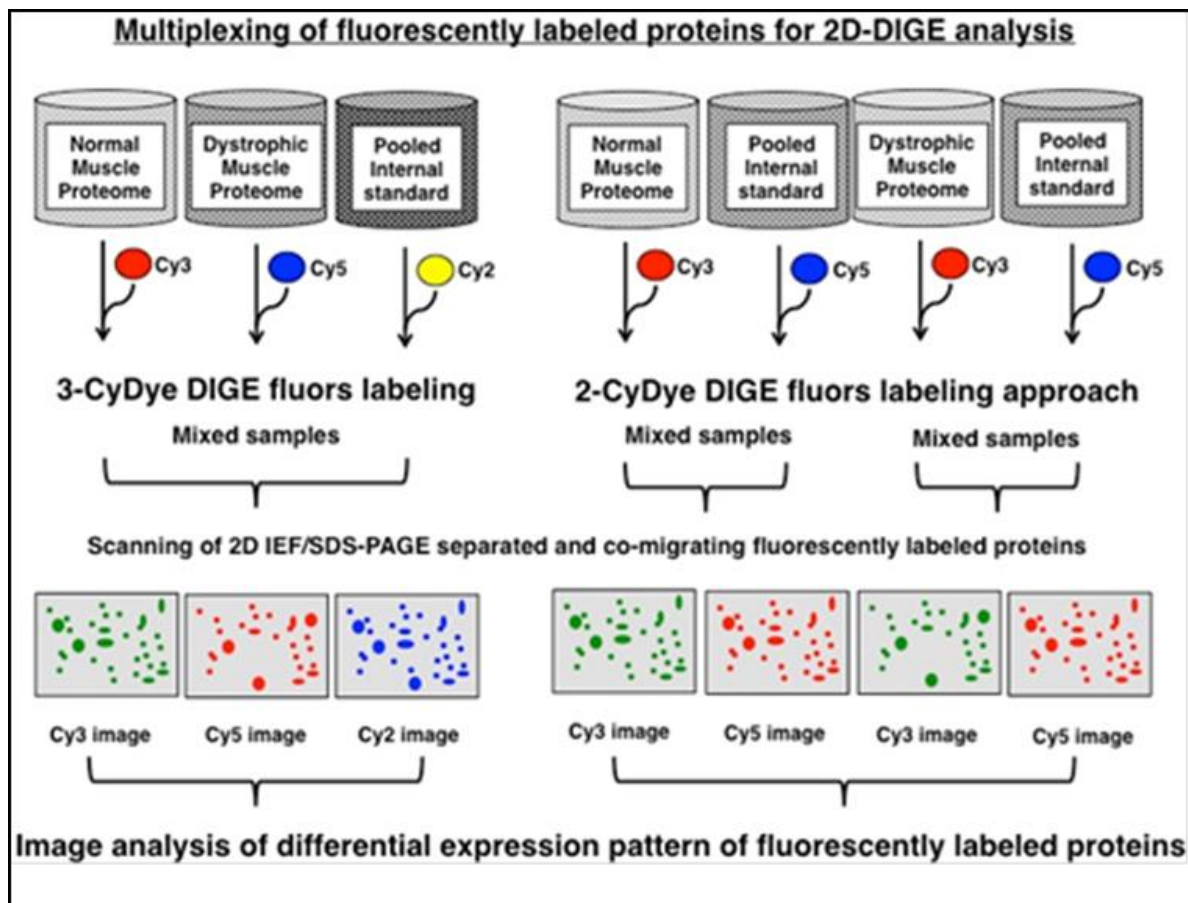


**Figure 1-8 Overview of the main approaches used in fluorescence difference in-gel electrophoresis (DIGE) gel-based proteomics**

The 2-dye or 3-dye DIGE system is most commonly applied method of labelling for studying global changes in complex protein populations. Specimens (A) and (B) are labelled with CyDyes pre-electrophoresis, samples then separated based by their isoelectric point and molecular masses. The gels scanned and image analysis of differential expression pattern of fluorescently labelled proteins.

#### 1.10.4 Protein identification

Quantitative comparative proteomic analysis of the 2-D gel images highlight changes between samples. The identification of these protein changes is achieved using mass spectrometry. Firstly, sample is cleaned up to remove contaminants by desalting and destaining the protein plug. This is then followed by enzymatic digestion using trypsin to cleave the proteins at lysine and arginine amino acid residues. With mass spectrometry following ionisation, analysis and detection steps the amino acid sequences of the peptides are provided and used to identify the protein from a database.

#### 1.10.5 Mass Spectrometry

An ion trap liquid chromatography mass spectrometry LC/MS with an electrospray ionisation (ESI) has been used for protein identification in this study. Whereby the peptide samples are dissolved in a polar solution tube upon exiting tubes tip an electric field is applied which charges the solvent. Thus results in the emerging sample drop to divide into fine spray of droplets which are directed towards the mass spectrometer by nitrogen gas. The warm nitrogen gas flowing through the chamber causes the droplets to evaporate till the droplets are small enough allowing free ions to enter the mass spectrometer and be analysed (Yamashita and Fenn, 1984; Fenn et al., 1989).

#### 1.11 Aims of proposed project

Duchenne muscular dystrophy represents one of the most frequently inherited childhood diseases affecting 1 in 3,500 live male births, due to genetic abnormalities in the dystrophin gene. Absence of dystrophin protein compromises the link between the cytoskeleton to the extracellular matrix and leads to muscle degeneration. Degeneration of muscle fibers and sequent fibrosis leads to DMD patients being

wheelchair bound in early childhood and severe cardiorespiratory complications in older children, the leading cause of death in individuals. Although DMD is progressive, interestingly different subtypes of skeletal muscles are not all affected to the same degree. While *mdx* diaphragm and cardiac muscle are severely dystrophic and hind limb moderately affected, there also appear to be spared phenotypes such as the *interosseus* and extraocular muscle.

The purpose of this research was to perform a detailed proteomic profile on differentially distressed dystrophic muscles, to determine potential muscle subtype-specific changes in secondary alterations and potential age-related changes in the dystrophic phenotype. Therefore, we carried out fluorescence labelling such as DIGE and RuBPs, mass spectrometry, histology and immunoblotting of dystrophic and normal tissue to establish the global proteomic expression patterns for a number of skeletal muscles from aged diaphragm, *interosseus* and *flexor digitorum brevis* muscle to hind limb muscles such as *tibialis anterior*, *extensor digitorum longus* and *soleus* muscle using the *mdx* animal model.

However, since the main proteins of the actomyosin apparatus and its supporting sarcomeric components frequently negate weak signals from minor muscle protein species during proteomic analyses, we also employed a pre-fractionation step to remove certain parts of this analytical problem. In order to eliminate a large portion of highly abundant contractile proteins, differential centrifugation of the crude skeletal muscle extracts were performed to reduce the samples complexity.

Mass spectrometry-based proteomics has been important in determining the global protein expression pattern and effects of the disintegration of the dystroglycan complex DAGC as well as the identification of compensatory mechanisms and establishment of novel biomarkers in dystrophic tissue.

## 2 Materials & Methods

### 2.1 Materials

#### 2.1.1 Equipment

Gel electrophoresis equipment and gel imaging systems used for the proteomic analysis of muscle proteins were from Amersham Biosciences/GE Healthcare, Little Chalfont, Buckinghamshire, UK, including immobilized pH gradient IPG DryStrip rehydration tray, IPGphor IEF unit, manifold, 6 gel casting box, cassette racks, Ettan DALT *twelve* multiple vertical slab gel electrophoresis system, fluorescent glass plates for gel electrophoretic analysis and a Typhoon Trio variable mode scanner.

A Vortex Genie-2 from Scientific Industries, New York, NY, a SSL4 Stuart shaker from Lennox Laboratory Supplies Ltd., Dublin, Ireland, a model 5417R centrifuge from Eppendorf, Cambridge, UK and a Heto speedvac concentrator Medical Supply Company, Dublin, Ireland were used for routine mixing, shaking, centrifugation and concentrating steps, respectively. Identification of protein species was performed on an electrospray ionization Agilent 6340 Ion Trap LC mass spectrometer from Agilent Technologies, Santa Clara, CA, USA. With a nanoflow Agilent 1200 series system, fitted with a Zorbax 300SB C18  $\mu\text{m}$  and 4mm 40nl pre-column was equipped for the separation of peptides.

#### 2.1.2 Reagent solutions

All reagent solutions were prepared with ultrapure water using a Millipore Mill-Q apparatus, to reduce contamination of protein samples to a minimum. General solutions and chemicals were purchased from Sigma Chemical Company in Dorset, UK and were of proteomic/analytical grade, unless stated otherwise. Protease inhibitors were from Roche Diagnostics in Mannheim, Germany.

### 2.1.3 1-D and 2-D gel electrophoresis

For gel electrophoretic protein separation, ultrapure Protogel acrylamide stock solution and 4X Protogel Resolving Buffer stock solutions were purchased from National Diagnostics (Atlanta, GA, USA). Isoelectric focusing immobilized pH gradient (IPG) strips of pH 3-10 24cm and pH 3-11 non-linear (NL) 24cm for 2-D electrophoresis, IPG buffer and ampholytes were purchased from Amersham Biosciences/GE Healthcare (Little Chalfont, Buckinghamshire, UK), and protein molecular weight markers and laemmli buffer were obtained from Biorad Laboratories (Hemel-Hempstead, Hertfordshire, UK).

### 2.1.4 Protein staining

Ruthenium batho-phenanthrolinedisulfonate chelate for the production of RuBPs dye was from Reagecon Diagnostic Limited (Shannon, Ireland). Sodium Ascorbate for RuBPs dye was purchased from Sigma Chemical Company (Dorset, U.K). Coomassie Brilliant Blue G-250 was purchased from Bio-Rad Labs, (Herts, UK). DIGE fluor minimal dyes Cy3 and Cy5 were purchased from GE Healthcare (Little Chalfont, Bucks., UK).

### 2.1.5 Mass spectrometry

Mass Spectrometry grade solvents were purchased for mass spectrometry analysis from Sigma Chemical Company (Dorset, UK). LC-MS Chromaslv water and formic acid were obtained from Fluka (Dorset, UK). Acetonitrile was from Amersham Biosciences/GE Healthcare (Little Chalfont, Bucks., UK) For protein digestion sequencing grade modified trypsin was purchased from Promega (Madison, WI, USA). Model 6340 Ion Trap LC/MS, LC/MS vials and ProtID-Chip-150 II 300A C18 150nm column were from Agilent Technologies Ireland Ltd. (Santa Clara, CA, USA).

### 2.1.6 Western blotting

Chemiluminescence substrate was purchased from Roche Diagnostics (Mannheim, Germany). Nitrocellulose transfer membrane was obtained from Millipore (Bedford, MA, USA). X-ray film was from Fuji Photo Film Co.Ltd. (Tokyo, Japan). Developer/Fixer was purchased from Sigma Chemical Company (Dorset, UK). Ponceau S-Red Staining Solution were purchased from Sigma Chemical Company (Dorset, UK). All secondary antibodies used were purchased from Chemicon International (Temecula, CA., USA). All antibodies used in this research are shown in Table 2-1 with company details and dilutions.

**Table 2.1 Antibodies**

List of antibodies used for immunoblotting this project including the dilutions used for both primary and secondary antibodies, host species (species), company and ordering information. Species= Host species; mouse (Ms), rabbit (Rb), chicken (Ck), 1<sup>0</sup>= primary; 2<sup>0</sup>= secondary; AB= abcam; NC= Novocastra; SC= Santa Cruz; SGN= Enzo Stressgen; SGC= Sigma Chemicals and BIO= Affinity Bioreagents.

<b>Antibody</b>	<b>1<sup>0</sup>Ab Dilutions</b>	<b>Species</b>	<b>2<sup>0</sup>Ab Dilutions</b>	<b>1<sup>0</sup> Order No.</b>	<b>Company</b>
αB-crystallin	1:500	Ms	1:1000	ab13496	AB
Actinin	1:1000	Ms	1:2000	ab9465	AB
ATP synthase	1:500	Ck	1:1000	ab43176	AB
βDystroglycan	1:100	Ms	1:500	NCL-b-DG	NC
βDystroglycan	1:100	Ms	1:500	ab sc-33701	SC
Calsequestrin	1:500	Ms	1:1000	VIIID1 <sub>2</sub>	BIO
Carbonic anhydrase	1:1000	Rb	1:2000	ab54913	AB
Collagen	1:1000	Rb	1:2000	ab6588	AB
cvHSP	1:500	Rb	1:1000	ab111233	AB
Ferritin light chain	1:500	Rb	1:1000	ab69090	AB
Hsp27	1:500	Rb	1:1000	ab12351	AB
Hsp70/72	1:250	Rb	1:1000	ab ADI-SPA-811	SG
Laminin	1:500	Rb	1:1000	ab L-9393	SGC
MLC-2	1:500	Rb	1:1000	ab92721	AB
Myoglobin	1:500	Rb	1:1000	ab77232	AB
Parvalbumin	1:1000	Rb	1:2000	ab11427	AB
Phosphoglycerate kinase	1:1000	Rb	1:2000	ab75223	AB
Prohibitin	1:500	Rb	1:1000	ab28172	AB
Serpina	1:1000	Ck	1:2000	ab14226	AB
Transferrin	1:500	Rb	1:1000	ab9033-1	AB

## 2.2 Methods

### 2.2.1 Dystrophic *mdx* animal model

Proteomic analysis was carried out using dystrophic *mdx* and aged matched C57 control mice. All tissue samples were obtained from the Animal House in the University of Greifswald in Karlsburg, Germany. The mice were maintained under standard living conditions and in accordance to all German and Irish procedures relating to the use of animals for scientific experiments. Mice were sacrificed by cervical dislocation and freeze frozen in liquid nitrogen.

### 2.2.2 Preparation of crude skeletal muscle extracts

The various skeletal muscle extracts for each study were prepared separately. For the proteomic profiling control C57 and age matched *mdx* muscles were taken. The diaphragm (DIA), *tibialis anterior* (TA), *soleus* (SOL), *extensor digitorum longus* (EDL), *interosseus* (INT), *flexor digitorum brevis* (FDB) and crude hind limb muscle extracts were washed in distilled water to remove any skin, bone, hair and blood.

For the initial break-up of the tough contractile fibres the tissue was dissected with a blade. Using appropriate safety equipment and protective clothing liquid nitrogen was added to freeze the tissue followed by grinding of the tissue into a fine powder with mortar and pestle. Each of the ground up muscle powder was solubilised in lysis buffer at a ratio of 1:10 (w/v) respectively. With lysis buffer containing 7M urea, 2M thiourea, 4% (w/v) (3-[3-Cholamidopropyl)-Dimethylammonio]-1-Propane sulfonate) CHAPS, 2% (v/v) IPG buffer pH3-10, 2% (w/v) (dithiothreitol) DTT and protease inhibitors. Samples undergoing DIGE analyses were limited to buffer consisting 9.5M urea, 2% (w/v) CHAPS and a protease inhibitor cocktail (Doran et al., 2006a).

The suspension was vortexed and gently left rocking for 1 hour at room temperature

followed by centrifugation at 4 °C for 20 min at 20,000g. The protein containing middle layer was retained. In the case of further subcellular fractionation an extra differential centrifugation step was performed at 100,000g for 1 hour at 4 °C. With sucrose buffer containing 20mM sodium pyrophosphate, 20mM sodium phosphate, 1mM MgCl<sub>2</sub>, 0.303M sucrose, 0.5mM EDTA, pH 7.0 and protease inhibitors. Pellets were resuspended in lysis buffer and the protein concentration determined using the Bradford assay system (Bradford, 1976).

### 2.2.3 1-D Gel Electrophoresis

One dimensional SDS polyacrylamide gel electrophoresis was carried out using a Bio-Rad Mini-Protean III gel system from Bio-Rad Laboratories (Hemel-Hempstead, Herts., UK) and performed according to Laemmli (1970). Ten percent resolving gel were used containing 10% (w/v) acrylamide from protogel acrylamide stock, 4X Protogel resolving buffer, 0.69M APS, 0.438M SDS and 0.1% (v/v) TEMED (N, N, N', N'-tetramethylethylenediamine). The stacking gel consisted of 5% (w/v) acrylamide, 0.69M APS, 0.5M Tris-PO<sub>4</sub> at pH 6.7, 0.438M SDS and 0.1% (v/v) TEMED. When casting the resolving gel was poured first and stacking gel poured over the resolving gel once it had time to polymerise. Samples were heated for 10 min at 96°C in a 1:1 dilution of Laemmli buffer with 350mM DTT before loading onto the gel. 10mg of protein was loaded per lane. Electrophoresis was carried out using running buffer (125mM Tris, 0.96M glycine, 0.1% (w/v) SDS) and run at 60 volts till sample passed the stacking gel were increased to 120 volts until the tracking dye ran off the bottom of the gel.

### 2.2.4 2-D Gel Electrophoresis

For isoelectric focusing IPG strips were in-gel rehydrated with sample (and equal volume 2x lysis buffer for DIGE analysis) and made up with rehydration buffer (7M urea, 2M thiourea, 4% (w/v) CHAPS, 2% (v/v) IPG buffer pH3-10, 2% (w/v) DTT, protease

inhibitors and 1.2% (v/v) DeStreak rehydration solution from Amersham Biosciences/GE Healthcare. ). Different volumes were used according to the length of the IPG strip and amount of sample required depending on the staining technique. For the IPG 24cm strips a total volume (rehydration buffer and sample) of 450ml is required.

Rehydrated strips were run on an IPGphor IEF instrument and isoelectric focusing was carried as followed: 80V for 4h, 100V for 2h, 500V for 1.5h, 1000V for 1h, 2000V for 1h, 4000V for 1h, 6000V for 2h and finally 8000V for 2.5h. After completion of isoelectric focusing, the IPG strips were initially incubated in equilibration buffer (6M urea, 30% (v/v) glycerol, 2% (w/v) SDS, 100mM Tris-HCl, pH 8.8) with addition of 100mM DTT for 20 min followed by an additional equilibration step with 0.25M (iodoacetamide) IAA for 20 min (Lewis et al., 2009).

Strips were then washed briefly in (sodium dodecyl sulphate) SDS containing running buffer (125mM Tris, 0.96M glycine, 0.1% (w/v) SDS) and placed onto a 12.5% (v/v) resolving slab gel. Sealing solution containing 1x SDS running buffer plus 1% (w/v) agarose and Bromophenol Blue was heated to seal the strip gels. Gel slabs were then loaded into an Ettan DALT-*two* tank system from GE Healthcare (Little Chalfont, Bucks., UK) and electrophoresis carried out at 0.5W/gel for 1 hour followed by 15W/gel until the Bromophenol Blue dye front ran off the gel.

## 2.2.5 Protein Staining

### 2.2.5.1 Colloidal Coomassie Staining

Colloidal Coomassie staining is a post electrophoretic staining method and was performed according to Neuhoff and co-workers (1988). The gels were washed in dH<sub>2</sub>O and placed into the Colloidal Coomassie staining solution, 1part Stock Solution A (5% (w/v) Coomassie Brilliant Blue G250), 40 parts Stock Solution B (10% (w/v) ammonium sulfate, 2% (v/v) phosphoric acid) and 10 parts methanol and left rocking overnight. The gels were

then washed with neutralisation buffer (0.1M Tris-PO<sub>4</sub> pH 6.5) for 3 min. Followed by 25% methanol wash step for 1 min to help reduce the background and gels fixed overnight in fixation solution (20% (w/v) ammonium sulphate). The Colloidal Coomassie Staining method was repeated until sufficient protein pattern is visualised.

### 2.2.5.2 RuBPs Stain Preparation

Ruthenium II Bathophenanthroline Disulfonate Chelate (RuBPs) 20mM stock solution was synthesised as outlined by Rabilloud and colleagues (2001). Potassium pentachloroaquo ruthenate (0.2g) was dissolved into 20ml of boiling dH<sub>2</sub>O and kept under reflux, resulting in a deep red-brown colour solution. Bathophenanthroline disulfonate (3M) was then added and kept under reflux for 20 min, resulting in a greenish-brown colour solution. 500mM sodium ascorbate solution made up to 5mls was then added and kept under reflux for 20 min, resulting in a deep orange-brown colour solution. The solution was then cooled and adjusted to pH 7 with sodium hydroxide. The RuBPs stain was then adjusted with dH<sub>2</sub>O to give a final volume of 26ml and stored at 4°C till use.

### 2.2.5.3 RuBPs staining

Following electrophoresis gels were placed in fixation solution (30% ethanol, 10% acetic acid) for 1 hour. The gels were then washed in 20% ethanol for 30 min and repeated three times. The gels were then incubated for 6 hours in 20% (v/v) ethanol containing 200nM of ruthenium chelate staining dye. Following ruthenium staining the gels were destained for overnight in 40% ethanol, 10% acetic acid. Gels were then equilibrated in dH<sub>2</sub>O twice for 10 min. RuBPs gels were scanned using variable mode imager from Amersham Biosciences/GE Healthcare Typhoon Trio apparatus. The RuBPs labelled muscle proteins were scanned at wavelength of  $\lambda=532\text{nm}$ . The Photomultiplier tube PMT-values for gels analysed were between 500V and 600V and the maximum pixel volume was between 80,000 and 99,000. The RuBPs stained gels were scanned at 100  $\mu\text{m}$  resolution.

## 2.2.6 Fluorescence difference in-gel electrophoretic analysis

Similar to RuBP's staining DIGE labelling was used to determine potential differences in expression patterns of the skeletal muscle soluble proteome (Viswanathan et al., 2006), as recommended by Karp and Lilley (2005). Prior to use the CyDye's were taken from  $-20^{\circ}\text{C}$  and left at room temperature. Cy3 and Cy5 dyes were reconstituted in freshly prepared (dimethylformamide) DMF to give a working solution of 400pmol/ul. Samples were labelled with 400pmols of Cy3 fluor dye per 50 $\mu\text{g}$  protein. The internal pooled standard for each sample were labelled with Cy5 fluor dye containing 25 $\mu\text{g}$  control and 25 $\mu\text{g}$  mdx. The labelled samples were mixed and centrifuged briefly and left on ice for 30 min in the dark. The reaction was stopped with 10mM lysine for 10 min in the dark. The labelled samples and pooled internal standards were combined according to the experimental design. Equal amounts of 2x lysis buffer was added and left for 10 min prior to electrophoresis separation.

## 2.2.7 Protein visualization and data analysis

Fluorescent CyDye and RuBPs labelled proteins were visualised using an Amersham Biosciences/GE Healthcare Typhoon Trio variable mode. For image acquisition, RuBPs labelled proteins were scanned at a wavelength of  $\lambda=532\text{nm}$ . While Cy3 and Cy5 labelled proteins were scanned at a wavelength of  $\lambda=550\text{nm}$  and  $\lambda=650\text{nm}$ , respectively. The photomultiplier tube PMT values were adjusted so that the volume of the most abundant spot on the gel images was between 80,000 and 99,000 when scanned at 100 $\mu\text{m}$  resolution. Allowing for an accurate analysis of the gel images as no spot would be saturated. The RuBPs and DIGE CyDye gel images were then analysed using an alignment based approach with SameSpots Progenesis software version 3.2.3 from NonLinear Dynamics (Newcastle upon Tyne, UK). RuBPs based experiments were normalised against their biological replicates while Cy3 images in the DIGE experiments used their corresponding Cy5 image. All the gels in an experiment were then aligned to a reference gel. Spots were then detected and filtered.

Following filtering, gel images were then placed into groups (control versus disease) and analysed to determine significant differences in the abundance of distinct protein spots. A list was generated of spots with changed abundance. Each spot was given a power score or principal component analysis PCA and any below  $<0.8$  were excluded from analysis. Similarly, spots with a P value  $<0.05$  were included with those  $>0.05$  being excluded from the experiment. An anova score was established using the one way anova test, an ANOVA score above  $>0.5$  was required for consideration. Any spots that met the significance criteria were subsequently identified by LC-MS/MS analysis.

### 2.2.8 In-gel digestion of proteins for Mass spectrometric identification

Preparative gels containing 800 $\mu$ g of protein (1:1 disease to control) were labelled with RuBPs stain and scanned at a wavelength of  $\lambda=532\text{nm}$  as previously discussed above. These images were attached to the Progenesis Samespots report and aligned to the experiments reference gel, highlighting the key protein spots of interest. Prior to identification via LC-MS/MS these key protein spots were excised, washed and digested according to Shevchenko and colleagues (2006). The gel pieces were destained and treated with 400ng of trypsin per gel plug and left at  $4^{\circ}\text{C}$  for 30 min before being digested at  $37^{\circ}\text{C}$  overnight. 100 $\mu$ l of extraction buffer (1:2 v/v of 5% (v/v) formic acid/acetonitrile) was added to the digested plugs and incubated at  $37^{\circ}\text{C}$  for 15min. Resulting supernatant fractions were transferred into fresh tubes and the peptides were dried down in a vacuum centrifuge.

### 2.2.9 Mass spectrometric identification of skeletal muscle proteins

Peptides were reconstituted in 16 $\mu$ l of 0.1% (v/v) formic acid. Followed by brief vortex, sonication and centrifugation for 20min in cellulose spin filter tubes at 14,000g. Samples were then transferred into individually labelled LC-MS vials and analysed on a 6340 Model Ion Trap LC mass spectrometer apparatus using electrospray ionization from Agilent

Technologies (Santa Clara, CA, USA). Samples were injected and followed previously optimised (Lewis et al., 2010b) running conditions of 10min gradient of 5-100% acetonitrile/0.1% formic acid and with a post run of 1min. Peptide separation was achieved with a nanoflow Agilent 1200 series system from Agilent Technologies, equipped with Zorbax 300SB C18 5 $\mu$ m, 4mm 40nl pre column and a Zorbax 300SB C18 5 $\mu$ m, 43mm x 75 $\mu$ m analytical reversed phase column with HPLC-Chip technology.

Mobile phases were (A): 0.1% (v/v) formic acid, (B): 90% (v/v) acetonitrile and 0.1% (v/v) formic acid. Samples (6 $\mu$ l) were loaded into the enrichment column at a capillary flow rate of 4 $\mu$ l/min with a mix of A and B at a ratio of 19:1. Elution of the tryptic peptides was carried out on a linear gradient with a constant nano pump flow rate of 0.6 $\mu$ l/min. To eliminate any sample carryover a 5 min post time of solvent A was carried out. Capillary voltage maintained at 2,000V with temperature and flow rate of the drying gas at 300<sup>0</sup>C and 41/min, respectively.

Distinct protein species were identified using database search engine, Mascot MS/MS Ion search from Matrix Science London, UK. Each search performed followed the same criteria (i) two missed cleavages by trypsin, (ii) species Mus "musculus" as taxonomic category, (iii) oxidation of methionine as variable modification, (iv) mass tolerance of precursor ions  $\pm$ 2.5Da and product ions  $\pm$ 1Da and (v) carboxymethylated cysteine fixed modification. Identification of protein of interest were accepted once a Mascot score >49 was confirmed with >2 peptides matched and p/ and molecular weight matched the reference gel. Mascot score of >49 (corresponding to <p 0.05) offers a 95% confidence the match is correct.

### 2.2.10 Immunoblot analysis

Key proteins of interest were selected and antibodies purchased. Samples (10 $\mu$ g) were loaded onto 1D gel according to the experimental design with a molecular weight marker. Gel electrophoretic separation of 1D gel was carried out with a Mini-Protean II

electrophoresis rig from Bio-Rad Laboratories (Hemel-Hempstead, Herts., UK) and transferred onto nitrocellulose membrane using transfer system from Bio-Rad. Muscle proteins were run at 100V for 70min at 4°C. Ponsceau S-Red staining was carried out on the nitrocellulose membrane and labelled appropriately.

Prior to immune decoration, nitrocellulose sheets were blocked with milk solution (5% (w/v) fat-free milk powder in phosphate-buffered saline PBS) for 1 hour. Membranes were then incubated overnight with sufficiently diluted primary antibody solution with gentle agitation. Membranes were washed and incubated with secondary peroxidase-conjugated antibodies in blocking solution for 1 hour at room temperature. Following another wash step the immune-decorated protein bands were visualised with enhanced chemiluminescence (ECL) method from Roche Diagnostics (Mannheim, Germany) in a darkroom. Immunoblots were then analysed, densitometric scanning was performed with Image J software (NIH, Bethesda, Maryland, USA) and Graphpad prism statistical software (Graphpad software Inc.)

### 2.2.11 Statistical Analysis

Densitometric scanning of Immunoblots was performed with Image J software (NIH, Bethesda, Maryland, USA) and Graphpad prism statistical software (Graphpad software Inc.). Throughout this project a probability (p) value of 0.05 was used within a Student's *t*-test, providing a 95% confidence our data is significant.

### **3 Proteomic profiling of age-related changes in the *tibialis anterior* muscle proteome of the *mdx* mouse model of dystrophinopathy**

#### **3.1 Introduction**

X-linked Duchenne muscular dystrophy is an extremely progressive childhood neuromuscular disorder and can be characterised by primary genetic abnormalities in the dystrophin gene. The established *mdx* mouse model of dystrophinopathy exhibits progressive muscle tissue deterioration with age as a result aged *mdx* muscle specimens were analysed on a large-scale survey of potential age-related changes in the dystrophic phenotype. Since the *mdx* mouse *tibialis anterior* muscle is a commonly used model system in muscular dystrophy research, we investigated this particular tissue to determine the global changes in the dystrophic skeletal muscle proteome.

##### **3.1.1 Duchenne muscular dystrophy and *tibialis anterior* skeletal muscle**

The *tibialis anterior* is one of the most active muscles in the lower leg (Mesin et al., 2010), displaying a relatively high level of resistance to fatigue or weakness during periods of intense exercise (Jones et al., 2009). This level of resistance makes the muscle particularly interesting to study with respect to the secondary effects of dystrophinopathy. Senescent *mdx* muscle has been studied as the dystrophic mouse muscle progressively deteriorates with age and as a result more closely resembles that of the neuromuscular pathology exhibited in Duchenne patients (Lefaucheur et al., 1995). Hence, aged *mdx* muscle represents an appropriate dystrophic phenotype for determining and identifying potential global alterations in the protein complement during aging.

### 3.1.2 Experimental design

Comparative gel-based proteomic analysis of aged *mdx tibialis anterior* muscle. Muscle protein extracts were separated by two-dimensional gel electrophoresis and labelled with the fluorescent dye ruthenium II tris bathophenanthroline disulfonate. Then proteins with a significant change in their concentration were identified by mass spectrometry. Key proteomic findings were verified by immunoblot analysis. This report describes the analysis of RuBPs labelled aged dystrophic *tibialis anterior* tissue across 8 week, 12 month and 22 month-old dystrophin-deficient mice along 3-10 pH range. Proteomic profiling established a change in abundance of 8 protein species across the *tibialis anterior* muscle age groups. Identified proteins were involved in various processes form cytosolic cycle, muscle metabolism and the cellular stress response.

## 3.2 Results

### 3.2.1 Comparative proteomic analysis of *mdx tibialis anterior* muscle

High-resolution two-dimensional gel electrophoresis was carried out to separate the proteome from aged dystrophic *mdx tibialis anterior* muscle tissues. A pH-range of 3-10 in the first dimension was employed to establish a global proteomic pattern. Followed by post-electrophoretic labelling of the protein spots with fluorescent dye RuBPs. With the help of a Typhoon Trio variable imager and Progenesis 2-D analysis software, *mdx* skeletal muscle proteomes were compared. An altered concentration was revealed for 8 protein species, with 4 proteins being increased and 4 proteins showing decreased expression in aged *mdx* tissue. Mass spectrometry was then used to identify a number of unchanged landmark proteins and the significant muscle-associated proteins of interest from the *tibialis anterior* muscle and listed in Tables 3-1 and 3-2, respectively.

### 3.2.2 RuBPs analysis of landmark proteins in normal *tibialis anterior* muscle

A list of unchanged landmark 2D protein spots from the *tibialis anterior* muscle are numbered 1 to 20 and marked by circles in the landmark master gel shown in figure 3-1. The mass spectrometric identification of these unchanged landmark muscle proteins is listed in Table 3-1. This table contains the identified muscle-associated proteins names, international accession number, relative molecular masses, *pI*-values, number of matched peptide sequences, Mascot scores, and percentage sequence coverage of major individual muscle protein species in aged dystrophic *mdx tibialis anterior*.

Identified protein species ranged from a molecular mass of 17 kDa (myoglobin) to 71 kDa (spot 2 unknown protein product) and with a *pI*-range from 4.6 *pI* (myosin light chain MLC3) to 8.7 *pI* (troponin TnI). Spots 1 to 22 represent major muscle-associated protein species from ATP synthase (spot 1), unnamed protein product (spot 2), pyruvate kinase (spot 3), enolase (spot 4), creatine kinase (spot 5), actin (spot 6), tropomyosin (spots 7 and 8), malate dehydrogenase (spot 9), aldolase (spot 10), phosphate dehydrogenase (spot 11), carbonic anhydrase (spot 12), triosephosphate (spots 13 and 14), troponin TnI (spot 15), adenylate kinase (spot 16), various myosin light chains consisting of MLC1/3, MLC2, MLC3 (spots 17-20), parvalbumin (spot 21) and myoglobin (spot 22). A significant number of the landmark proteins identified are part of the contractile apparatus.

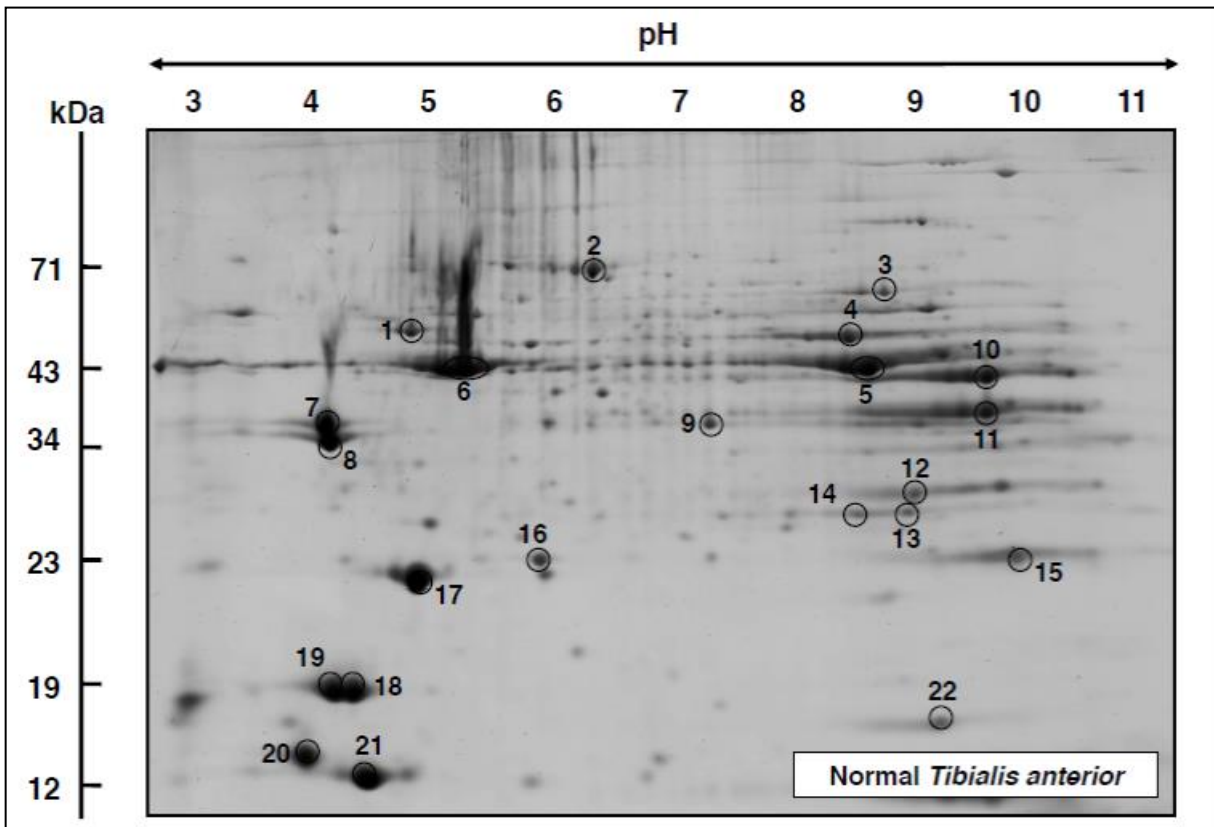


**Figure 3-1 landmark 2D gel of normal mouse *tibialis anterior* muscle**

Figure 3-1 Two-dimensional gel electrophoretic analysis of normal *tibialis anterior* mouse muscle. Shown is a RuBPs-stained gel with 8 weeks old *tibialis anterior* muscle extracts. Major protein spots are numbered 1 to 22 and marked by circles. See Table 3-1 for the mass spectrometric identification of the 2D landmark proteins with no change during aging of the *mdx* model of Duchenne muscular dystrophy. The pH-values of the first dimension and molecular mass standards of the second dimension are shown on the top and on the left of the panels, respectively

**Table 3.1 List of unchanged landmark 2D protein spots from normal mouse *tibialis anterior* muscle**

<b>Spot No.</b>	<b>Protein Name</b>	<b>Accession No.</b>	<b>Isoelectric point (pI)</b>	<b>Molecular mass (Da)</b>	<b>Number of peptides</b>	<b>Coverage (%)</b>	<b>Mascot Score</b>
1	Mitochondrial ATP synthase	AAH37127	5.24	56,632	23	64	456
2	Unnamed protein [Mus musculus]	BAC34145	5.75	70,730	12	21	230
3	Pyruvate kinase, isozymes M1/M2	NP_001240812	6.69	58,461	25	51	1149
4	Enolase, beta, isoform 1	NP_031959	6.73	47,337	21	56	450
5	Creatine Kinase, M-type	NP_031736	6.58	43,250	23	47	509
6	Actin, beta	CAA27396	5.78	39,446	12	41	103
7	Tropomyosin, beta chain	NP_033442	4.66	32,931	22	59	395
8	Tropomyosin, beta chain	NP_033442	4.66	32,933	15	32	241
9	Malate dehydrogenase, cytosolic	AAA37423	6.16	36,625	9	36	190
10	Aldolase A, isoform 2	NP_031464	8.31	39,795	24	75	498
11	Glyceraldehyde- 3-phosphate dehydrogenase	NP_032110	8.44	36,072	14	57	238

12	Carbonicanhydrase CA3	NP_031632	6.89	29,638	12	43	431
13	Triosephosphate isomerase	AAB48543	5.62	22,720	11	62	248
14	Triosephosphate isomerase	AAB48543	5.62	22,720	11	68	638
15	Troponin Tnl, fast skeletal muscle	NP_033431	8.65	21,515	5	20	150
16	Adenylate kinase, isoenzyme 1	NP_067490	5.7	23,330	14	70	184
17	Myosin light chain MLC1/3	NP_067260	4.98	20,697	17	79	426
18	Myosin light chain MLC2	NP_058034	4.82	19,057	15	61	216
19	Myosin light chain MLC2	NP_058034	4.82	19,059	19	81	391
20	Myosin light chain MLC3	AAH59087	4.63	18,968	11	60	222
21	Parvalbumin, alpha	NP_038673	5.02	11,923	12	89	622
22	Myoglobin	NP_038621	7.07	17,116	5	37	98

### 3.2.3 Proteomic analysis of dystrophic *tibialis anterior* muscle during aging

Following the optimisation and initial mass spectrometric identification of landmark muscle proteins in normal *tibialis anterior* mouse muscle, fluorescence high-resolution two-dimensional gel electrophoresis was performed to determine potential differences in aging-related protein expression patterns in *mdx tibialis anterior* mouse muscle proteome. Figure 3-2 shows the analytical gels with 4 biological repeats of 8 week, 12 month and 22 month old total *mdx* mouse muscle extracts. Panels labelled TA MDX 1-4, TA MDX 5-8 and TA MDX 9-12 represent 8 week, 12 month and 22 month old *tibialis anterior* muscle preparations, respectively.

A detailed densitometric analysis was performed on the 2D spot patterns of normal versus dystrophic mouse *tibialis anterior* muscle in order to determine potential differences in individual protein species. Densitometric analysis was carried out using a Typhoon Trio variable imager scanner and Samespot Progenesis 2-D analysis software was performed to establish differential expression patterns during the muscle aging. The detailed proteomic profiling of dystrophic *tibialis anterior* showed distinct age-related changes in 8 muscle protein species between 8 week and 22 month old total *mdx* mouse muscle preparations.

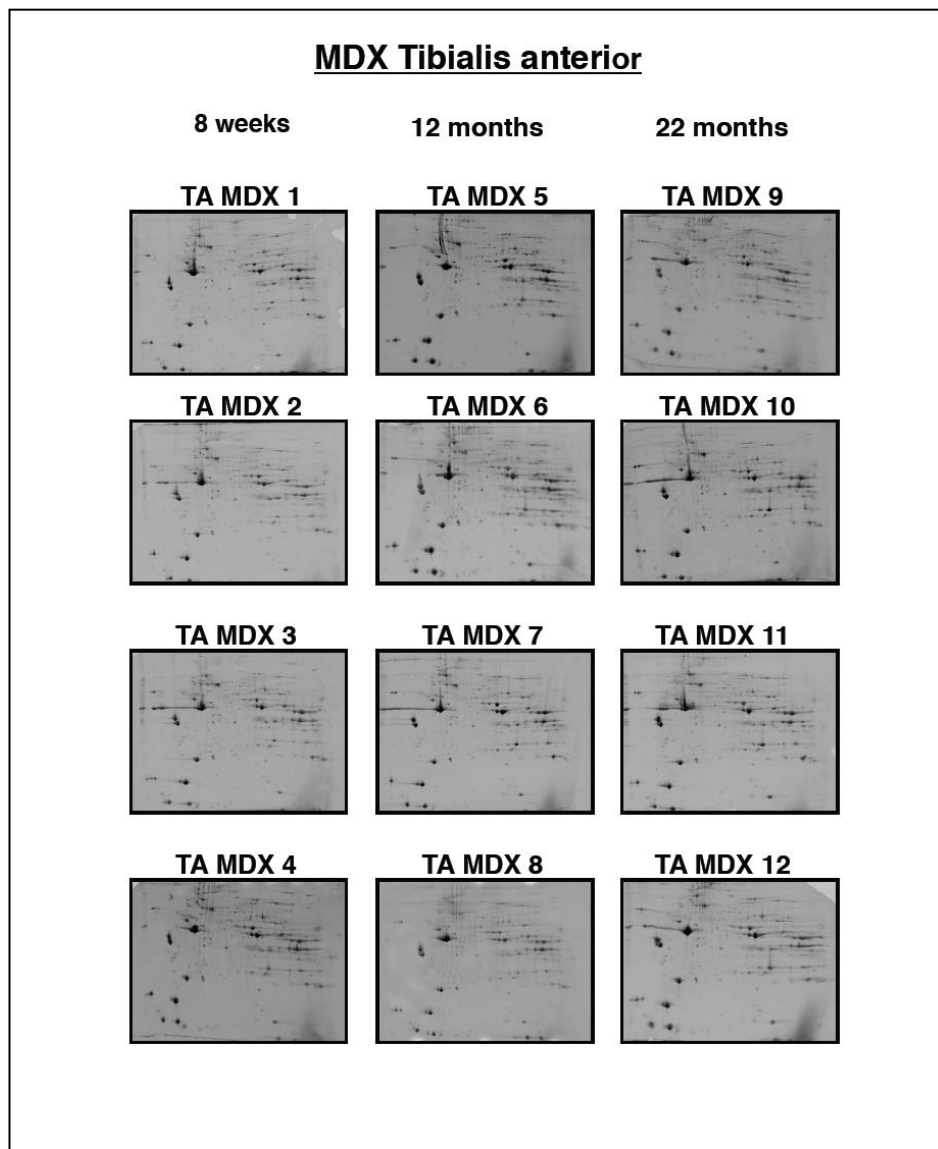


**Figure 3-2 Two-dimensional gel electrophoretic analysis of aging *mdx* mouse *tibialis anterior* muscle**

Shown are RuBPs-stained gels from 8 weeks (TA MDX 1-4), 12 months (TA MDX 5-8) and 22 months (TA MDX 9-12) old *tibialis anterior* muscle extracts. Fluorescent images are shown along the pH 3-10 range.

### 3.2.4 RuBPs analysis of dystrophic *tibialis anterior* muscle

A list of the *tibialis anterior* proteins with significantly altered expression level in age-related dystrophic *mdx* tissue is shown in Table 3-2. Proteins with significant changes in expression levels are numbered 1 to 8 and marked by circles in the master gel Fig 3-3. The mass spectrometric identification of these altered muscle proteins is listed in Table 3-2. This table contains the identified muscle-associated proteins names, international accession number, relative molecular masses, *pI*-values, number of matched peptide sequences, Mascot scores, percentage sequence coverage, and fold-change of individual muscle proteins affected in aged dystrophic *mdx tibialis anterior*.

Protein species with an altered concentration in aged *mdx tibialis anterior* muscle ranged from a molecular mass of 23 kDa (heat shock protein Hsp27) to 224 kDa (myosin 3) and with a *pI*-range from 4.7 *pI* (tropomyosin) to 8.5 *pI* (electron transferring flavoprotein). The expression levels showed an increased abundance for the carbonic anhydrase CA3 isoform (spots 1 and 4), the glycolytic enzyme aldolase protein (spot 2) and electron transferring flavoprotein (spot 3). While the expression levels of key cytosolic enzyme pyruvate kinase (spot 5), myosin 3 (spot 6), tropomyosin beta chain (spot 7) and the molecular chaperone Hsp27 (spot 8) were shown to be decreased in *mdx* aged tissue.

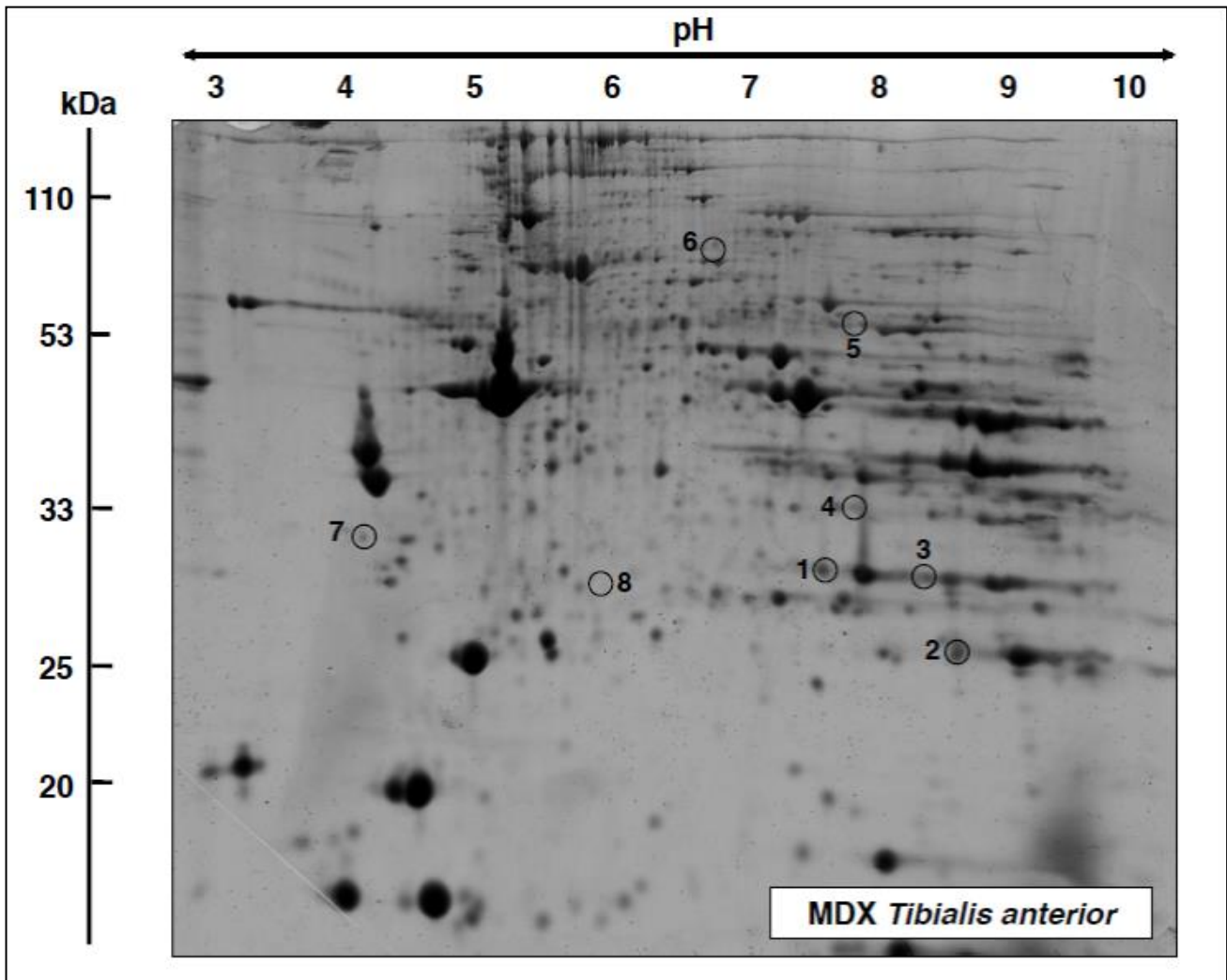


**Figure 3-3 Fluorescence two-dimensional gel electrophoretic analysis of *mdx tibialis anterior* muscle**

Figure 3-3 Fluorescence gel electrophoretic analysis of aged *mdx mouse tibialis anterior* muscle. Shown is a representative RuBPs-stained master gel with crude tissue extracts from *mdx tibialis anterior* muscle. Proteins with an age-related change in expression levels are numbered 1 to 8 and marked by circles. See Table 3-2 for the mass spectrometric identification of the individual muscle-associated proteins. The pH-values of the first dimension and molecular mass standards of the second dimension are shown on the top and on the left of the panels, respectively.

**Table 3.2 List of identified muscle proteins with a significant change of abundance in aging *mdx tibialis anterior* muscle**

Spot No.	Protein Name	Accession No.	Isoelectric point (pI)	Molecular mass (Da)	Number of peptides	Coverage (%)	Mascot Score	Fold Change 8w-22m MDX
1	Carbonic anhydrase CA3	NP031632	6.89	29,638	4	26	181	2.9
2	Aldolase A isoform 2	NP031464	8.31	39,795	2	14	85	2.3
3	Electron transferring flavoprotein, beta	EDL22660	8.50	29,177	13	42	190	1.9
4	Carbonic anhydrase CA3	NP031632	6.89	29,638	12	53	182	1.7
5	Pyruvate kinase	NP035229	7.18	58,388	7	18	440	-1.4
6	Myosin 3	NP001078 847	5.62	224,75 5	9	5	141	-1.4
7	Tropomyosin, beta chain	NP033442	4.66	32,933	3	14	126	-1.6
8	Heat shock protein Hsp27	AAA18335	6.45	22,945	2	15	550	-1.9

### 3.2.5 Immunoblot analysis of dystrophic *tibialis anterior* muscle

In order to further characterise the *tibialis anterior* phenotype, comparative immunoblotting was carried out following the mass spectrometric establishment of the age-related changes in the urea-soluble *mdx* muscle proteome. Immunoblotting was performed to investigate the concentration of the two most extensively altered new biomarkers, carbonic anhydrase CA3 and heat shock protein Hsp27 in normal versus dystrophic muscle preparations.

Antibodies to  $\beta$ -dystroglycan ( $\beta$ -DG), a dystrophin-associated glycoprotein which forms the main trans-sarcolemmal linker among the extracellular matrix and the cytoskeleton in the fibre periphery, were used to confirm the dystrophic status of *mdx* muscle samples during aging. Immunoblotting of the glycoprotein (Figure 3-4) clearly shows the drastic reduction of  $\beta$ -DG in both 8 week and 22 month old *mdx* mouse *tibialis anterior* muscle, which is characteristic of dystrophinopathy.

Immunoblotting of young versus old muscle samples with the CA3 isoform of carbonic anhydrase antibody (Figure 3-5) showed an increased abundance of the metabolic enzyme. While immunoblotting with the molecular chaperone Hsp27 antibody (Figure 3-6) showed a decreased concentration of the small heat shock protein in dystrophin-deficient *mdx* muscle. Thus, both the CA3 fibre type-specific protein and the Hsp27 molecular stress protein represent suitable biomarker candidates of the dystrophic phenotype.

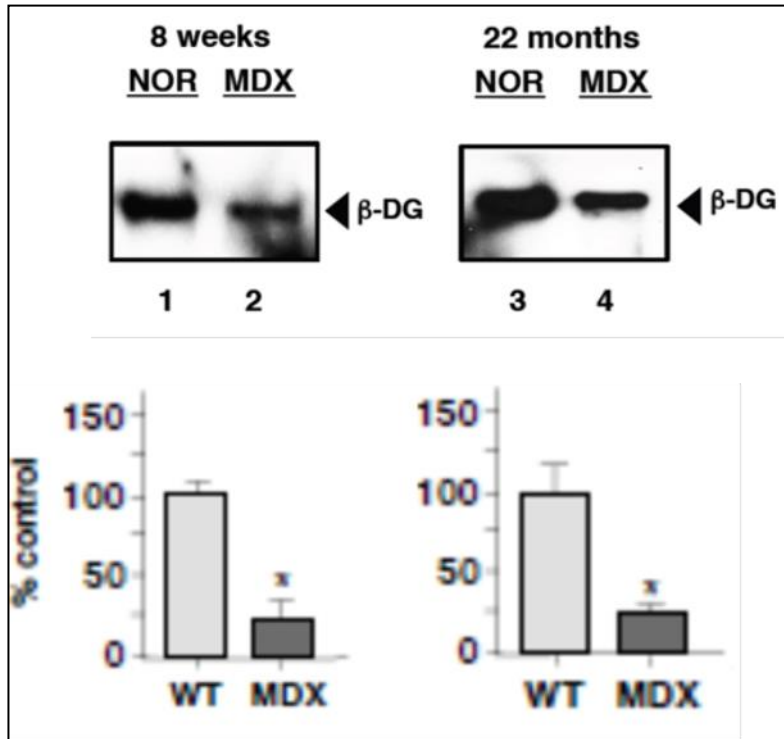


**Figure 3-4 Immunoblotting analysis of dystrophin-associated glycoprotein  $\beta$ -dystroglycan**

Shown are representative blots with expanded views of immuno-decorated protein bands indicated by the arrowhead, with graphical presentation of the statistical evaluation. Immunoblots were labelled with the  $\beta$ -dystroglycan ( $\beta$ -DG) antibody. Lanes 1, 2 and 3, 4 represent 8 week vs 22 month-old normal wild type vs dystrophic *mdx tibialis anterior* muscle, respectively. The comparative blotting was statistically verified using an unpaired Student's *t*-test ( $n=4$  replicates). Standard deviation represented by Error bars, (\* $p < 0.05$ ).

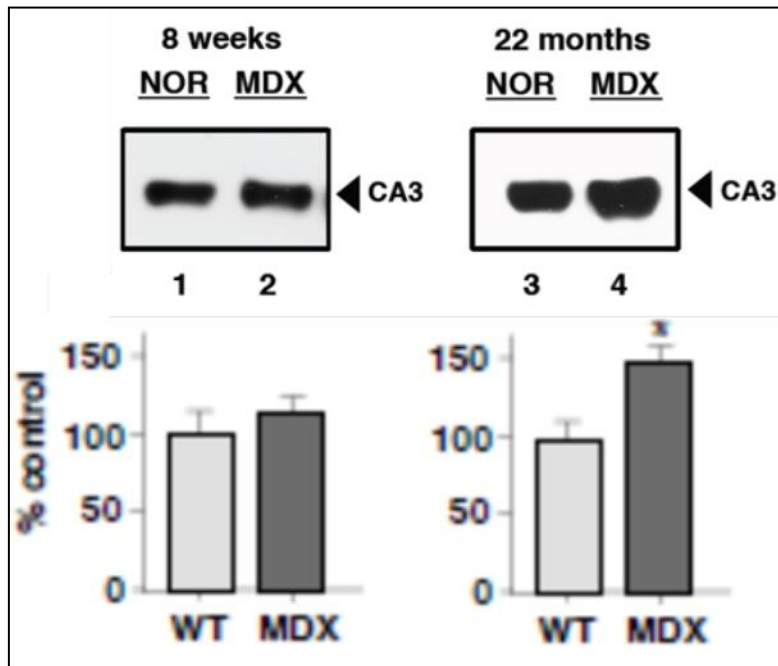


**Figure 3-5 Immunoblotting analysis of carbonic anhydrase enzyme**

Shown are representative blots with expanded views of immuno-decorated protein bands indicated by the arrowhead, with graphical presentation of the statistical evaluation. Immunoblots were labelled with the fiber type-specific enzyme carbonic anhydrase (CA3) antibody. Lanes 1, 2 and 3, 4 represent 8 week vs 22 month-old normal wild type vs dystrophic *mdx tibialis anterior* muscle, respectively. The comparative blotting was statistically verified using an unpaired Student's *t*-test ( $n=4$  replicates). Standard deviation represented by Error bars, (\* $p<0.05$ ).

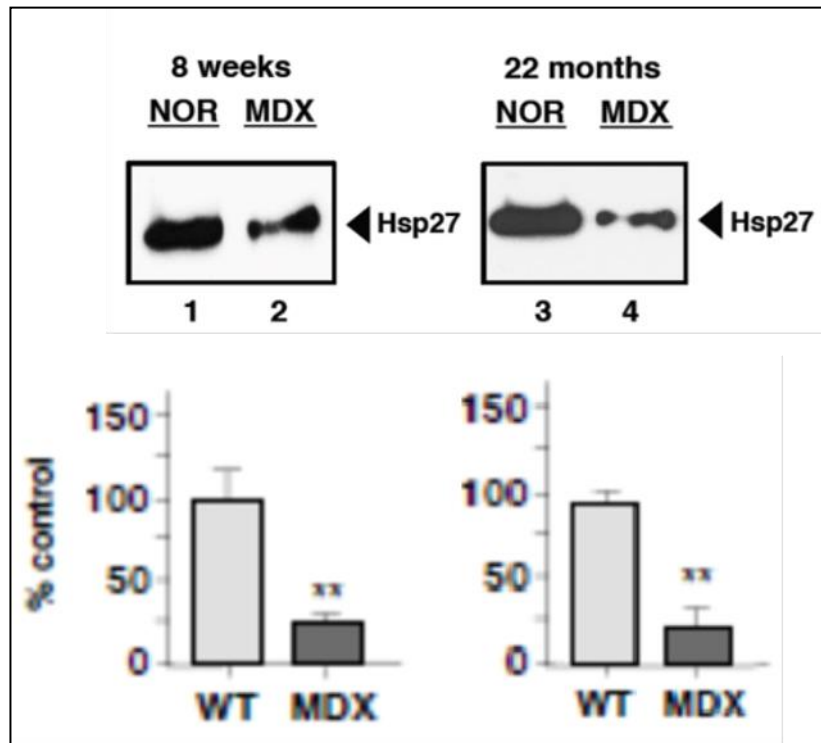


**Figure 3-6 Immunoblotting analysis of the small heat shock protein 27**

Shown are representative blots with expanded views of immuno-decorated protein bands indicated by the arrowhead, with graphical presentation of the statistical evaluation. Immunoblots were labelled with the molecular chaperone heat shock protein 27 (Hsp27) antibody. Lanes 1, 2 and 3, 4 represent 8 week vs 22 month-old normal wild type vs dystrophic *mdx tibialis anterior* muscle, respectively. The comparative blotting was statistically verified using an unpaired Student's *t*-test (n=4 replicates). Standard deviation represented by Error bars, (\*\* $p < 0.005$ ).

### 3.3 Discussion

Duchenne muscular dystrophy is one of the most crippling childhood neuromuscular disorders (Emer, 2002), therefore meriting comprehensive large-scale studies into the establishment of detailed biomarker signatures of dystrophinopathy (Lewis et al., 2009; Griffin and Rosiers, 2009). In dystrophinopathy, the loss or almost complete absence of the crucial 427kDa cytoskeletal membrane protein dystrophin result in a drastic reduction of a large number of surface glycoproteins which leads to a loss of sarcolemmal integrity.

In this chapter, proteomic profiling revealed that during the natural aging of the moderately dystrophic mouse *tibialis anterior* muscles a key number of skeletal muscle proteins change in abundance. Senescent *mdx* muscle has been studied as the dystrophic mouse muscle progressively deteriorates with age and as a result more closely resembles that of the neuromuscular pathology exhibited in Duchenne patients (Lefaucheur et al., 1995). Hence, aged *mdx* muscle represents an appropriate dystrophic phenotype for determining and identifying potential global alterations in the protein complement during aging.

#### 3.3.1 Proteomic expression changes of *tibialis anterior* analysis

This chapter has summarised the results of a comparative proteomic analysis of moderately affected *mdx tibialis anterior* muscle from 8 week, 12 month and 22 month old mice. The identification of carbonic anhydrase, aldolase, electron transferring flavoprotein, tropomyosin, myosin, pyruvate kinase, and Hsp27 small heat shock protein as new markers of progressive muscular dystrophy might be helpful for the establishment of a detailed biomarker signature of Duchenne muscular dystrophy.

### 3.3.2 Elevated metabolic enzymes in *mdx* tissue

The protein spot with the highest age-related increase was carbonic anhydrase isoform CA3 (Fremont et al., 1988). In general, carbonic anhydrases are involved in catalysing the reversible hydration of CO<sub>2</sub> and are commonly distributed throughout the body (Geers, 2000). Several isoforms of this key metabolic enzyme are expressed by skeletal muscles in a fiber type-specific manner. The principal CA3 isoform is mostly located in the cytosolic fraction of type I and IIa fibers (Fremont et al., 1988). Interestingly, altered neuromuscular activity patterns, disuse atrophy, stretch-induced hypertrophy and metabolic adaptations significantly influence the expression of muscle carbonic anhydrases (Brownson et al., 1988; Brownson and Loughna, 1996; Cote et al., 1999).

The increased concentration of the carbonic anhydrase CA3 isoform in aged *mdx* muscle, as revealed in this survey by mass spectrometry-based proteomics, could suggest an increased demand for effective CO<sub>2</sub>-removal during *mdx* fibre aging. That or perhaps since the CA3 isoform is mainly located in slower-twitching fibre populations, its change in density could also be contributed to age-related fibre type shifting in the *mdx* mouse *tibialis anterior* muscle.

### 3.3.3 Perturbed stress response in *mdx* tissue

The muscle-associated protein spot with the greatest reduction during aging of the *mdx* mouse *tibialis anterior* muscle was shown to be anti-apoptotic small heat shock protein, Hsp27. This suggests a potentially diminished anti-oxidative stress response in the dystrophic *tibialis anterior* muscle fibers and establishes that clear differences exist with respect to expression levels of small cellular heat shock proteins in moderately affected hind limb muscles compared to severely dystrophic diaphragm muscle in the *mdx* mouse model of dystrophinopathy, shown in chapter 4 (Doran et al., 2006a; Doran

et al., 2009a).

### 3.3.4 Altered glycolytic and oxidative enzymes in *mdx* tissue

The enzyme aldolase and pyruvate kinase catalyses the reversible cleavage of fructose-1,6-bisphosphate into glyceraldehyde-3-phosphate and dihydroxyacetone phosphate and the important oxidation-reduction-phosphorylation step that transforms ADP and phosphoenolpyruvate to yield ATP and pyruvate, respectively (Ohlendieck, 2001). These changes in glycolytic enzymes and mitochondrial proteins in *mdx* mouse *tibialis anterior* muscle suggest altered flux rates through the key metabolic pathway. With regards to the glycolytic pathway, pyruvate kinase is central for the regulation of an enzymatic level (Ohlendieck, 2001). This vital role of pyruvate kinase in muscle metabolism makes its altered abundance in the *mdx* mouse *tibialis anterior* muscle a key finding. Mass spectrometry-based proteomics has clearly confirmed a glycolytic-to-oxidative metabolic shift during *mdx* skeletal muscle aging.

Previously published surveys have shown pyruvate kinase as a potential biomarker for the overall aging process in skeletal muscle tissues (Doran et al., 2008; Doran et al., 2009a). The altered metabolic enzymes in the aged *mdx* mouse *tibialis anterior* muscle agree with the proteomic profiling of the golden retriever muscular dystrophy GRMD. In the dog model of dystrophinopathy various glycolytic and oxidative enzymes, were found to be reduced, such as the aldolase and pyruvate kinase enzymes (Guevel et al., 2011).

### 3.3.5 Other proteins

While alterations of the contractile apparatus elements indicate down-stream effects of dystrophin deficiency on myosin and tropomyosin organisation, changed expression

levels in electron transferring flavoprotein suggest perturbed *mdx* muscle metabolism. The electron transferring flavoprotein beta polypeptide chain plays an important role in amino acid and mitochondrial fatty acid catabolism, and facilitates the transporting of electrons between flavoprotein dehydrogenases (Toogood and Scrutton, 2007).

### 3.4 Conclusion

In conclusion, the comparative proteomic profiling of dystrophic *tibialis anterior* muscle from 8 week versus 22 month-old *mdx* mice has revealed changes in expression levels in a number of key proteins during skeletal muscle aging. However, the level of concentrations altered was less evident in the moderately dystrophic *tibialis anterior* mouse muscle as compared to previously analysed aged *mdx* mouse diaphragm (Carberry et al., 2012a). These differing proteomic results agree with the pathophysiological notion that the aged *mdx* mouse diaphragm muscle is more severely dystrophic as compared to moderately affected *mdx* hind limb muscle.

In the long-term, the continued proteomic identification of novel biomarkers of dystrophinopathy may potentially be useful for the establishment of a detailed and muscle subtype-specific biomarker signature of Duchenne muscular dystrophy. This would be important for monitoring disease progression, identifying novel therapeutic targets, improving diagnostic procedures and aid in the evaluation of new treatments, such as stem cell therapy or exon-skipping therapy.

## **4 Proteomic profiling of age-related changes in severely dystrophic Diaphragm muscle proteome of the *mdx* mouse model of dystrophinopathy**

### 4.1 Introduction

Aging is a complex and fundamental biological process. The established *mdx* mouse model of dystrophinopathy exhibits progressive muscle tissue deterioration with age and more closely resembles the human pathology as a result aged *mdx* muscle specimens were analysed on a large-scale survey of potential age-related changes in the dystrophic phenotype. Thus, since senescent *mdx* mouse diaphragm muscle appears to represent a more suitable dystrophic phenotype, we investigated this particular tissue to determine the global changes in the protein complement during the natural aging process of the *mdx* muscle.

#### 4.1.1 Duchenne muscular dystrophy and Diaphragm skeletal muscle

In contrast to the *mdx* hind limb muscles, the dystrophic *mdx* diaphragm exhibits severe symptoms of skeletal muscle fibre degeneration that more closely resembles that of the neuromuscular pathology exhibited in Duchenne patients than any other muscle (Lefaucheur et al., 1995). The Diaphragm is one of the most severely affected muscles in Duchenne patients and is the primary cause of death leading from respiratory problems in late twenties. Senescent *mdx* muscle has been studied as the severely dystrophic diaphragm mouse muscle progressively deteriorates with age making it more comparable to Duchenne muscular dystrophy.

The age-related pathogenesis of *mdx* mouse muscle is characterised by

progressive motor weakness (Lynch et al., 2001), a shortened life span with increased susceptibility to spontaneous rhabdomyosarcoma (Chamberlain et al., 2007), muscle periphery weakening triggered by the presence of branched fibres (Mouisel et al., 2010), severe loss of myofibres with concomitant replacement by connective tissue (Wineinger et al., 1998; Pastoret and Sebille, 1995a; Pastoret and Sebille, 1995b), a reduction in regenerative potential and changes in the crucial mTOR signaling pathway (Mouisel et al., 2010), and impaired structural and functional recovery after injury (Irintchev et al., 1997). Hence, aged *mdx* muscle represents an appropriate dystrophic phenotype for determining and identifying potential global alterations in the protein complement during aging.

#### 4.1.2 Experimental design

Comparative gel-based proteomic analysis of *mdx* Diaphragm muscle. Muscle protein extracts were separated by two-dimensional gel electrophoresis and labelled with the fluorescent dyes. Then proteins with a significant change in their concentration were identified by mass spectrometry. Key proteomic findings were verified by immunoblot analysis. This report describes both the analysis of RuBPs labelled aged dystrophic Diaphragm muscle across 8 week, 12 month and 22 month-old dystrophin-deficient mice along 3-10 pH range. Proteomic findings established an age-related change in abundance of 11 protein species across the aged *mdx* Diaphragm muscle.

This was followed by a detailed comparative DIGE analysis of 22 month-old dystrophin-deficient mice versus age-matched control mice across 3-11 NL pH range. Proteomic profiling established a significant change in abundance of 84 protein species in the aged *mdx* Diaphragm muscle. Identified proteins were involved in various processes from the extracellular matrix, contractile apparatus, metabolite transport, mitochondrial energy metabolism and the cellular stress response.

## 4.2 Results

### 4.2.1 Comparative proteomic analysis of *mdx* diaphragm muscle

High-resolution two-dimensional gel electrophoresis was carried out to separate the proteome from aged dystrophic *mdx* diaphragm muscle tissues. A pH-range of 3-10 in the first dimension was employed to establish a global proteomic pattern. Followed by post-electrophoretic labelling of the protein spots with fluorescent dye RuBPs. With the help of a Typhoon Trio variable imager and Progenesis 2-D analysis software, *mdx* skeletal muscle proteomes were compared. An altered concentration was revealed for 11 protein species, with 10 proteins being increased and 1 protein showing decreased expression in senescent *mdx* tissue. Mass spectrometry was then used to identify these significant muscle-associated proteins of interest and listed in Table 4-1.

### 4.2.2 Proteomic analysis of dystrophic diaphragm muscle during aging

Fluorescence high-resolution two-dimensional electrophoresis in combination with MS analysis was performed to determine potential differences in aging-related protein expression patterns in *mdx* diaphragm muscle proteome. Figure 4-1 shows the analytical gels with 4 biological repeats of 8 week, 12 month and 22 month-old total *mdx* mouse muscle extracts. Panels labelled DIA MDX 1-4, DIA MDX 5-8 and DIA MDX 9-12 represent 8 week, 12 month and 22 month-old dystrophic diaphragm muscle preparations, respectively.

The overall 2D protein spot patterns of differently aged dystrophic muscle preparations were relatively comparable as a result a detailed denitometric analysis was performed in order to determine potential differences in individual protein species. Densitometric analysis was carried out using a Typhoon Trio variable imager scanner and Samespot Progenesis 2-D analysis software was performed to establish differential expression

patterns during the muscle aging. The detailed proteomic profiling of dystrophic diaphragm showed distinct age-related changes in 8 muscle protein species between 8 week and 22 month old total *mdx* mouse muscle preparations.

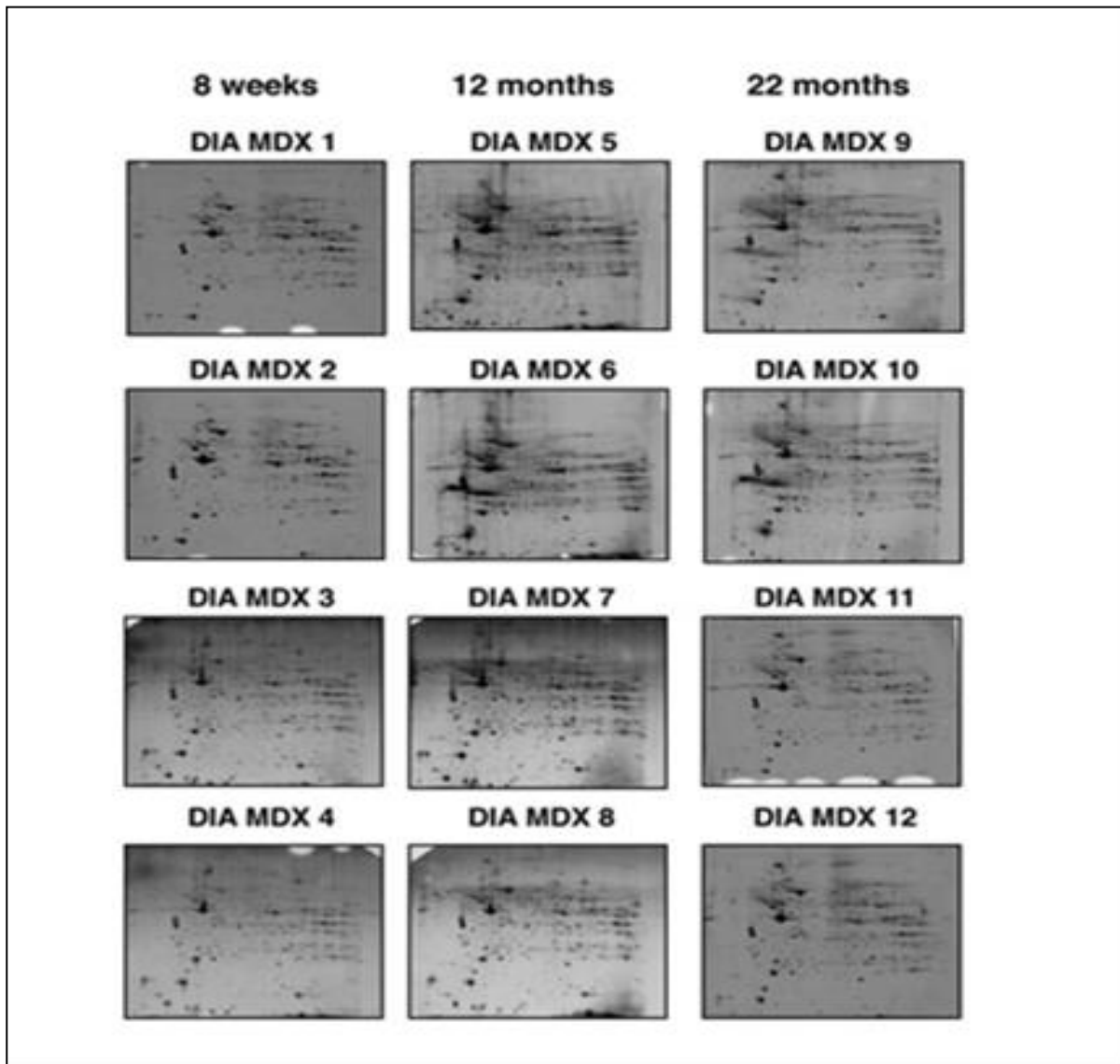


**Figure 4-1 Two-dimensional gel electrophoretic analysis of aging *mdx* mouse diaphragm muscle**

Shown are RuBPs-stained gels from 8 week (DIA MDX 1-4), 12 month (DIA MDX 5-8) and 22 month (DIA MDX 9-12) old diaphragm muscle extracts. Fluorescent images are shown along the pH 3-10 range.

### 4.2.3 RuBPs analysis of dystrophic diaphragm muscle

The overall degree of diaphragm proteins with significantly altered expression levels in age-related dystrophic *mdx* tissue was striking. Proteins with significant changes in expression levels are numbered 1 to 11 and marked by circles in the master gel Figure 4-2. The mass spectrometric identification of these altered muscle proteins is listed in Table 4-1. This table contains the identified muscle-associated proteins names, international accession number, relative molecular masses, *pI*-values, number of matched peptide sequences, Mascot scores, percentage sequence coverage, and fold-change of individual muscle proteins affected in aged dystrophic *mdx* diaphragm.

Protein species with an altered concentration in aged *mdx* diaphragm muscle ranged from a molecular mass of 20 kDa ( $\alpha$ B-crystallin) to 110 kDa (collagen) and with a *pI*-range from 4.7 *pI* (dermatopontin) to 8.6 *pI* (myozenin). The expression levels showed an increased abundance for the collagen  $\alpha$ -1(VI) chain (spot 1), the dermatopontin extracellular matrix protein (spot 2), the ubiquitin carboxyl-terminal hydrolase enzyme (spot 3), the  $\alpha$ B-crystallin small heat shock protein (spot 4),  $\alpha$ -2 actinin (spot 5), the ferritin heavy chain (spot 6), vimentin (spot 7), the fibrinogen  $\gamma$  chain (spot 8) mimecan (spot 9) and apolipoprotein E (spot 10). While the expression level of myozenin (spot 11) was shown to be decreased in *mdx* aged diaphragm muscle.

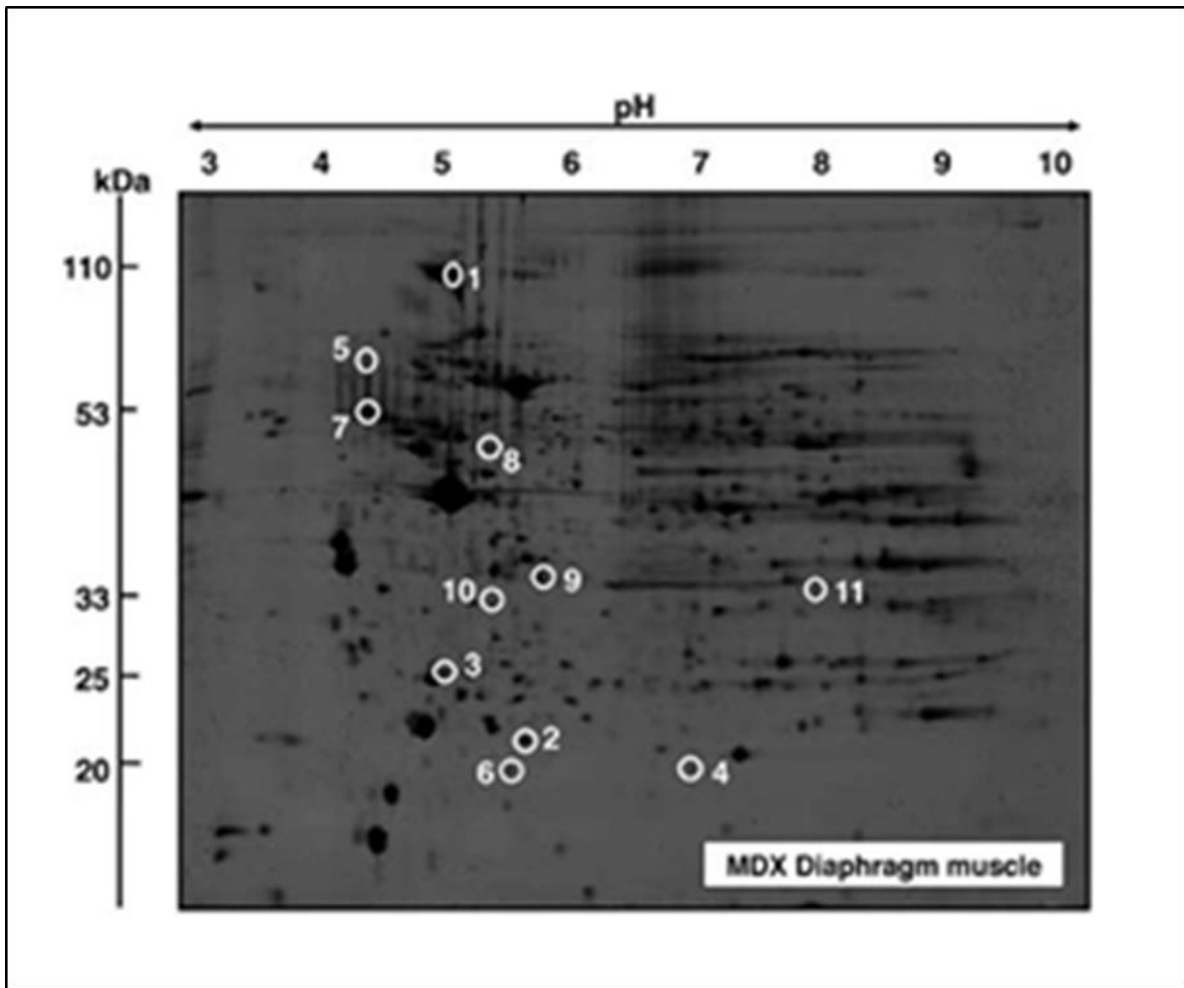


**Figure 4-2 Fluorescence gel electrophoretic analysis of aged *mdx* mouse diaphragm muscle**

Shown is a representative RuBPs-stained master gel with crude tissue extracts from *mdx* diaphragm muscle. Proteins with an age-related change in expression levels are numbered 1 to 11 and marked by circles. See Table 4-1 for the mass spectrometric identification of the individual muscle-associated proteins. The pH-values of the first dimension and molecular mass standards of the second dimension are shown on the top and on the left of the panels, respectively.

**Table 4.1 List of identified muscle proteins with a significant change of abundance in aging *mdx* diaphragm muscle**

<b>Spot No.</b>	<b>Protein Name</b>	<b>Accession No.</b>	<b>Isoelectric point (pI)</b>	<b>Molecular mass (Da)</b>	<b>Number of peptides</b>	<b>Coverage (%)</b>	<b>Mascot Score</b>	<b>Fold Change 8w-12m MDX</b>	<b>Fold Change 8w-22m MDX</b>
1	Collagen $\alpha$ -1(VI) chain	NP034063	5.20	109,582	12	15	259	3.6	6.3
2	Dermatopontin	NP062733	4.70	24,559	4	21	122	5.4	6.1
3	Ubiquitin carboxyl-terminal hydrolase enzyme	AAD51029	5.33	25,170	4	30	83	3.5	4.1
4	$\alpha$ B-crystallin	NP034094	6.76	20,056	7	38	113	3.7	4
5	$\alpha$ -2 actinin	AAK64510	5.34	104,447	4	5	196	4.3	3.6
6	Ferritin heavy chain	NP034369	5.53	21,227	3	18	50	2.6	2.6
7	Vimentin	CAA39807	5.06	53,747	14	37	140	2.5	2.5
8	Fibrinogen $\gamma$ chain	NP598623	5.54	50,056	4	12	65	1.9	2.5
9	Mimecan	NP032786	5.52	34,339	5	19	293	1.8	2.2
10	Apolipoprotein E	AAA37252	5.82	33,206	8	32	169	2	1.5
11	Myozenin-1	NP067483	8.57	31,438	9	54	174	3	-3.6

#### 4.2.4 Comparative proteomic analysis of *mdx* versus wild-type diaphragm muscle

In order to establish the extent of secondary changes in the senescent *mdx* mouse diaphragm proteome due to absence in the membrane cytoskeletal dystrophin protein, the urea-soluble protein complement from 22 month-old wild type versus age-matched dystrophic diaphragm mouse muscle was investigated. Following fluorescent labelling of wild type or *mdx* samples with the CyDyes Cy3, as well as fluor tagging of the pooled standard using the CyDye Cy5, high-resolution two-dimensional gel electrophoresis was carried out to separate the proteome from aged dystrophic *mdx* diaphragm muscle.

A pH-range of 3-11NL in the first dimension was employed to establish a global proteomic pattern. Detailed densitometric analysis was carried out using a Typhoon Trio variable imager scanner and Samespot Progenesis 2-D analysis software was performed to establish differential expression patterns of the aged muscle. Figure 4-3 shows the 2-D DIGE analysis of 22 month-old dystrophic *mdx* versus aged-matched normal diaphragm skeletal muscle with 4 biological repeats.

Panels labelled (MDX 1-4) and (WT 1-4) represent the Cy3-labelled gels of total muscle extracts from *mdx* versus normal wild type mice as well as pooled standard Cy5-labelled gels, respectively. DIGE images are shown for the pH 3-11NL range. The detailed proteomic profiling of dystrophic diaphragm revealed distinct changes in concentration for 84 protein species, with 27 proteins being increased and 57 proteins showing decreased expression in the total *mdx* mouse muscle preparations (Fig 4-4). Mass spectrometry was then used to identify these significant muscle-associated proteins of interest and listed in Table 4-2.

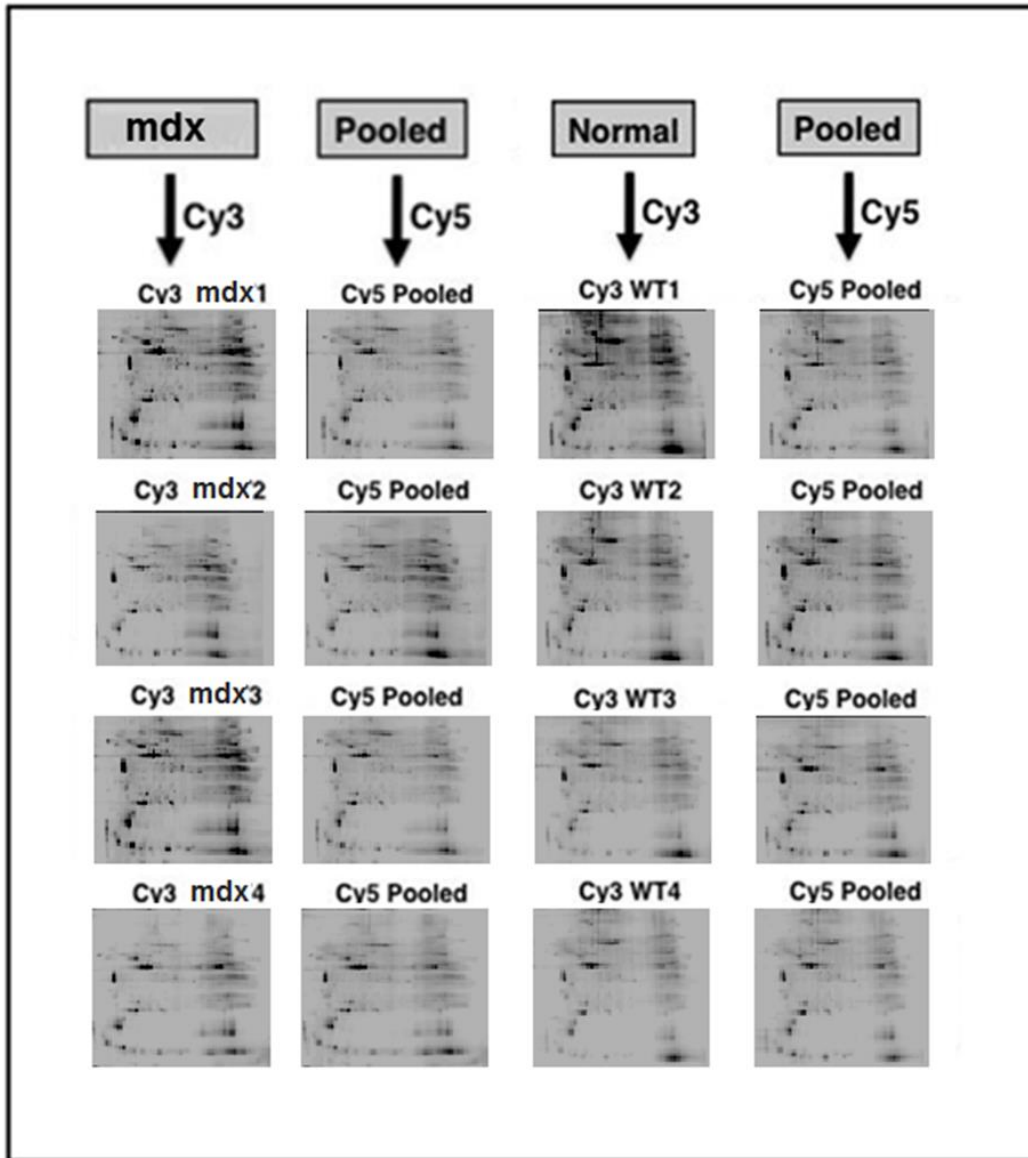


**Figure 4-3 Shown is the 2-D DIGE analysis of dystrophic *mdx* versus normal diaphragm skeletal muscle**

Shown are Cy3-labelled gels of total muscle extracts from *mdx* (MDX1 to MDX4) versus normal wild type (WT1 to WT4) mice, as well as pooled standard Cy5-labelled gels. DIGE images are shown for the pH 3-11NL range.

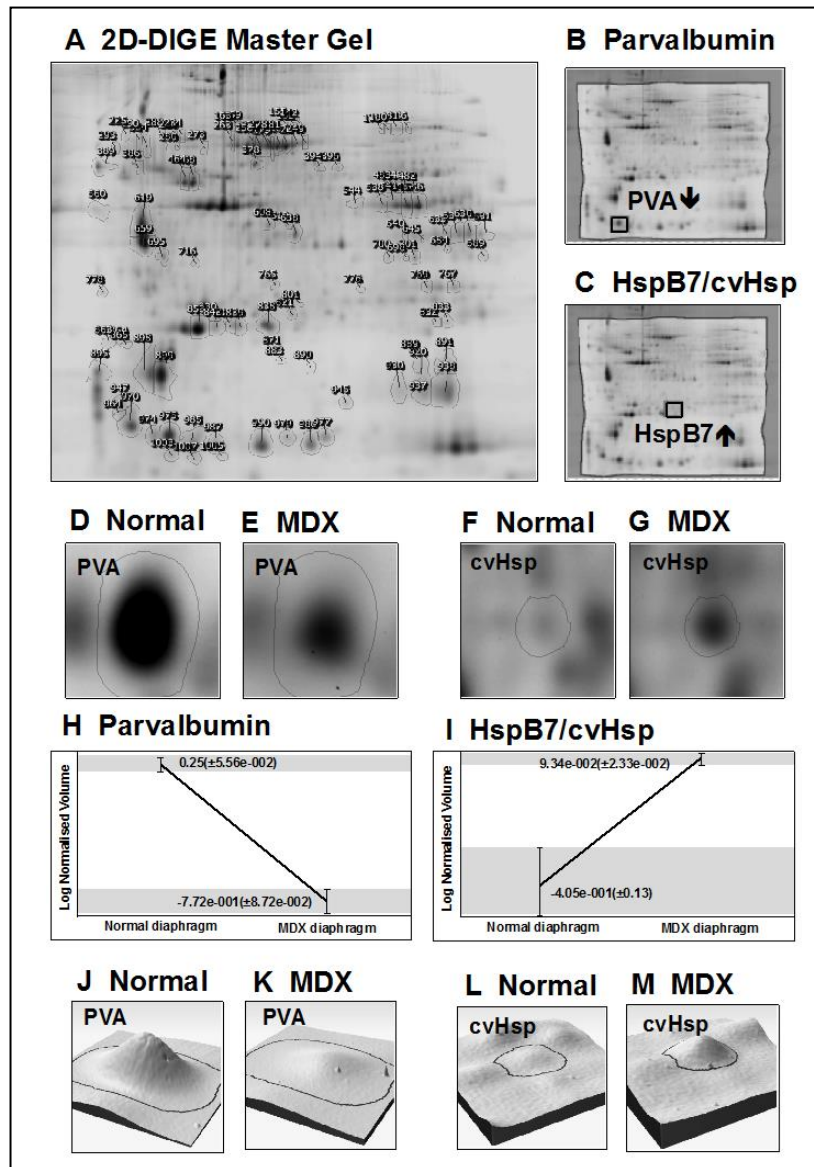


**Figure 4-4 Overview of the standard 2D-DIGE image analysis process used in muscle proteomics**

Shown are a 2D-DIGE master gel of the analysis of normal versus dystrophic aged diaphragm muscle (A), the visualization of the altered levels of parvalbumin (B, D, E) and cvHsp (C, F, G), the range of detected alterations between normal and dystrophic samples (H, I) and the graphical 3D montage of the drastic reduction in parvalbumin (J, K) and increase in expression of cvHsp (L, M) in dystrophic muscle.

#### 4.2.5 DIGE analysis of dystrophic Diaphragm muscle

The overall number and degree of diaphragm proteins with significantly altered expression levels in aged dystrophic *mdx* tissue was drastic with 84 changes. Showing a significant increase in 27 and decrease in 57 proteins in dystrophin-deficient and aged diaphragm. Proteins with significant changes in expression levels are numbered 1 to 84 and marked by circles in the master gel Fig 4-5. The mass spectrometric identification of these altered muscle proteins is listed in Table 4-2. This table contains the identified muscle-associated proteins names, international accession number, relative molecular masses, *p*-values, number of matched peptide sequences, Mascot scores, percentage sequence coverage, and fold-change of individual muscle proteins affected in aged dystrophic *mdx* diaphragm. Protein species with an altered concentration in aged *mdx* diaphragm muscle ranged from a molecular mass of 11.9 kDa (Parvalbumin) to 87.7 kDa (Nebulin fragment) and with a *p*-range from 4.07 *p* (Troponin C) to 9.19 *p* (Nebulin fragment). Identified proteins were involved in various processes from the extracellular matrix, contractile apparatus, ion homeostasis, mitochondrial energy metabolism and the cellular stress response.

The expression levels showed an increased abundance for the extracellular matrix protein dermatopontin (spot 1, 2, 3), the HspB7/cvHsp small heat shock protein (spot 4), the myosin light chain 6B (spot 5), unnamed protein product (spots 7, 17, 26), beta actin (spot 10), Hsp70 heat shock protein cognate (spots 11, 21, 22), mitochondrial stress 70 protein (spots 12, 24), gamma actin smooth muscle (spot 13), nebulin fragment (spot 14), lumican (spot 15), prohibitin protein (spot 16), transferrin (spot 18), annexin A5 (spot 19), Hsp8 heat shock protein (spot 23), Fmod protein (spot 25) and glucose regulated 78 kDa protein (spot 27).

In contrast, a decreased expression level was shown for alpha parvalbumin (spots 29, 80, 84), for various isoforms of malate dehydrogenase (spots 30, 39, 41, 46, 49, 57, 77), ATP-synthase (spots 31, 43, 59, 63), isocitrate dehydrogenase (spot 35),

alpha actin (spot 36), coiled-coil-helix-coiled-coil-helix domain-containing mitochondrial protein 3 (spot 37), Cu/Zn superoxide dismutase (spot 38), peroxiredoxin (spot 40), cytochrome c oxidase (spot 42), Hsp beta-6 heat shock protein (spot 44), creatine kinase (spots 45, 52, 74), troponin C (spots 47, 48), myoglobin (spots 50, 71, 72, 76, 79, 81), FABP3 fatty acid-binding protein (spots 53, 78, 82, 83), NCS-1 calcium-binding protein (spot 54), electron transferring flavoprotein (spots 55, 60), isocitrate dehydrogenase (spot 56), cofilin-2 (spot 61), AK1adenylate kinase (spot 62), MLC2 myosin light chain (spots 65, 73), fumarate hydratase (spot 66), ubiquinone biosynthesis COQ9 protein (spot 68) and calsequestrin (spot 69).

A number of proteins with differential expression patterns were identified as tropomyosin beta chain, myosin light chain 1/3 and the alpha-fetoprotein. Individual 2D protein spots representing the tropomyosin beta chain isoforms exhibited both increased (spots 6, 9) and decreased (spots 32, 64) levels. In the case of the myosin light chain 1/3 1f muscle isoform, both increased (spot 8) and decreased (spots 28, 51, 67, 75) concentrations were determined. The alpha-fetoprotein was shown to be increased (spot 20) and decreased (spot 33) in concentration. Although spots 12, 50, 54, 72 were only had 1 matched peptide, they were included in Table 4-2 based on their mascot scores of 57, 61, 48, 59, respectively. All other proteins species were identified by at least 2 peptides or more.

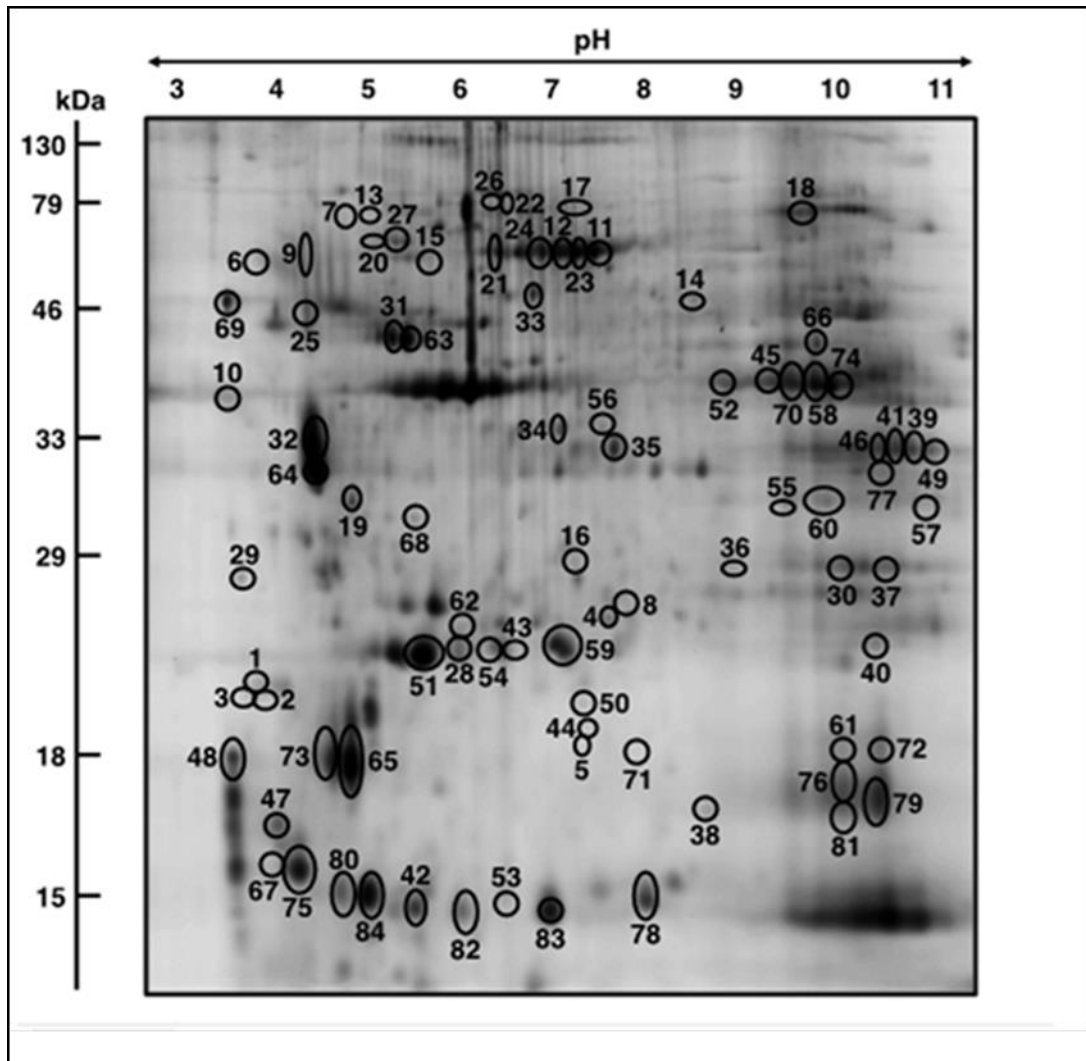


**Figure 4-5 Fluorescence 2D-DIGE master gel of aged *mdx* diaphragm muscle**

Shown is a representative DIGE master gel of aged *mdx* diaphragm muscle. Proteins with a significant change in expression levels are numbered 1 to 84 and marked by circles. See Table 4-2 for the mass spectrometric identification of the individual muscle-associated proteins. The pH-values of the first dimension and molecular mass standards of the second dimension are shown on the top and on the left of the panels, respectively.

**Table 4.2 List of identified proteins from 2D-DIGE analyses that exhibit a drastic change in abundance in the aged *mdx* diaphragm**

Spot No.	Protein Name	Accession No.	Isoelectric point (pI)	Molecular mass (Da)	Number of peptides	Coverage (%)	Mascot Score	Fold Change 22m WT v MDX
1	Dermatopontin	NP_062733	4.7	24,559	5	28	73	5.9
2	Dermatopontin	NP_062733	4.7	24,559	7	37	111	4.4
3	Dermatopontin	NP_062733	4.7	24,559	6	26	100	3.4
4	Heat shock protein HspB7 (beta7, cvHsp)	NP_038896	5.95	18,681	5	38	87	3.3
5	Myosin light chain 6B	NP_758463	5.41	22,851	14	74	181	3.1
6	Tropomyosin, beta chain isoform 1	NP_033442	4.66	32,933	22	61	319	2.9
7	Unnamed protein product	BAE35818	5.78	70,776	15	30	286	2.8
8	Myosin light chain 1/3, isoform 1f, muscle	NP_067260	4.98	20,697	2	12	97	2.7
9	Tropomyosin, beta chain isoform 1	NP_033442	4.66	32,933	11	35	107	2.7
10	Actin, beta (aa 27–375)	CAA27396	5.78	39,451	9	21	124	2.6
11	Heat shock protein Hsp70 cognate	AAA37869	5.37	71,025	11	23	110	2.6
12	Mitochondrial stress-70 protein	BAA04493	5.91	73,773	1	1	57	2.6
13	Actin, gamma, smooth muscle	AAC52237	5.36	43,258	5	16	81	2.6

14	Nebulin (fragment)	AAF59979	9.19	87,694	4	7	53	2.5
15	Lumican	AAB35361	5.84	38,733	2	5	103	2.4
16	Prohibitin	NP_032857	5.57	29,860	15	69	350	2.4
17	Unnamed protein product	BAC34145	5.75	70,766	8	14	129	2.4
18	Transferrin	AAL34533	6.92	78,832	19	24	168	2.3
19	Annexin A5	NP_033803	4.83	35,788	16	45	249	2.3
20	Alpha-fetoprotein	AAA37190	5.47	48,819	2	6	112	2.2
21	Heat shock protein Hsp70 cognate	AAA37869	5.37	71,025	11	23	110	2.2
22	Heat shock protein Hsp70 cognate	AAA37869	5.37	71,025	4	6	77	2.2
23	Heat shock protein 8	AAH66191	5.28	71,060	11	23	110	2.2
24	Mitochondrial stress-70 protein	BAA04493	5.91	73,773	5	9	71	2.1
25	Fmod protein	AAH52673	5.56	46,637	2	4	92	2.1
26	Unnamed protein product	BAC34145	5.75	70,766	8	17	254	2.1
27	78 kDa glucose-regulated protein	BAA11462	5.09	72,528	7	15	112	2.0
28	Myosin light chain 1/3, isoform 1f, muscle	NP_067260	4.98	20,697	15	63	222	-2.0
29	Parvalbumin, alpha	NP_038673	5.02	11,923	6	57	156	-2.0
30	Malate dehydrogenase	AAA39509	8.93	36,052	3	11	90	-2.1
32	Tropomyosin, beta chain	gi 11875203	4.66	32,933	11	32	180	-2.1
33	Alpha-fetoprotein	AAA37190	5.47	48,819	2	5	95	-2.1

34	Isocitrate dehydrogenase subunit alpha	NP_083849	6.27	40,077	6	20	242	-2.1
35	L-lactate dehydrogenase B chain	NP_032518	5.7	36,839	5	12	54	-2.1
36	Actin, alpha, cardiac	gi 387090	5.23	42,048	2	7	51	-2.1
37	Coiled-coil-helix-coiled-coil-helix domain-containing protein 3, mitochondrial	NP_079612	8.56	26,550	5	24	80	-2.1
38	Cu/Zn superoxide dismutase	1513495A	6.03	15,926	5	41	147	-2.1
39	Malate dehydrogenase mitochondrial	NP_032643	8.93	36,053	12	45	256	-2.1
40	Peroxiredoxin Prdx1	NP_035164	8.26	22,394	11	47	97	-2.1
41	Malate dehydrogenase mitochondrial	NP_032643	8.93	36,053	15	56	343	-2.1
42	Cytochrome c oxidase, subunit Va	CAA34085	6.08	16,252	8	48	125	-2.2
43	ATP synthase, mitochondrial F0 complex	AAH16547	5.52	18,810	5	47	148	-2.2
44	Heat shock protein Hsp beta-6	NP_001012401	5.64	17,568	6	51	130	-2.2
45	Creatine kinase, M-type	NP_031736	6.58	43,250	9	27	276	-2.2

46	Malate dehydrogenasemitochondrial	NP_032643	8.93	36,053	9	36	243	-2.2
47	Troponin C, skeletal muscle	NP_033420	4.07	18,156	3	28	238	-2.2
48	Troponin C, skeletal muscle	NP_033420	4.07	18,156	8	53	774	-2.3
49	Malate dehydrogenase 2, mitochondrial	ABD77283	7.7	32,121	7	28	365	-2.3
50	Myoglobin	NP_038621	7.07	17,117	1	9	61	-2.3
51	Myosin light chain 1/3, isoform 1f, muscle	NP_067260	4.98	20,697	4	17	93	-2.3
52	Creatine kinase, M-type	NP_031736	6.58	43,250	10	28	297	-2.3
53	Fatty acid-binding protein FABP3	NP_034304	6.11	14,810	6	48	157	-2.3
54	Calcium-binding protein NCS-1-like	XP_003945963	6.49	12,957	1	17	48	-2.4
55	Electron transferring flavoprotein, alpha	AAH03432	8.62	35,366	11	44	449	-2.4
56	Isocitrate dehydrogenase subunit alpha	NP_083849	6.27	40,077	6	19	167	-2.4
57	Malate dehydrogenase 2, mitochondrial	ABD77283	7.7	32,121	2	8	85	-2.4
58	Creatine kinase, M-type	NP_031736	6.58	43,250	11	33	404	-2.4

59	ATP synthase, subunit d, mitochondrial	NP_082138	5.52	18,796	11	70	168	-2.4
60	Electron transfer flavoprotein, subunit alpha	NP_663590	8.62	35,336	8	39	195	-2.5
61	Cofilin-2	NP_031714	7.66	18,814	5	36	158	-2.5
62	Adenylate kinase, isoenzyme AK1	NP_067490	5.7	23,334	6	36	104	-2.5
63	ATP synthase, beta-subunit	AAB86421	5.14	56,344	6	16	301	-2.6
64	Tropomyosin, beta chain	gi 11875203	4.66	32,920	10	25	129	-2.6
65	Myosin light chain MLC2, skeletal muscle	NP_058034	4.82	19,059	2	8	93	-2.7
66	Fumarate hydratase 1	AAH06048	9.12	54,568	6	17	173	-2.8
67	Myosin light chain 1/3, isoform 1f, muscle	NP_067260	4.98	20,697	11	53	201	-2.9
68	Ubiquinone biosynthesis protein COQ9	NP_080728	5.6	35,235	5	21	150	-3.0
69	Calsequestrin, skeletal muscle	AAC63616	3.93	45,619	8	22	143	-3.1
70	Creatine kinase, M-type	NP_031736	6.58	43,250	10	31	505	-3.1
71	Myoglobin	NP_038621	7.07	17,117	6	48	124	-3.1
72	Myoglobin	NP_038621	7.07	17,117	1	11	59	-3.2
73	Myosin light chain MLC2, skeletal muscle	NP_058034	4.82	19,059	15	68	267	-3.4

74	Creatine kinase, M-type	NP_031736	6.58	43,250	11	31	266	-3.5
75	Myosin light chain 1/3, isoform 1f, muscle	NP_067260	4.98	20,697	2	12	87	-3.6
76	Myoglobin	NP_038621	7.07	17,117	2	21	91	-3.7
77	Malate dehydrogenase	AAA39509	8.93	36,052	5	20	126	-3.7
78	Fatty acid-binding protein FABP3	NP_034304	6.11	14,810	11	77	426	-3.7
79	Myoglobin	NP_038621	7.07	17,117	6	46	129	-4.0
80	Parvalbumin, alpha	NP_038673	5.02	11,923	6	57	285	-4.0
81	Myoglobin	NP_038621	7.07	17,117	6	41	89	-4.3
82	Fatty acid-binding protein FABP3	NP_034304	6.11	14,810	7	63	188	-5.3
83	Fatty acid-binding protein FABP3	NP_034304	6.11	14,810	9	71	532	-5.3
84	Parvalbumin alpha	NP_038673	5.02	11,923	8	57	431	-10.5

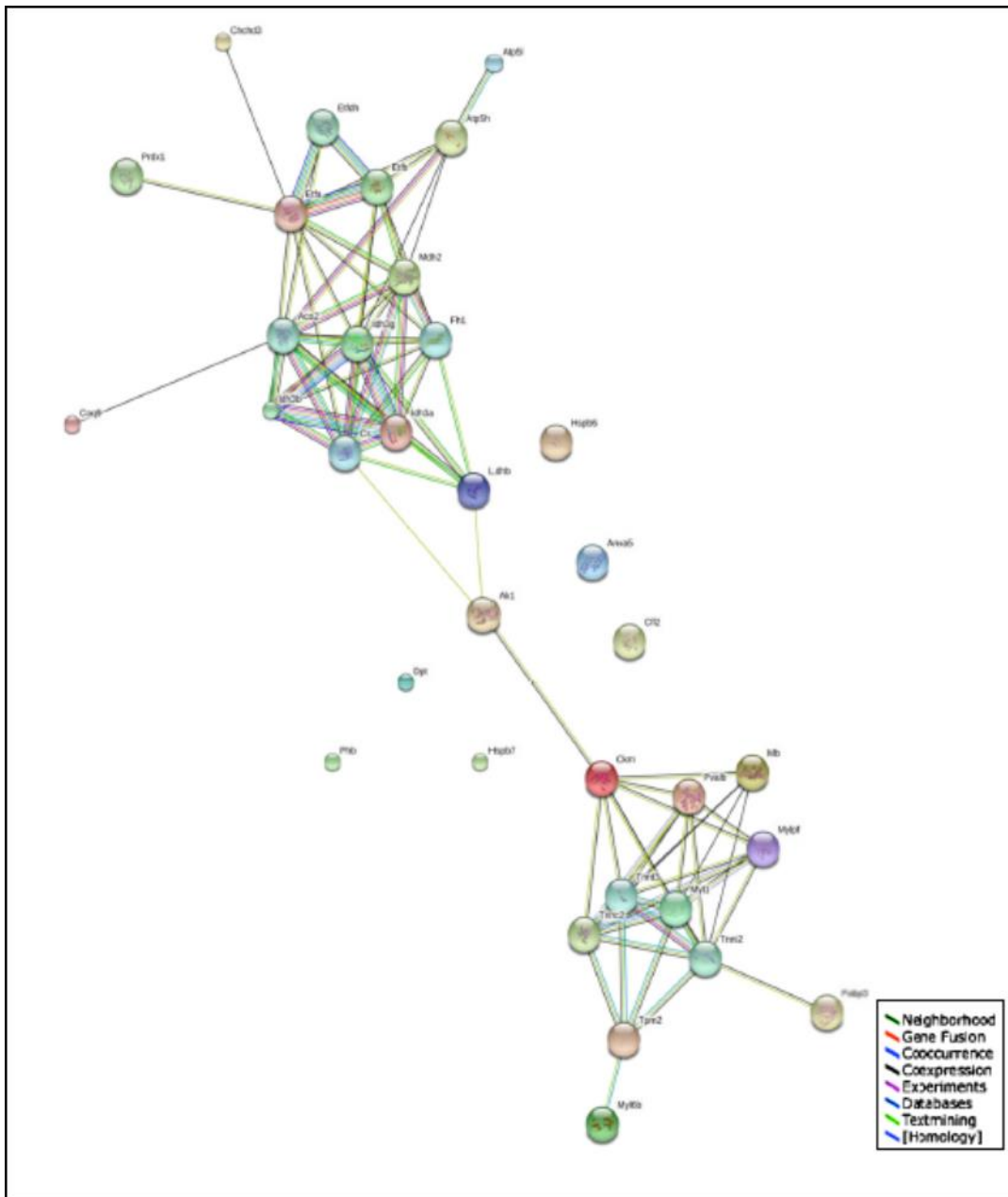


**Figure 4-6 Protein interaction map of *mdx* diaphragm muscle proteins**

The STRING database of known and predicted protein associations (version 9.1) was used to generate a protein interaction map that includes direct physical and indirect functional protein linkages. This analysis was performed with proteins that exhibited a changed abundance in aged *mdx* diaphragm (Table 4.2).

#### 4.2.6 Immunoblot analysis of altered proteins in aged *mdx* diaphragm muscle

In order to further characterise the most drastic changes in aged *mdx* diaphragm as shown by proteomics, comparative immunoblotting was carried out. While laminin expression was shown not to be affected in muscular dystrophy (Fig 4-7B), the dystrophin-associated glycoprotein b-dystroglycan showed a drastic reduction in dystrophic muscle (Fig 4-7C) confirming the mutant status of the *mdx* tissue used in this study. In contrast, the extracellular matrix protein collagen was shown to be increased during the aging process (Fig 4-7A), which agrees with the previous senescent and dystrophic aged *mdx* diaphragm muscle study. This exhibited a general increase of collagen in 12 month and 22 month-old muscle. However, aged dystrophic *mdx* diaphragm muscle showed a significantly higher increase in collagen expression as compared to aged normal muscle.

FigureS 4-7(D-I) shows immunoblot labelling of key proteins with an increased or decreased expression in aged *mdx* diaphragm muscle. Increased markers of the senescent *mdx* diaphragm were verified to be the small heat shock protein  $\alpha$ Hsp, the molecular chaperone Hsp70 and the mitochondrial protein prohibitin figures 4-7D, E and F, respectively. In contrast the cytosolic  $\text{Ca}^{2+}$ - binding  $\alpha$  parvalbumin protein, the luminal  $\text{Ca}^{2+}$ - binding calsequestrin protein of the sarcoplasmic reticulum and mitochondrial ATP synthase figures 4-7G, H and I, respectively were shown to be decreased markers of senescent *mdx* diaphragm. The immunoblot of calsequestrin showed besides the major 60kDa band of its monomer there are also several high molecular mass bands that represent calsequestrin-like proteins. All bands labelled by antibodies to calsequestrin showed a reduced abundance in the dystrophic diaphragm.

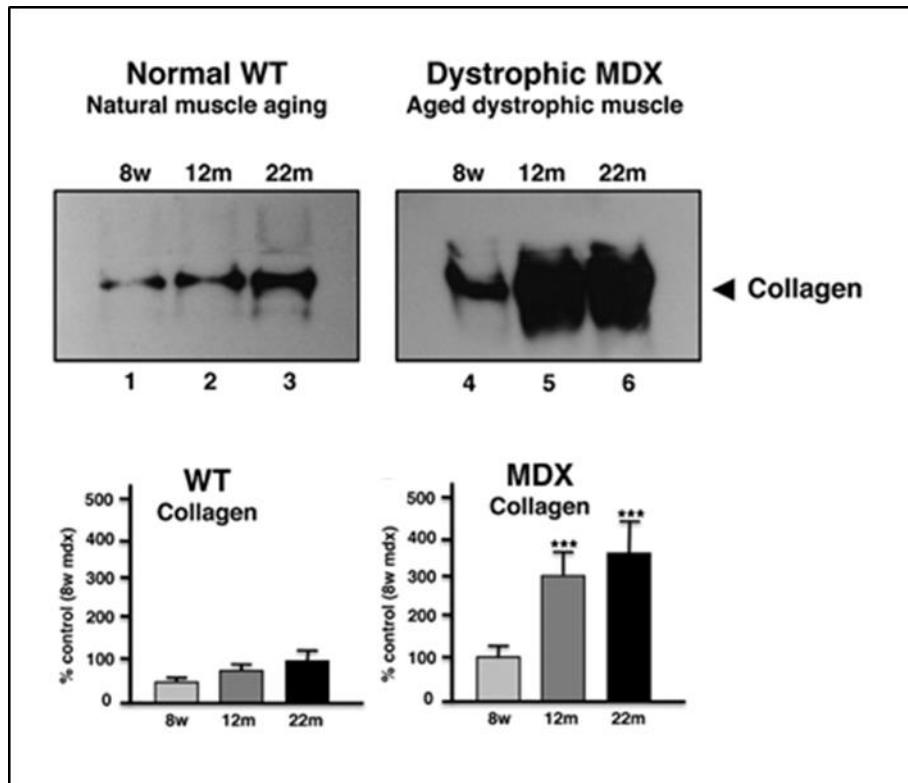


**Figure 4-7A Immunoblotting analysis of extracellular matrix protein collagen**

Shown are representative blots with expanded views of immuno-decorated protein bands indicated by the arrowheads, with graphical presentation of the statistical evaluation. Immunoblots were labelled with the collagen antibody. Lanes 1-3 and 4-6 represent 8 week, 12 month and 22 month-old normal wild type vs dystrophic *mdx* diaphragm muscle, respectively. The comparative blotting was statistically verified using an unpaired Student's *t*-test (n=4 replicates). Standard deviation represented by Error bars, (\*\*\*) $p < 0.001$ ).

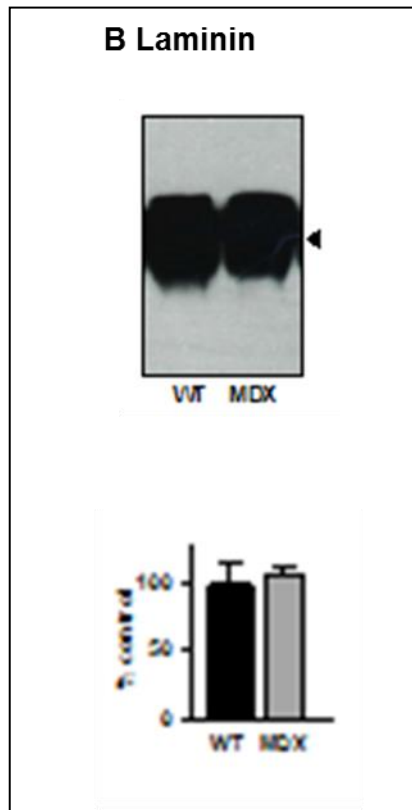


**Figure 4-7B Immunoblotting analysis of unchanged extracellular matrix laminin**

Shown are representative blots with expanded views of immuno-decorated protein bands indicated by the arrowhead, with graphical presentation of the statistical evaluation. Immunoblots were labelled with the laminin antibody. Lanes 1, 2 represent 22 month-old normal wild type vs dystrophic *mdx* diaphragm muscle, respectively. The comparative blotting was statistically verified using an unpaired Student's *t*-test (n=4 replicates).

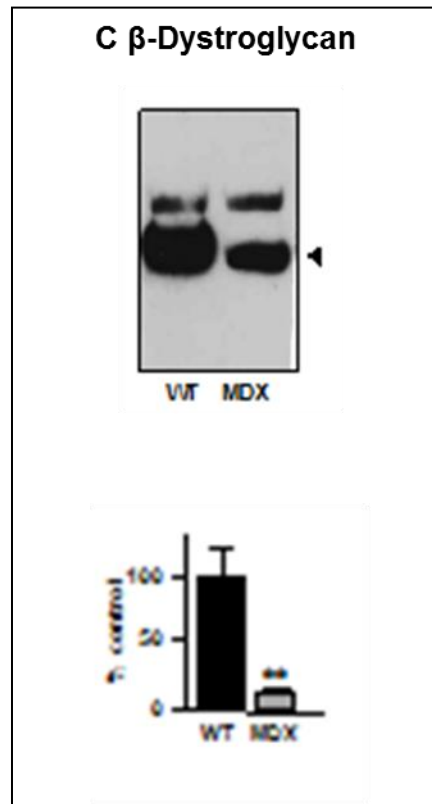


**Figure 4-7C Immunoblotting analysis of of dystrophin-associated glycoprotein  $\beta$ -dystroglycan**

Shown are representative blots with expanded views of immuno-decorated protein bands indicated by the arrowhead, with graphical presentation of the statistical evaluation. Immunoblots were labelled with the dystrophin-associated glycoprotein  $\beta$ -dystroglycan antibody. Lanes 1, 2 represent 22 month-old normal wild type vs dystrophic *mdx* diaphragm muscle, respectively. The comparative blotting was statistically verified using an unpaired Student's *t*-test ( $n=4$  replicates). Standard deviation represented by Error bars, (\*\* $p<0.005$ ).

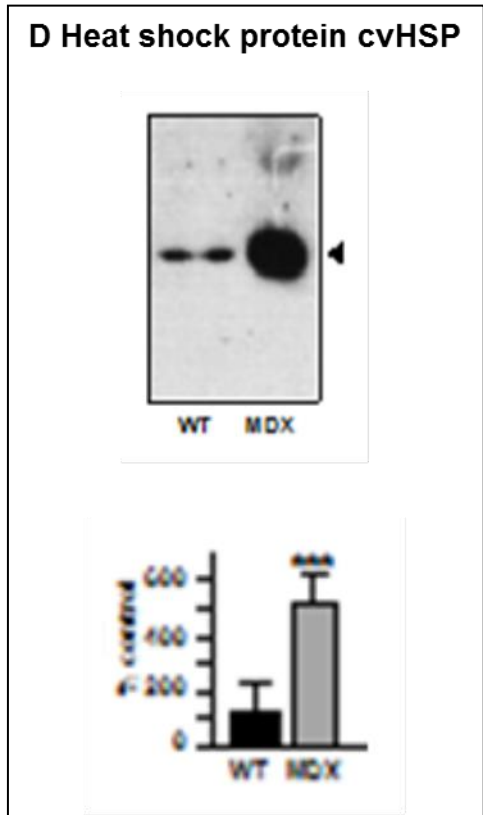


**Figure 4-7D Immunoblotting analysis of small heat shock protein cvHSP**

Shown are representative blots with expanded views of immuno-decorated protein bands indicated by the arrowhead, with graphical presentation of the statistical evaluation. Immunoblot analysis of novel biomarker proteins in normal versus aged *mdx* diaphragm muscle. Immunoblots were labelled with the cvHSP antibody. Lanes 1, 2 represent 22 month-old normal wild type vs dystrophic *mdx* diaphragm muscle, respectively. The comparative blotting was statistically verified using an unpaired Student's *t*-test (n=4 replicates). Standard deviation represented by Error bars, (\*\*\*) $p < 0.001$ ).

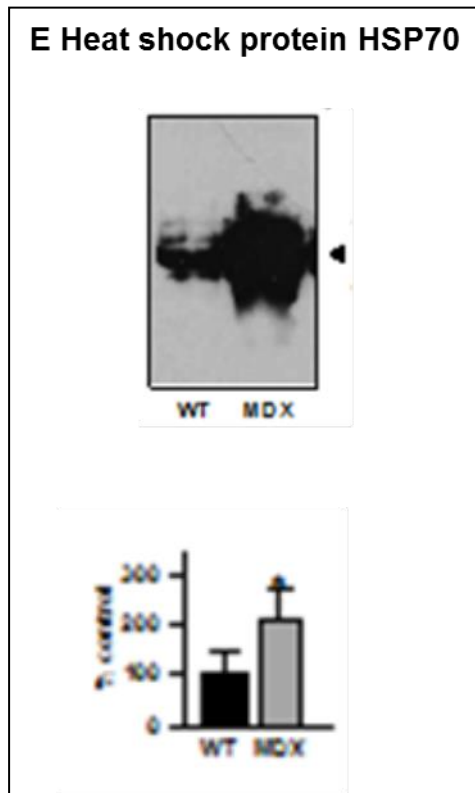


**Figure 4-7E Immunoblotting analysis of large heat shock protein 70**

Shown are representative blots with expanded views of immuno-decorated protein bands indicated by the arrowhead, with graphical presentation of the statistical evaluation. Immunoblot analysis of novel biomarker proteins in normal versus aged *mdx* diaphragm muscle. Immunoblots were labelled with the Hsp70 antibody. Lanes 1, 2 represent 22 month-old normal wild type vs dystrophic *mdx* diaphragm muscle, respectively. The comparative blotting was statistically verified using an unpaired Student's *t*-test (n=4 replicates). Standard deviation represented by Error bars, (\* $p < 0.05$ ).

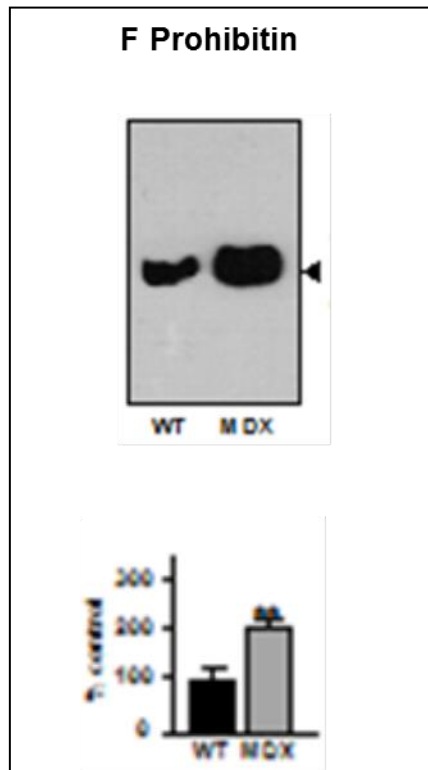


**Figure 4-7F Immunoblotting analysis of prohibitin protein**

Shown are representative blots with expanded views of immuno-decorated protein bands indicated by the arrowhead, with graphical presentation of the statistical evaluation. Immunoblot analysis of novel biomarker proteins in normal versus aged *mdx* diaphragm muscle. Immunoblots were labelled with the prohibitin antibody. Lanes 1, 2 represent 22 month-old normal wild type vs dystrophic *mdx* diaphragm muscle, respectively. The comparative blotting was statistically verified using an unpaired Student's *t*-test (n=4 replicates). Standard deviation represented by Error bars, (\*\*p<0.005).

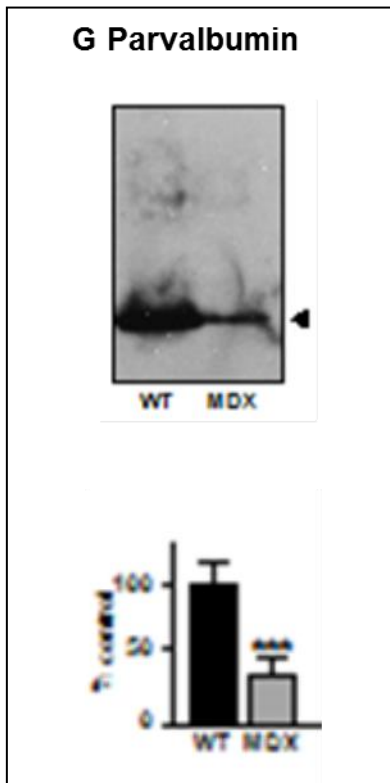


**Figure 4-7G Immunoblotting analysis of calcium-binding protein parvalbumin**

Shown are representative blots with expanded views of immuno-decorated protein bands indicated by the arrowhead, with graphical presentation of the statistical evaluation. Immunoblot analysis of novel biomarker proteins in normal versus aged *mdx* diaphragm muscle. Immunoblots were labelled with the parvalbumin antibody. Lanes 1, 2 represent 22 month-old normal wild type vs dystrophic *mdx* diaphragm muscle, respectively. The comparative blotting was statistically verified using an unpaired Student's *t*-test (n=4 replicates). Standard deviation represented by Error bars, (\*\*\*) $p < 0.001$ ).

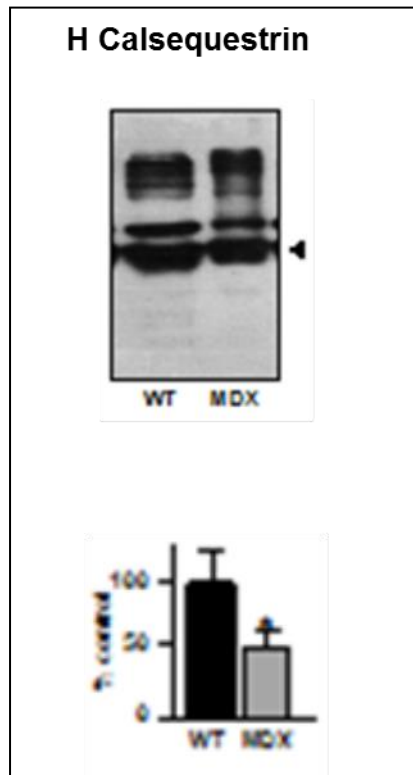


**Figure 4-7H Immunoblotting analysis of the luminal  $\text{Ca}^{2+}$ -binding protein calsequestrin**

Shown are representative blots with expanded views of immuno-decorated protein bands indicated by the arrowhead, with graphical presentation of the statistical evaluation. Immunoblot analysis of novel biomarker proteins in normal versus aged *mdx* diaphragm muscle. Immunoblots were labelled with the calsequestrin antibody. Lanes 1, 2 represent 22 month-old normal wild type vs dystrophic *mdx* diaphragm muscle, respectively. The comparative blotting was statistically verified using an unpaired Student's *t*-test ( $n=4$  replicates). Standard deviation represented by Error bars, ( $*p<0.05$ ).

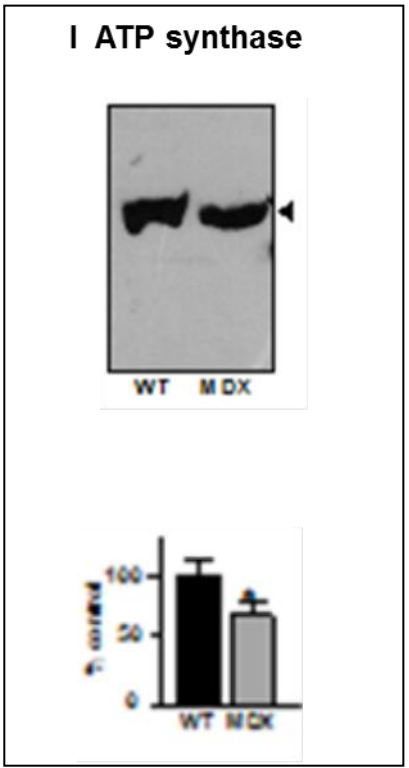


**Figure 4-7I Immunoblotting analysis of mitochondrial enzyme ATP synthase**

Shown are representative blots with expanded views of immuno-decorated protein bands indicated by the arrowhead, with graphical presentation of the statistical evaluation. Immunoblot analysis of novel biomarker proteins in normal versus aged *mdx* diaphragm muscle. Immunoblots were labelled with the mitochondrial ATP synthase antibody. Lanes 1, 2 represent 22 month-old normal wild type vs dystrophic *mdx* diaphragm muscle, respectively. The comparative blotting was statistically verified using an unpaired Student's *t*-test ( $n=4$  replicates). Standard deviation represented by Error bars, ( $*p<0.05$ ).

## 4.3 Discussion

In this chapter, proteomic profiling revealed that during the natural aging of the severely dystrophic *mdx* diaphragm muscles a key number of skeletal muscle proteins change in abundance. Senescent *mdx* muscle has been studied as the dystrophic muscle progressively deteriorates with age and as a result more closely resembles that of the neuromuscular pathology exhibited in Duchenne patients (Lefaucheur et al., 1995).

The age-related pathogenesis of *mdx* mouse muscle is characterised by progressive motor weakness (Lynch et al., 2001), a shortened life span with increased susceptibility to spontaneous rhabdomyosarcoma (Chamberlain et al., 2007), muscle periphery weakening triggered by the presence of branched fibres (Head, 2010), severe loss of myofibres with concomitant replacement by connective tissue (Wineinger et al., 1998; Pastoret and Sebille, 1995a; Pastoret and Sebille, 1995b), a reduction in regenerative potential and changes in the crucial mTOR signaling pathway (Mouisel et al., 2010), and impaired structural and functional recovery after injury (Irintchev et al., 1997). Hence, aged *mdx* muscle represents an appropriate dystrophic phenotype for determining and identifying potential global alterations in the protein complement during aging. This chapter has summarised the results of a comparative proteomic analysis of severely affected *mdx* diaphragm muscle from aging 8 week versus 22 month-old mice as well as a comprehensive aged-matched 22 month-old dystrophic diaphragm versus 22 month-old control mice.

### 4.3.1 Proteomic expression changes of diaphragm analysis during aging

Dystrophic *mdx* diaphragm muscle exhibited changed expression levels in 11 protein species during skeletal muscle aging. Alterations in the aging *mdx*

diaphragm proteome indicate elevated levels of fibrosis, an increased stress response and an escalation in cytoskeletal elements perhaps compensating the lack of dystrophin. These proteomic results support the idea of more extensively perturbed protein concentrations in dystrophin-deficient *mdx* diaphragm tissue as compared to other *mdx* muscle subtypes (Lewis et al., 2009).

#### 4.3.2 Increased extracellular matrix proteins in aging *mdx* tissue

The approximately 6-fold increase of collagen and dermatopontin in aging *mdx* diaphragm muscle are key proteomic findings and reveal the dystrophic status of this muscle type. Immunoblotting analysis clearly shows the dramatic increase of collagen in the *mdx* diaphragm supporting the mass spectrometric results in table 4-1 and 4-2. While it is known that collagen levels are elevated in the extracellular matrix of the skeletal muscle during the natural aging process (Kragstrup et al., 2011), the *mdx* dystrophic phenotype demonstrates an intensified age-related increase of collagen  $\alpha$ -1(VI) chain. Collagen is the key protein component of connective tissue and is particularly enriched in the endomysium of the skeletal muscles. Previous studies have highlighted increase amounts of mRNA in the *mdx* diaphragm (Goldspink et al., 1994), which agrees with the elevated collagen protein levels and supports the notion of severe fibrosis in the *mdx* tissue (Graham et al., 2010; Trenz et al., 2010)

Dermatopontin the non-collagenous extracellular matrix protein plays a role in matrix assembly and cell-matrix interactions (Okamoto and Fujiwara, 2006) and also known as tyrosine-rich acidic matrix protein (TRAMP) (Forbes et al., 1994)). TRAMP seems to regulate interactions of transforming growth factor beta (TGF- $\beta$ ), fibronectin and decorin (Kato et al., 2011). Its increased abundance in *mdx* diaphragm is possibly due to greater demands for collagen matrix organisation within the dystrophic muscle tissues.

### 4.3.3 Perturbed stress response and cytoskeletal disruption in aging *mdx* tissue

The increased levels of  $\alpha$ B-crystallin and vimentin suggests an intensified cellular stress response and an up-regulation of cytoskeletal elements in *mdx* dystrophic muscle, respectively, which supports previous proteomic reports (Doran et al., 2006a).

### 4.3.4 Other proteins

Increased concentrations of fibrinogen protein in aged *mdx* diaphragm, as indicated by proteomics, agree with a previous report (Vidal et al., 2008). Fibrinogen appears to play a crucial role in fibrosis through a TGF- $\beta$  or alternative macrophage activation pathway in dystrophinopathy.

### 4.3.5 Proteomic expression changes of aged diaphragm analysis

The comparative proteomic analysis of the naturally aged diaphragm versus dystrophin-deficient *mdx* diaphragm shown here establishes that the fluorescence difference in-gel electrophoresis with optimised animal model proteomics can be important for the identification of new protein biomarkers candidates involved in the molecular pathogenesis of dystrophinopathy. Figure 14 illustrates an overview of the proteomic results from the senescent *mdx* mouse model survey for Duchenne muscular dystrophy.

Global changes in structural proteins, extracellular proteins, contractile proteins, molecular chaperones, calcium-binding proteins, glycolytic enzymes, mitochondrial enzymes and metabolite transporters suggest changes in the cytoskeletal complex and its indirect linkage to the extracellular matrix, reorganisations within the

actomyosin apparatus, an intensified cellular stress response, compromised ion handling and metabolic disturbances. Overall, this analysis revealed that protein expression patterns are severely changed in the dystrophin-deficient *mdx* diaphragm muscle and that these pathobiochemical alterations are more intense as compared to that of the *mdx* hind limb muscles examined in this thesis (Rayavarapu et al., 2013; Ge et al., 2003; Carberry et al., 2012b).

#### 4.3.6 Increased extracellular matrix proteins in aged *mdx* tissue

Elevated levels of dermatopontin and the resulting increase in collagen, as indicated here by proteomics and immunoblotting, respectively, supports the initial RuBPs aging survey of increased connective tissue in the dystrophic *mdx* diaphragm (Carberry et al., 2012a).

#### 4.3.7 Perturbed stress response in aged *mdx* tissue

Increased levels of fibrosis appear to be accompanied by an intensified cellular stress response with the up-regulation of various heat shock proteins. In the form of several isoforms of Hsp70 and the muscle-specific molecular chaperone cvHsp, this supports the general principle of severe cellular stress in dystrophinopathy (Carberry et al., 2013a). The various isoforms of Hsp70 play a main role in skeletal muscle stress in response to injury, oxidative conditions, reperfusion-induced ischemia, excessive exercise and neuromuscular disorders (Liu et al., 2006).

During periods of muscle stress molecular chaperone regulation has been shown to be crucial in protecting muscle from damage (Maglara et al., 2003). In general, stress proteins facilitate in protein-protein interactions by helping to stabilise misfolded proteins or peptide clusters as well as regulating their degradation and elimination in

order to prevent harmful unwanted accumulation of non-functional protein aggregates (Boluyt et al., 2006). Hence, the observed increase in expression of mitochondrial Hsp70 isoforms can be seen as a compensatory mechanism to protect dystrophic fibres from excessive oxidative stress and supporting previous reports on elevated levels of the small heat shock protein  $\alpha$ Hsp in dystrophic skeletal muscle (Doran et al., 2006a).

#### 4.3.8 Increased expression of Iron handling proteins in aged *mdx* tissue

The 2-fold increase in transferrin concentration suggests fluctuations in iron absorption and use in muscular dystrophy. Since circulating transferrin acts as an iron transporter delivering needed iron to tissue proteins (Wang and Pantopoulos, 2011), the elevated abundance suggests impaired iron homeostasis in the degenerating *mdx* diaphragm muscle. During the aging dystrophic diaphragm study which investigated 8-week to 22-month range (Carberry et al., 2012a), we also examined the 8-week to 12-month range and recorded a drastic increase in ferritin light chain levels in *mdx* muscle. Deficiency in dystrophin seems to impair iron homeostasis and the elevated iron transporter and binding-protein concentrations possibly suggest a compensatory mechanism to help prevent harmful iron overloading in muscle tissues.

#### 4.3.9 Reduced mitochondrial enzymes in aged *mdx* tissue

Previous reports have shown that skeletal muscles from the dystrophin-deficient *mdx* mouse exhibit disturbed mitochondrial metabolism leading to decreased intramuscular ATP concentrations. Mitochondrial abnormalities consist of the pathophysiological uncoupling of oxidative phosphorylation and the resulting reduction in maximal ATP synthesis capacity (Kuznetsov et al., 1998) and a

disturbance of the subsarcolemmal localisation of mitochondria which leads to metabolic inefficiency and thus limits the maximal generation of ATP (Percival et al., 2013). This bioenergetic dysfunction of mitochondria in the senescent *mdx* diaphragm indicates that aged mitochondria are incapable of meeting the ATP demand of the dystrophic muscle fibres, which agrees with recent proteomic study in aged *mdx* heart (Holland et al., 2013a).

A reduced concentration was shown for essential mitochondrial enzymes, including cytochrome c oxidase, electron transferring flavoprotein, isocitrate dehydrogenase, malate dehydrogenase and ATP synthase. In addition, the proteomic findings of a decreased concentration of the vital and rate-limiting metabolite transporters for the utilisation of oxygen and fatty acids, intracellular oxygen transporter myoglobin and the fatty acid binding protein FABP3, suggest the idea of impaired mitochondrial metabolism.

#### 4.3.10 Other proteins

The contractile apparatus degeneration and/or remodeling, as indicated here with actin, troponins, tropomyosin and myosin light chains, and interestingly, possible compensatory mechanism to stabilise the deteriorated sarcomeric structure was observed with elevated levels of a nebulin fragment perhaps strengthening the nebulin-associated thin filament in dystrophic tissue fibres (Holland and Ohlendieck, 2013).

#### 4.3.11 Predicted interaction patterns of altered proteins in aged *mdx* diaphragm muscle

The STRING database of direct physical and indirect functional protein interactions (Franceschini et al., 2013) was employed to evaluate potential protein networks within the

proteomic data set generated by this study of the aged *mdx* diaphragm. Figure 4-6 shows the result of this bioinformatics analysis, which revealed a relatively complex interaction map. Two large clusters were shown to exist that are linked via adenylate kinase and creatine kinase interactions. Since both proteins were shown to be reduced in dystrophin-deficient fibers, this indicates that more severe downstream effects on various proteins may occur within these apparent protein clusters. The upper protein network consists especially of enzymes involved in mitochondrial metabolism, such as ATP synthase, isocitrate dehydrogenase, aconitase and malate dehydrogenase. The lower protein cluster contains several major contractile elements, including tropomyosin, troponin and myosins. Important ion handling proteins and metabolite transporters are also proposed to interact with these protein complexes.

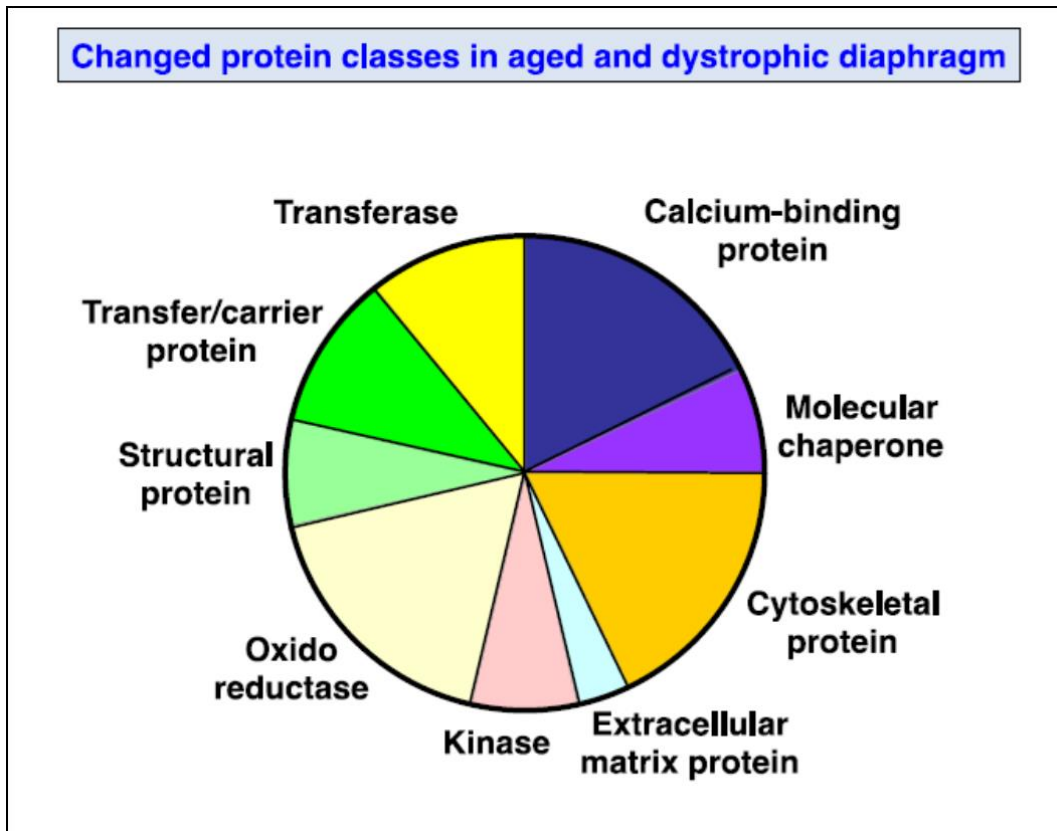


**Figure 4-8 Overview of the molecular function of altered diaphragm-associated proteins**

Shown is the application of the bioinformatics software program PANTHER (database; version 8.1) to identify the clustering of molecular functions of the mass spectrometrically identified proteins with a changed abundance in aged *mdx* diaphragm (Table 4.2). The molecular functions of the identified muscle proteins have been catalogued as being involved in ion homeostasis, the cellular stress response, cytoskeletal stabilization, extracellular matrix organization, structural integrity, metabolic transportation and metabolism. The largest groups of proteins were represented by calcium-binding proteins, cytoskeletal proteins and oxidoreductase. Frequent changes were also observed in molecular chaperones, kinases, structural proteins, transferases and carrier proteins. Relatively small alterations were shown to occur in extracellular matrix proteins.

## 4.4 Conclusion

In recent years, comparative proteomic studies with *mdx* muscle tissue extracts have shown significant alterations in the enzyme adenylate kinase AK1 (Marouga et al., 2005; Ng et al., 2012; Theodoridis et al., 2012), the actin binding protein profilin, the fatty acid binding protein FABP3 (Okamoto and Fujiwara, 2006), the cytosolic Ca<sup>2+</sup>-binding protein parvalbumin (Stastna and van Eyk, 2012), the Ca<sup>2+</sup>-binding protein calsequestrin CSQf (Cox and Mann, 2011), the enzyme carbonic anhydrase CA3 (Carberry et al., 2012b), the molecular chaperone cvHsp/HspB7 (Marouga et al., 2005; Kato et al., 2011), the oxygen carrier myoglobin (Stastna and van Eyk, 2012), different isoforms of annexin (Okamoto and Fujiwara, 2006), the ion transporter transferrin (Forbes et al., 1994; Graham et al., 2010), the mitochondrial enzyme isocitrate dehydrogenase (Kornegay et al., 2012; Stastna and van Eyk, 2012; Mallick and Kuster 2010) and the extracellular matrix protein dermatopontin (Mouisel et al., 2010).

These proteomic profiles of the *mdx* mouse were performed with multiple muscle subtypes, variety of tissue extracts or subcellular fractions, various protein separation techniques, opposing labelling methods and different mass spectrometric techniques. The proteomic results in this chapter has established that the abundance of annexin, carbonic anhydrase CA3, cvHsp, prohibitin, transferrin and dermatopontin is significantly increased and that the concentration of adenylate kinase, calsequestrin, isocitrate dehydrogenase, myoglobin, and parvalbumin is drastically reduced in the aged *mdx* diaphragm model of DMD.

This makes these proteins suitable biomarker candidates of dystrophinopathy, which might be helpful to evaluate diagnostic, prognostic or therapeutic approaches. In conclusion, the proteomic results presented here indicate that the aged *mdx* diaphragm, which shows severe respiratory impairment following fibrosis (Ishizaki et al., 2008), is a suitable model system to study the molecular pathogenesis of Duchenne muscular dystrophy.

## **5 Comparative proteomic profiling of *soleus*, *extensor digitorum longus*, *flexor digitorum brevis* and *interosseus* muscle from the *mdx* mouse model of Duchenne muscular dystrophy**

### 5.1 Introduction

In the *mdx* animal model of dystrophinopathy, different skeletal muscle subtypes are affected to varying degrees resulting from the same single base substitution of the dystrophin gene. Thus, to establish potential muscle subtype-specific alterations in secondary changes due to dystrophin-deficiency, we have performed a comparative proteomic survey of multiple *mdx* muscles. We included those specific skeletal muscles that are frequently used for studying the muscular dystrophy pathomechanism, *soleus*, *extensor digitorum longus*, *flexor digitorum brevis* and *interosseus* muscle.

#### 5.1.1 Duchenne muscular dystrophy and skeletal muscle subtypes

In humans, the corresponding mouse muscle tissue subtypes examined relate to (i) *soleus* (SOL), a muscle of the lower back part of the leg located just below the *gastrocnemius* that contains predominantly oxidative type 1 fibers, (ii) *extensor digitorum longus* (EDL), a muscle lying in the lateral front part of the leg that contains a high number of glycolytic type 2B and 2X fibers, (iii) *flexor digitorum brevis* (FDB), muscles of the foot located in the middle part of the sole and contains a large portion of oxidative-glycolytic type 2A fibers, and (iv) *interosseus* (INT), a muscle of the hand positioned near the metacarpal bones that contains almost exclusively type 2 fibers (Jarmey, 2006; Lieber, 2010; Stal et al., 1987; Staron et al.,

1997). All four muscles have been extensively used to investigate changes of *mdx* muscle structure, physiology, function and biochemistry.

However, each of these different muscle subtypes has strengths and weaknesses with respect to routine biological analyses. While SOL and EDL are ideal to study the biochemistry, force and fatigue in muscle, FDB and INT are suited to study muscles on the single fiber level, as they can be readily enzymatically dissociated into single fibers. Thus, numerous observations on subsarcolemmal  $\text{Ca}^{2+}$  levels,  $\text{Ca}^{2+}$  influx and the function of cation channels have been made with FDB (Boittin et al., 2010; Mallouk et al., 2000; Teichmann et al., 2008) and INT (Mallouk et al., 2000; Pritschow et al., 2011; Tutdibi et al., 1999) without knowing whether these results can be generalised. Thus, we included FDB and INT muscle preparations in this proteomic analyses to evaluate whether they exhibit similar abnormalities as compared to other *mdx* mice limb muscles. While different skeletal muscle subtypes are affected to varying degrees resulting from the same single base substitution of the dystrophin gene these distinct differences in the level of protein perturbation of different muscle subtypes from *mdx* mice are perhaps a result of dissimilar secondary processes in the molecular pathogenesis.

### 5.1.2 Experimental design

Comparative gel-based proteomic analysis of normal versus *mdx* *soleus*, *extensor digitorum longus*, *flexor digitorum brevis* and *interosseus* muscle, the urea-soluble protein complement was prepared from these four muscles from control and dystrophic mice. Muscle protein extracts were separated by two-dimensional gel electrophoresis and labelled with the fluorescent dye ruthenium II tris bathophenanthroline disulfonate. Then proteins with a significant change in their abundance were identified by mass spectrometry. Key proteomic findings were verified by immunoblot analysis. This report describes the analysis of RuBPs labelled normal and dystrophic SOL, EDL, FDB and INT tissue of 3-month-old dystrophin-deficient versus aged-matched wild type (WT) mice across 3-10 pH range.

Proteomic profiling established a change in abundance of 24, 17, 19 and 5 protein species in SOL, EDL FDB and INT muscle, respectively. Identified proteins were involved in various processes from the contraction-relaxation cycle, muscle metabolism, metabolite transport and the cellular stress response.

## 5.2 Results

### 5.2.1 Comparative proteomic analysis of *mdx* versus normal muscle

High-resolution two-dimensional gel electrophoresis was carried out to separate the proteome from normal versus dystrophic *mdx* SOL, EDL, FDB and INT muscle tissues. A pH-range of 3-10 in the first dimension was employed to establish a global proteomic pattern. Followed by post-electrophoretic labelling of the protein spots with fluorescent dye RuBPs, a Typhoon Trio variable imager and Progenesis 2-D analysis software were used to analyse the *mdx* skeletal muscle proteomes. An altered concentration was revealed for 24, 17, 19 and 5 protein species, with 19, 15, 8 and 1 proteins being increased and 5, 2, 9 and 4 proteins showing decreased expression in SOL, EDL, FDB and INT *mdx* tissue, respectively. Mass spectrometry was then used to identify these significant muscle-associated proteins of interest and listed in Tables (5-1 to 5-4).

### 5.2.2 Proteomic analysis of dystrophic skeletal muscle subtypes

Following optimisation, fluorescence high-resolution two-dimensional gel electrophoresis was performed to determine potential differences in protein expression patterns in *mdx* skeletal muscle proteomes. Figure 5-1 shows the total extracts from 3 month old normal wild-type vs dystrophic *mdx* (A) SOL, (B) EDL, (C) FDB and (D) INT muscles. The 32 RuBPs-stained gel images contain four biological repeats of each group of normal wild-type (WT 1-4) versus dystrophic (*MDX* 1-4)

muscle. Fluorescent images are shown along a pH 3-10 range. The overall 2D spot patterns of normal versus dystrophic skeletal muscle subtypes were relatively comparable as a result a detailed denitometric analysis was performed in order to determine potential differences in individual protein species. Densitometric analysis was carried out using a Typhoon Trio variable imager scanner and Samespot Progenesis 2-D analysis software was performed to establish differential expression patterns with the dystrophic muscles. The detailed proteomic profiling of dystrophic subtypes showed distinct changes in 24, 17, 19 and 5 muscle protein species in SOL, EDL FDB and INT tissue respectively, suggesting the INT to be a much milder affected phenotype.

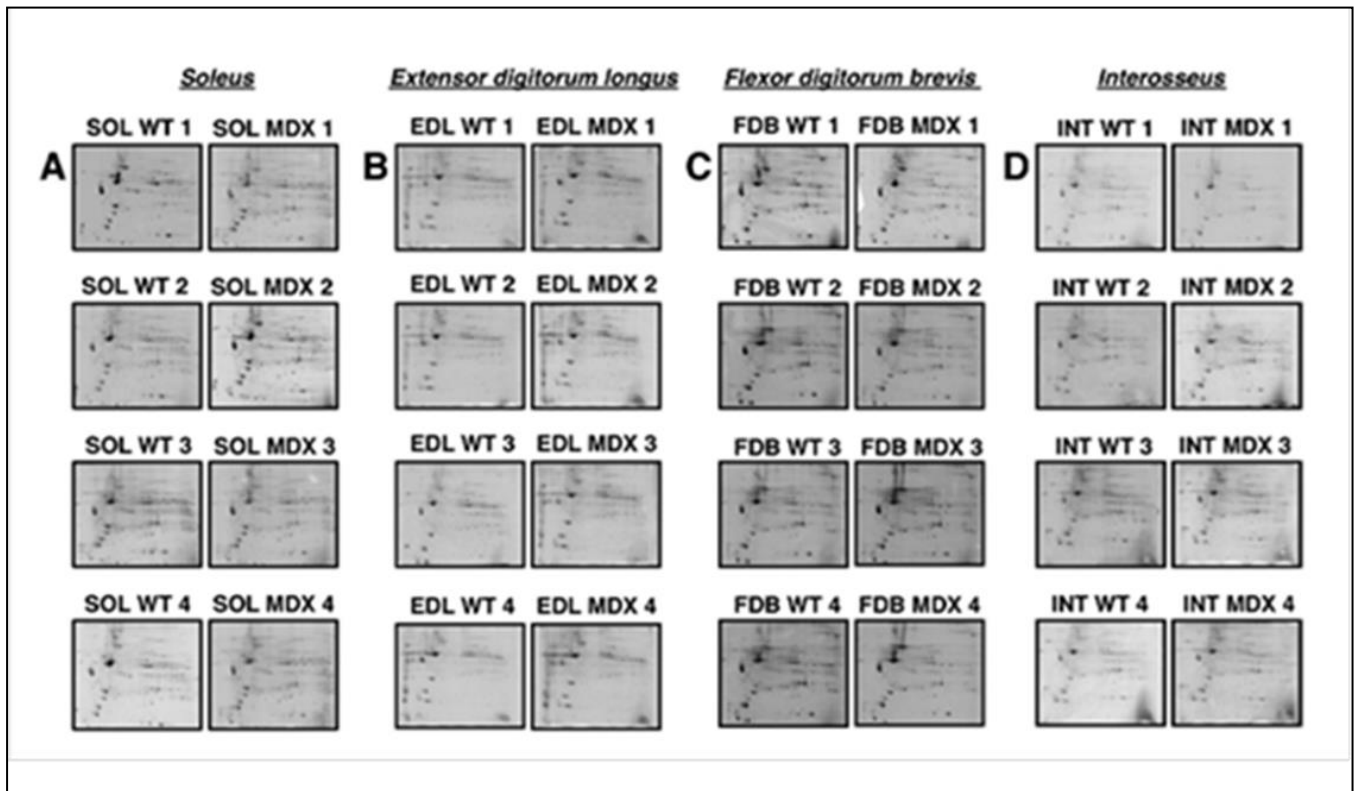


**Figure 5-1 Overview of two-dimensional gel electrophoretic analysis of the *mdx* mice skeletal muscles for x-linked muscular dystrophy**

Shown are RuBPs stained gels from 3-month-old normal wild type (WT) vs dystrophic (MDX) (A) *soleus* (SOL), (B) *extensor digitorum longus* (EDL), (C) *flexor digitorum brevis* (FDB) and (D) *interosseus* (INT) muscle extracts. The 32 gel images comprise of four biological repeats of each set of normal (wild-type; WT 1-4) vs diseased (MDX 1-4) muscles. Fluorescent images are shown across the pH 3-10 range.

### 5.2.3 RuBPs analysis of dystrophic *soleus* muscle

Proteins with significant changes in expression levels are numbered 1 to 24 and marked by circles in the master gel Fig 5-2. The mass spectrometric identification of these altered muscle proteins is listed in Table 5-1. This table contains the identified muscle-associated proteins names, international accession number, relative molecular masses, *pI*-values, number of matched peptide sequences, Mascot scores, percentage sequence coverage, and fold-change of individual muscle proteins affected in the dystrophic *mdx* SOL tissue.

Protein species with an altered concentration in *mdx* SOL muscle ranged from a molecular mass of 17 kDa (myoglobin) to 127 kDa (myosin binding protein) and with a *pI*-range from 4.7 *pI* (myosin light chain) to 8.9 *pI* (malate dehydrogenase). The expression levels showed an increased abundance for various myosin light chains consisting of MLC1/3, MLC2 and MLC3 (spots 1, 5, 11,17 and 19), cadherin 13 (spot 2), aldolase (spot 3), the molecular chaperone  $\alpha$ B-crystallin (spots 4, 9 and 14), troponin TnC (spot 6), glutathione transferase (spot 7), different subunits of 14-3-3 protein (spots 8 and 15), collagen (spot 10) phosphatase (spot 12), iron transporter ferritin (spot 13), myosin binding slow protein MyBP-C (spot 16) and peroxiredoxin (spot 18). A decreased abundance was established in the tumor metastatic process-associated protein NM23 (spot 20), oxygen carrier myoglobin (spot 21), ATP synthase Atp5b protein (spot 22), creatine kinase (spot 23) and for malate dehydrogenase (spot 24).

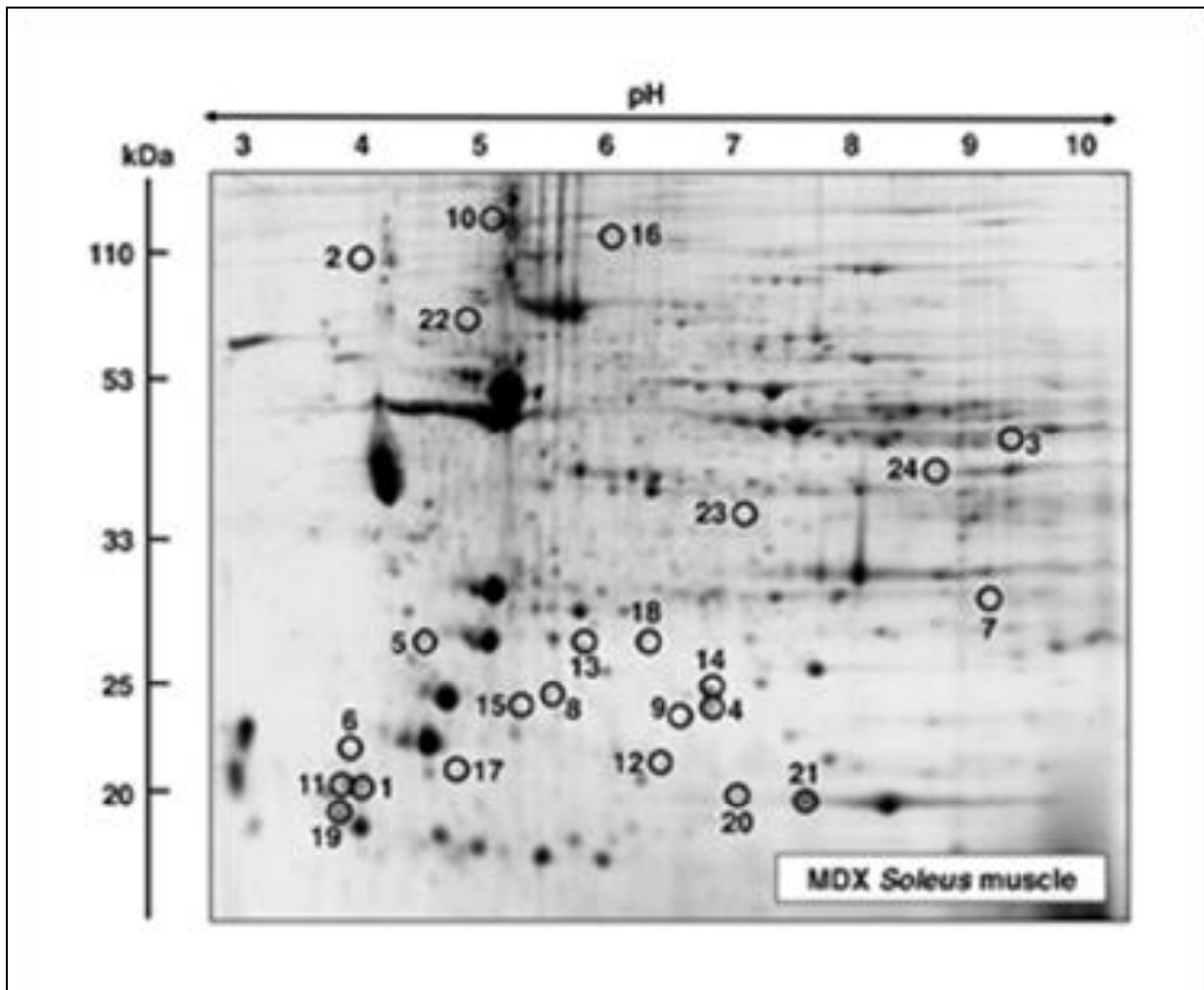


**Figure 5-2 Fluorescence two-dimensional gel electrophoretic analysis of *mdx soleus* muscle**

Shown is a representative RuBPs-stained master gel of crude muscle extracts from *mdx soleus* muscle. Protein spots with age-related alterations in abundance are numbered 1 to 24 and marked by circles. See Table 5-1 for the mass spectrometric identification of individual muscle-associated protein spots. The pH-values of the first dimension and molecular mass standards of the second dimension are shown on the top and on the left of the panels, respectively.

**Table 5.1 List of muscle-associated proteins with changes in abundance in the soleus muscle from *mdx* mice**

<b>Spot No.</b>	<b>Protein Name</b>	<b>Accession No.</b>	<b>Isoelectric point (pI)</b>	<b>Molecular mass (Da)</b>	<b>Number of peptides</b>	<b>Coverage (%)</b>	<b>Mascot Score</b>	<b>Fold Change</b>
1	Myosin light chain 2 (MLC2)	AAA39796	4.71	18870	9	60	401	5.0
2	Cadherin 13	AAH21628	4.9	78474	2	4	104	4.4
3	Aldolase A, isoform 2	NP031464	8.31	39795	17	40	136	4.3
4	$\alpha$ B-crystallin	NP034094	6.76	20056	3	28	121	4.2
5	Myosin light chain 3 (MLC3)	EDL09001	5.03	22523	6	38	268	3.3
6	Troponin C, skeletal muscle	NP033420	4.07	18156	2	20	190	3.1
7	Glutathione S-transferase	NP034488	7.71	26069	9	42	415	2.8
8	14-3-3 Protein $\gamma$	NP036611	4.8	28519	4	9	145	2.8
9	$\alpha$ B-crystallin	NP034094	6.76	20056	1	14	58	2.8
10	Collagen $\alpha$ -1 (VI) chain	NP034063	5.2	109582	13	16	224	2.6
11	Myosin light chain 2 (MLC2)	NP058034	4.82	19059	4	31	272	2.5

12	Mg-dependent phosphatase 1	NP075886	6.29	18629	3	29	98	2.4
13	Ferritin light chain 1	P29391	5.66	20848	6	44	372	2.3
14	$\alpha$ B-crystallin	NP034094	6.76	20056	13	60	141	2.3
15	14-3-3 Protein $\zeta$	BAA13421	4.7	27911	4	18	258	2.2
16	Myosin binding protein C, slow	HQ848554	5.74	127046	9	10	411	2.1
17	Myosin light chain 2 (MLC2)	NP058034.1	4.82	19059	5	44	161	2.1
18	Peroxiredoxin-1	NP035164	8.26	22394	5	24	170	2.0
19	Myosin light chain 1/3 (MLC1/3)	NP0672605	4.98	20697	11	53	514	2.0
20	Tumor metastatic process-associated protein NM23	AAA39826	8.44	18846	4	40	141	-2.0
21	Myoglobin	NP038621	7.07	17117	2	21	161	-2.1
22	Atp5b protein	BC037127	5.24	56632	7	20	488	-2.2
23	Creatine kinase M-type	NP031736	6.58	43250	2	7	97	-2.3
24	Malate dehydrogenase	AAA39509	8.93	36052	5	22	132	-4.2

#### 5.2.4 RuBPs analysis of dystrophic EDL muscle

Proteins with significant changes in expression levels are numbered 1 to 17 and marked by circles in the master gel Fig 5-3. The mass spectrometric identification of these altered muscle proteins is listed in Table 5-2. This table contains the identified muscle-associated proteins names, international accession number, relative molecular masses, *pI*-values, number of matched peptide sequences, Mascot scores, percentage sequence coverage, and fold-change of individual muscle proteins affected in the dystrophic *mdx* EDL tissue.

Protein species with an altered concentration in *mdx* EDL muscle ranged from a molecular mass of 17 kDa (myoglobin) to 224 kDa (myosin) and with a *pI*-range from 5.2 *pI* (actin) to 9.0 *pI* (Troponin TnT). Mass spectrometric analyses revealed an increased concentration in fast troponin TnT (spots 1 and 9), oxygen carrier myoglobin (spot 2), phosphoglycerate mutase 2 (spots 3 and 15), glyceraldehyde-3-phosphate dehydrogenase (spot 4), triosephosphate isomerase (spot 5), myosin protein (spot 6), lactate dehydrogenase B chain (spot 7), phosphoglycerate kinase (spot 8), creatine kinase (spot 10), the malate dehydrogenase (spot 11), , actin (spot 12), glycogen phosphorylase (spot 13) and for phosphoglycerate kinase (spot 14). In contrast, decreased concentrations were found for glycogen phosphorylase (spot 16) and actinin (spot 17).

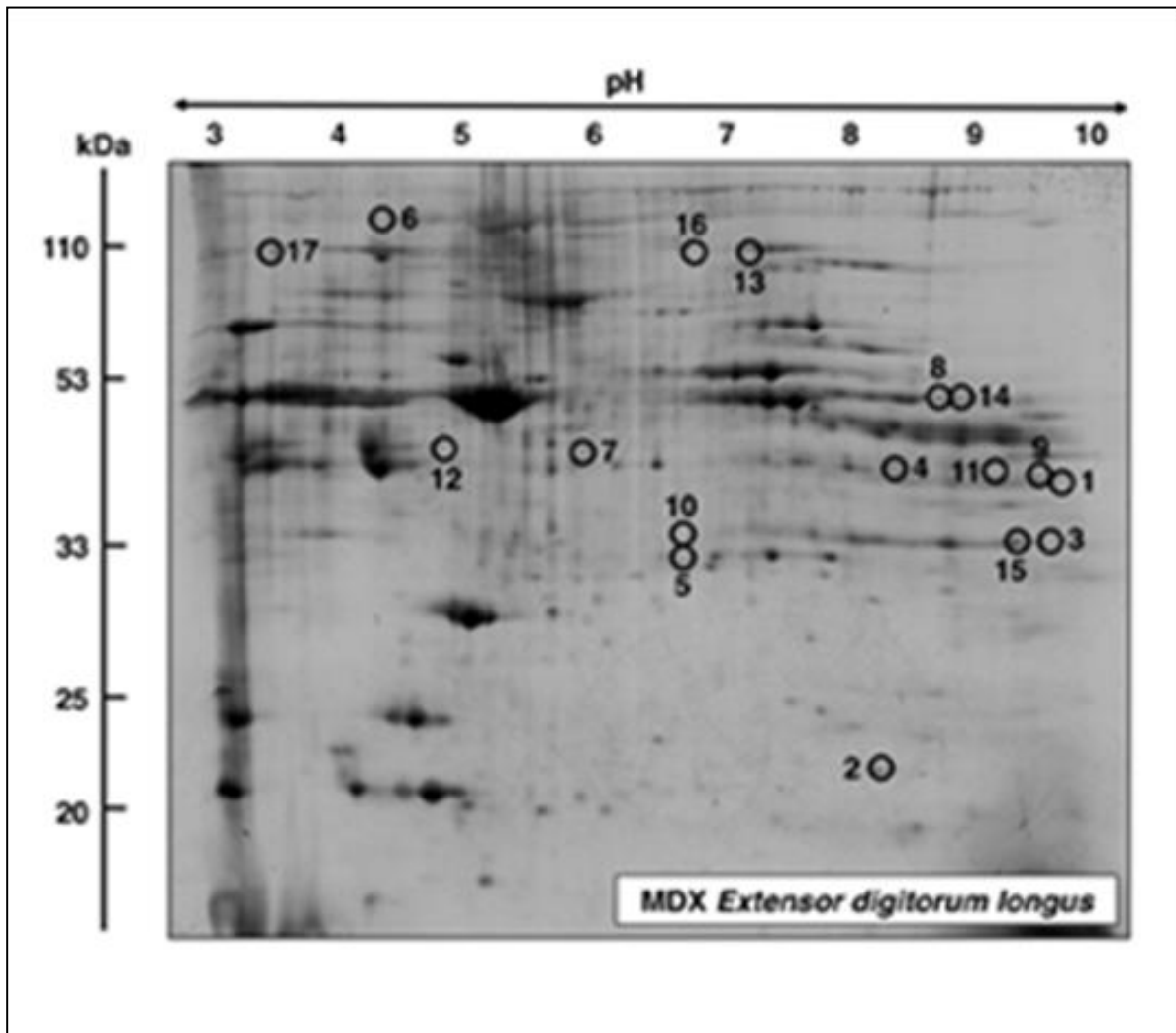


**Figure 5-3 Fluorescence two-dimensional gel electrophoretic analysis of *mdx extensor digitorum longus* muscle**

Shown is a representative RuBPs-stained master gel of crude muscle extracts from *mdx extensor digitorum longus* muscle. Protein spots with age-related alterations in abundance are numbered 1 to 17 and marked by circles. See Table 5-2 for the mass spectrometric identification of individual muscle-associated protein spots. The pH-values of the first dimension and molecular mass standards of the second dimension are shown on the top and on the left of the panels, respectively.

**Table 5.2 List of muscle-associated proteins with changes in abundance in the *extensor digitorum longus* muscle from *mdx* mice**

Spot No.	Protein Name	Accession No.	Isoelectric point (pI)	Molecular mass (Da)	Number of peptides	Coverage (%)	Mascot Score	Fold Change
1	Troponin T, fast skeletal muscle	AAB39743	9.01	29358	2	11	66	3.8
2	Myoglobin	NP038621	7.07	17117	11	68	547	3.7
3	Phosphoglycerate mutase 2	NP061358	8.65	28983	11	49	484	3.4
4	Glyceraldehyde-3-phosphate dehydrogenase	AAH85315	7.59	36099	7	30	347	3.0
5	Triosephosphate isomerase	AAB48543	5.62	22724	4	22	90	2.6
6	Myosin-1	NP109604	5.60	224131	19	11	774	2.6
7	Lactate dehydrogenase B chain	NP032518	5.70	36839	15	49	775	2.5
8	Phosphoglycerate kinase	AAA70267	7.53	44914	6	21	299	2.3
9	Troponin T, fast skeletal muscle	AAB39743	9.01	29358	6	31	131	2.3

10	Creatine kinase M-type	NP031736	6.58	43250	5	16	114	2.2
11	Malate dehydrogenase	AAA39509	8.93	36052	11	41	313	2.1
12	Actin, $\alpha$ skeletal muscle	NP001091	5.23	42372	10	31	136	2.1
13	Glycogen phosphorylase	NP035354	6.65	97689	25	35	1047	2.0
14	Phosphoglycerate kinase	AAA70267	7.53	44914	7	22	109	2.0
15	Phosphoglycerate mutase 2	NP061358	8.65	28983	14	51	637	2.0
16	Glycogen phosphorylase	NP035354	6.65	97689	2	4	54	-2.6
17	$\alpha$ -actinin-3	NP038484	5.31	103616	7	9	374	-2.8

### 5.2.5 RuBPs analysis of dystrophic FDB muscle

Proteins with significant changes in expression levels are numbered 1 to 19 and marked by circles in the master gel Fig 5-4. The mass spectrometric identification of these altered muscle proteins is listed in Table 5-3. This table contains the identified muscle-associated proteins names, international accession number, relative molecular masses, *pI*-values, number of matched peptide sequences, Mascot scores, percentage sequence coverage, and fold-change of individual muscle proteins affected in the dystrophic *mdx* FDB tissue.

Protein species with an altered concentration in *mdx* FDB muscle ranged from a molecular mass of 12 kDa (parvalbumin) to 130 kDa (collagen) and with a *pI*-range from 4.9 *pI* (vimentin) to 9.2 *pI* (collagen). MS-based proteomics revealed an increase in expression levels for fast troponin I (spot 1), serpin1 protein (spots 2, 6 and 9), the molecular chaperone  $\alpha$ B-crystallin (spot 3), vimentin (spot 4), phosphoglycerate mutase 2 (spot 5), desmin (spot 7), the leukocyte elastase inhibitor A (spot 8) and tropomyosin (spot 10). Decreased protein abundance was established in FDB muscle for the glycolytic enzyme aldolase (spots 11, 12, 15, 17 and 18), cytosolic Ca<sup>2+</sup>-binding protein parvalbumin (spots 13 and 16), the 14-3-3 protein (spot 14) and for collagen (spot 19).

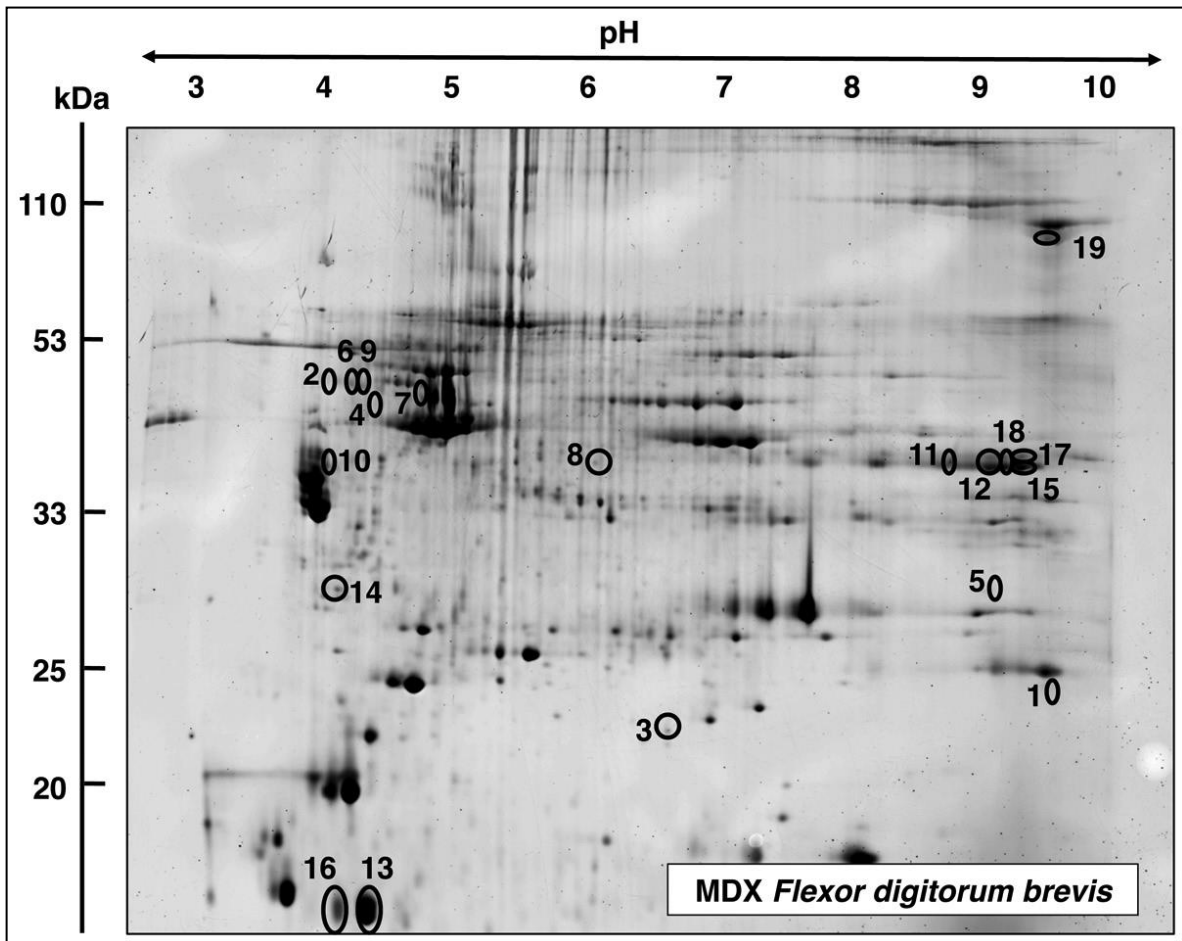


**Figure 5-4 Fluorescence two-dimensional gel electrophoretic analysis of *mdx flexor digitorum brevis* muscle**

Shown is a representative RuBPs-stained master gel of crude muscle extracts from *mdx flexor digitorum brevis* muscle. Protein spots with age-related alterations in abundance are numbered 1 to 19 and marked by circles. See Table 5-3 for the mass spectrometric identification of individual muscle-associated protein spots. The pH-values of the first dimension and molecular mass standards of the second dimension are shown on the top and on the left of the panels, respectively.

**Table 5.3 List of muscle-associated proteins with changes in abundance in the *flexor digitorum brevis* muscle from *mdx* mice**

Spot No.	Protein Name	Accession No.	Isoelectric point (pI)	Molecular mass (Da)	Number of peptides	Coverage (%)	Mascot Score	Fold Change
1	Troponin I, fast skeletal muscle	NP033431	8.65	21518	5	30	57	3.1
2	Serpina 1d protein	AAH21850	5.18	46140	9	24	104	2.7
3	$\alpha$ B-crystallin	NP034094	6.76	20056	8	45	324	2.4
4	Vimentin	CAA69019	4.96	51591	21	50	261	2.4
5	Phosphoglycerate mutase 2	NP061358	8.65	28983	2	8	75	2.3
6	Serpina 1d protein	AAH21850	5.18	46140	5	11	136	2.3
7	Desmin	NP034173	5.21	53523	10	32	206	2.2
8	Leukocyte elastase inhibitor A	NP079705	5.85	42722	9	30	178	2.1
9	Serpina 1d protein	AAH21850	5.18	46140	7	17	131	2.0
10	Tropomyosin, $\beta$ chain	NP033442	4.66	32933	17	47	176	2.0
11	Aldolase A, isoform 2	NP001170778	8.31	39795	15	48	202	-2.2

12	Aldolase A, isoform 2	NP001170778	8.31	39795	13	40	249	-2.2
13	Parvalbumin $\alpha$	NP038673	5.02	11923	8	65	228	-2.3
14	14-3-3 Protein $\gamma$	AAC14345	4.80	28519	8	38	116	-2.3
15	Aldolase A, isoform 2	NP001170778	8.31	39795	13	40	163	-2.7
16	Parvalbumin $\alpha$	NP038673	5.02	11923	8	65	219	-3.0
17	Aldolase A, isoform 2	NP001170778	8.31	39795	9	27	139	-3.1
18	Aldolase A, isoform 2	NP001170778	8.31	39795	20	55	215	-3.3
19	Pro- $\alpha$ -2(I) collagen	CAA41205	9.23	130046	2	2	51	-3.4

### 5.2.6 RuBPs analysis of dystrophic INT muscle

In contrast to the above listed results of extensive alterations in the proteomes from the *mdx* dystrophic SOL, EDL and FDB muscle, the MS-based proteomic analyse of INT muscle exhibited only a limited number of changed proteins. Proteins with significant changes in expression levels are numbered 1 to 5 and marked by circles in the master gel Fig 5-5. The mass spectrometric identification of these altered muscle proteins is listed in Table 5-4. This table contains the identified muscle-associated proteins names, international accession number, relative molecular masses, *pI*-values, number of matched peptide sequences, Mascot scores, percentage sequence coverage, and fold-change of individual muscle proteins affected in the dystrophic *mdx* INT tissue.

Protein species with an altered concentration in *mdx* INT muscle ranged from a molecular mass of 12 kDa (parvalbumin) to 33 kDa (40 kDa protein) and with a *pI*-range from 4.8 *pI* (40 kDa protein) to 8.65 *pI* (Toponin I). MS-based proteomics revealed an increase in expression levels for fast Toponin I (spots 1 and 2), the heat shock protein  $\alpha$ B-crystallin (spot 3) and the 40 kDa protein (spot 4). In contrast, decreased protein abundance was found in the cytosolic  $\text{Ca}^{2+}$ -binding protein parvalbumin in the INT muscle.

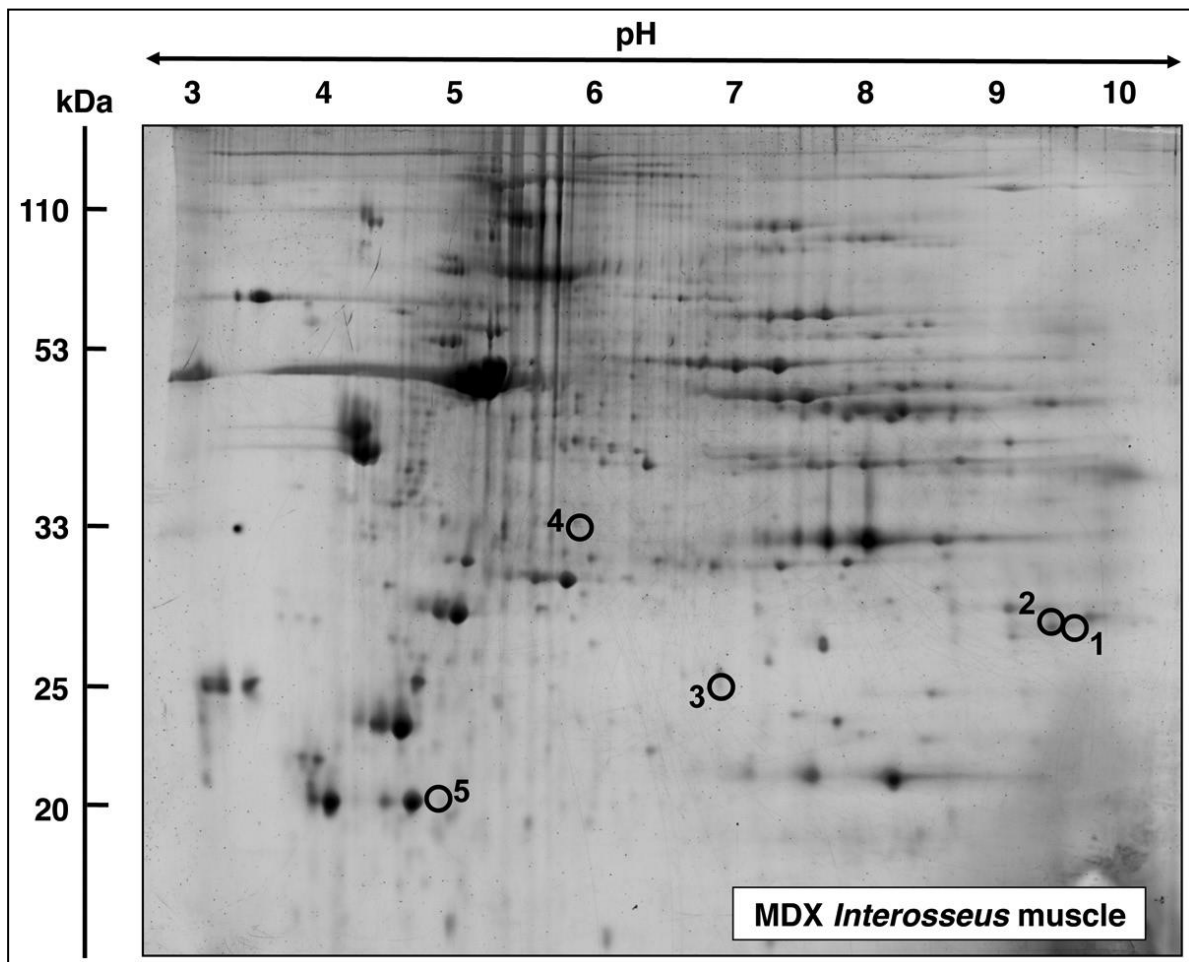


**Figure 5-5 Fluorescence two-dimensional gel electrophoretic analysis of *mdx interosseus* muscle**

Shown is a representative RuBPs-stained master gel of crude muscle extracts from *mdx interosseus* muscle. Protein spots with age-related alterations in abundance are numbered 1 to 5 and marked by circles. See Table 5-4 for the mass spectrometric identification of individual muscle-associated protein spots. The pH-values of the first dimension and molecular mass standards of the second dimension are shown on the top and on the left of the panels, respectively.

**Table 5.4 List of muscle-associated proteins with changes in abundance in the *interosseus* muscle from *mdx* mice**

<b>Spot No.</b>	<b>Protein Name</b>	<b>Accession No.</b>	<b>Isoelectric point (pI)</b>	<b>Molecular mass (Da)</b>	<b>Number of peptides</b>	<b>Coverage (%)</b>	<b>Mascot Score</b>	<b>Fold Change</b>
1	Troponin I, fast skeletal muscle	NP033431	8.65	21518	8	29	301	4.1
2	Troponin I, fast skeletal muscle	NP033431	8.65	21518	5	21	245	3.4
3	$\alpha$ B-crystallin	NP034094	6.76	20056	9	56	421	2.2
4	40 kDa Protein	1405340A	4.80	32848	3	15	164	2.1
5	Parvalbumin, $\alpha$	NP038673	5.02	11923	7	63	400	-2.2

### 5.2.7 Immunoblot analysis of dystrophic skeletal muscle subtypes

In order to further characterise the various skeletal muscles, comparative immunoblotting was carried out following the mass spectrometric establishment of the subtype specific changes in the urea-soluble *mdx* muscle proteomes. Lanes 1 and 2, 3 and 4, 5 and 6 and 7 and 8 shown in figure 5-6A were labelled with a laminin antibody for control purposes. The extracellular matrix protein presented relatively comparable quantities in normal versus dystrophic samples, with the exception of SOL muscle which exhibited an increased concentration in *mdx* preparations.

As shown in Figure 5-6B to 5-6I, antibody labelling was performed to verify the altered abundance of 2 marker proteins from each of the *mdx* muscle subtypes analysed. The reduced expression of myoglobin and increased concentration of collagen in the SOL muscle in figure 5-6B and 5-6C, respectively. The lower levels of actinin and higher levels of phosphoglycerate kinase in the EDL muscle in figure 5-6D and 5-6E, respectively. The reduced expression of parvalbumin and increased concentration of serpina in the FDB muscle in figure 5-6F and 5-6G, respectively and the reduced levels of parvalbumin and higher levels of  $\alpha$ B-crystallin in the INT muscle in figure 5-6H and 5-6I, respectively were all confirmed by immunoblot analysis.

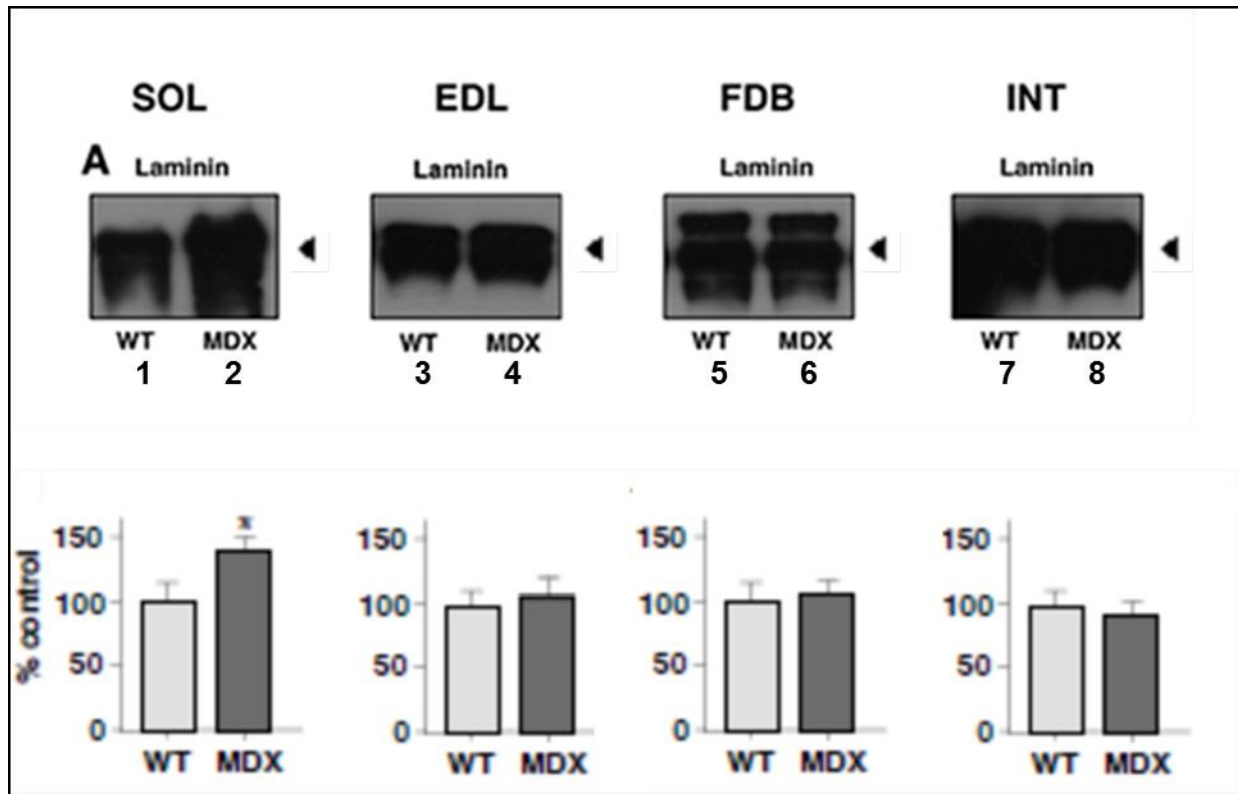


**Figure 5-6A Immunoblotting analysis of the extracellular matrix protein laminin in normal versus *mdx* skeletal muscle subtypes**

Shown are representative blots with expanded views of immuno-decorated protein bands indicated by the arrowhead, with graphical presentation of the statistical evaluation. Immunoblots were labelled with the Laminin antibody. Lanes 1 and 2, 3 and 4, 5 and 6 and 7 and 8 represent 3-month-old normal wild-type vs dystrophic *mdx* preparations from *soleus* (SOL), *extensor digitorum longus* (EDL), *flexor digitorum brevis* (FDB) and *interosseus* (INT) muscles, respectively. The comparative blotting was statistically verified using an unpaired Student's *t*-test ( $n=4$  replicates). Standard deviation represented by Error bars, ( $*p<0.05$ ).

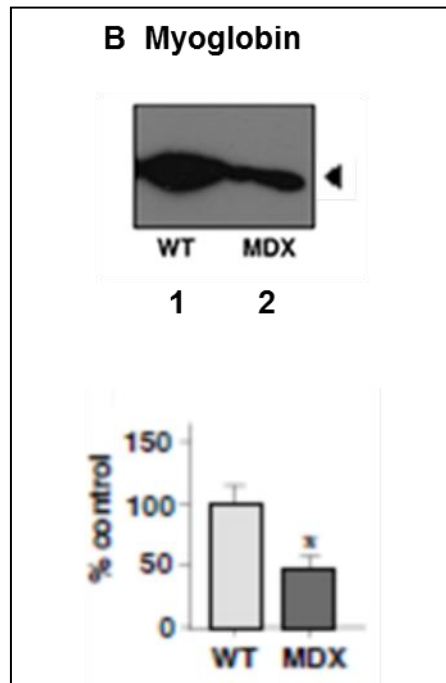


**Figure 5-6B Immunoblotting analysis of myoglobin in *soleus* muscle**

Shown are representative blots with expanded views of immuno-decorated protein bands indicated by the arrowhead, with graphical presentation of the statistical evaluation. Immunoblots were labelled with the myoglobin antibody. Lanes 1 and 2 represent 3-month-old normal wild type vs dystrophic *mdx soleus* (SOL), respectively. The comparative blotting was statistically verified using an unpaired Student's *t*-test (n=4 replicates). Standard deviation represented by Error bars, (\*p<0.05).

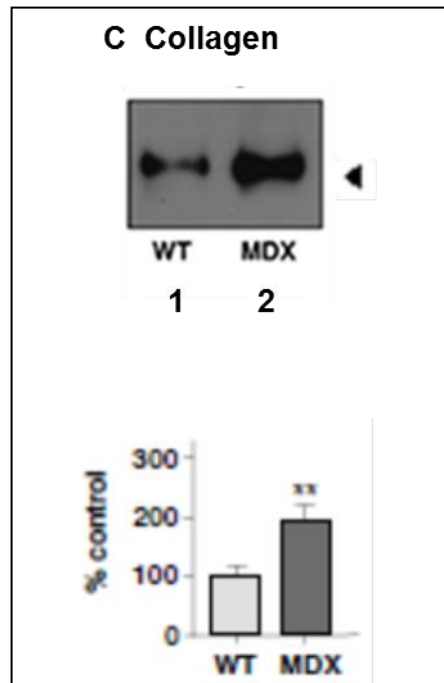


**Figure 5-6C Immunoblotting analysis of extracellular matrix protein collagen in *soleus* muscle**

Shown are representative blots with expanded views of immuno-decorated protein bands indicated by the arrowhead, with graphical presentation of the statistical evaluation. Immunoblots were labelled with the collagen antibody. Lanes 1 and 2 represent 3-month-old normal wild type vs dystrophic *mdx soleus* (SOL), respectively. The comparative blotting was statistically verified using an unpaired Student's *t*-test ( $n=4$  replicates). Standard deviation represented by Error bars, (\*\* $p<0.005$ ).

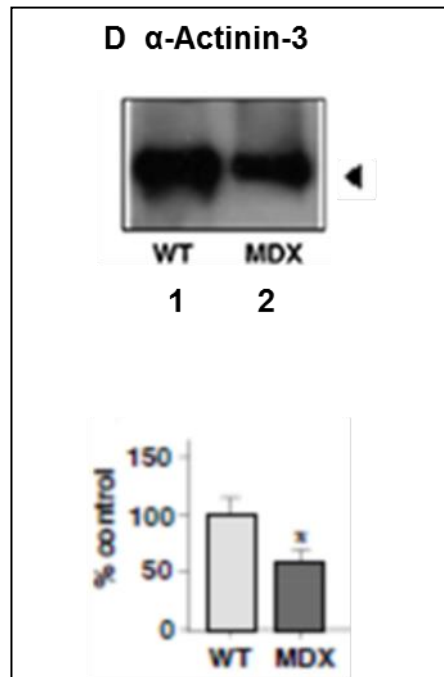


**Figure 5-6D Immunoblotting analysis of  $\alpha$ -actinin-3 in *extensor digitorum longus* muscle**

Shown are representative blots with expanded views of immuno-decorated protein bands indicated by the arrowhead, with graphical presentation of the statistical evaluation. Immunoblots were labelled with the  $\alpha$ -actinin-3 antibody. Lanes 1 and 2 represent 3-month-old normal wild type vs dystrophic *mdx extensor digitorum longus* (EDL), respectively. The comparative blotting was statistically verified using an unpaired Student's *t*-test (n=4 replicates). Standard deviation represented by Error bars, (\* $p < 0.05$ ).

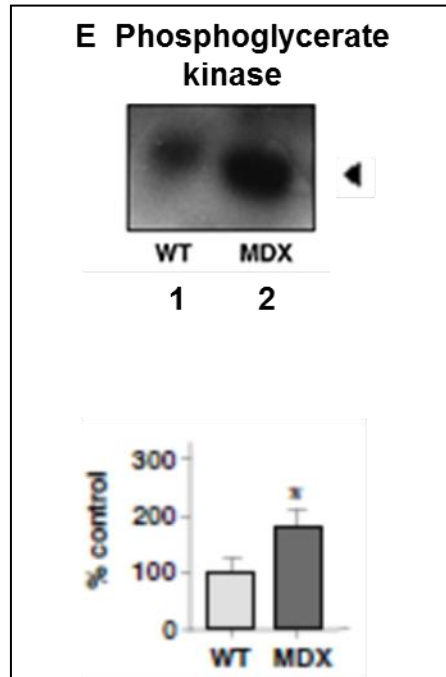


**Figure 5-6E Immunoblotting analysis of phosphoglycerate kinase in *extensor digitorum longus* muscle**

Shown are representative blots with expanded views of immuno-decorated protein bands indicated by the arrowhead, with graphical presentation of the statistical evaluation. Immunoblots were labelled with the phosphoglycerate kinase antibody. Lanes 1 and 2 represent 3-month-old normal wild type vs dystrophic *mdx extensor digitorum longus* (EDL), respectively. The comparative blotting was statistically verified using an unpaired Student's *t*-test (n=4 replicates). Standard deviation represented by Error bars, (\*p<0.05).

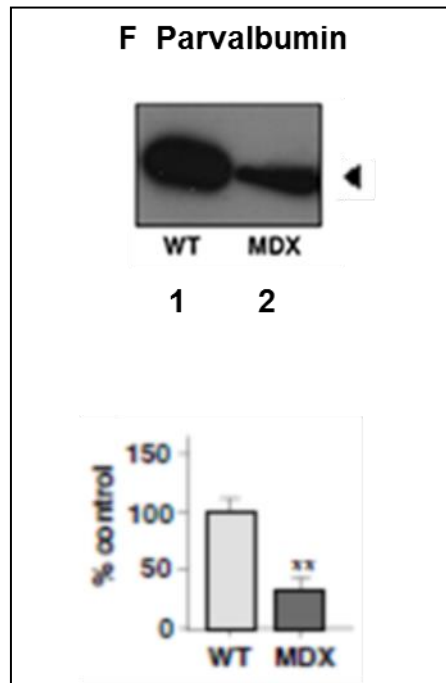


**Figure 5-6F Immunoblotting analysis of calcium-binding protein parvalbumin in flexor digitorum brevis muscle**

Shown are representative blots with expanded views of immuno-decorated protein bands indicated by the arrowhead, with graphical presentation of the statistical evaluation. Immunoblots were labelled with the parvalbumin antibody. Lanes 1 and 2 represent 3-month-old normal wild type vs dystrophic *mdx flexor digitorum brevis* (FDB), respectively. The comparative blotting was statistically verified using an unpaired Student's *t*-test (n=4 replicates). Standard deviation represented by Error bars, (\*\*p<0.005).

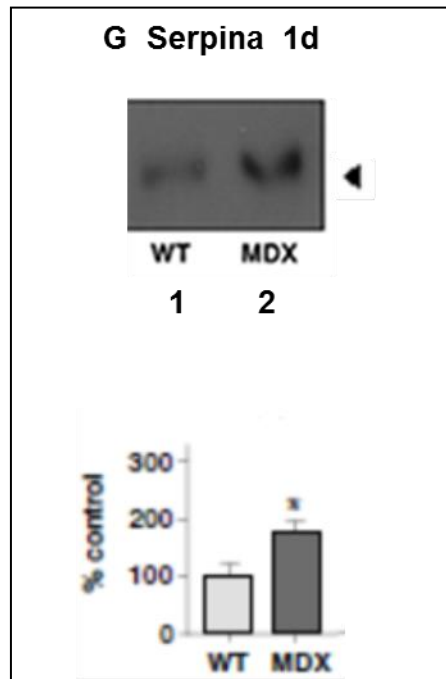


**Figure 5-6G Immunoblotting analysis of serpina 1d in flexor digitorum brevis muscle**

Shown are representative blots with expanded views of immuno-decorated protein bands indicated by the arrowhead, with graphical presentation of the statistical evaluation. Immunoblots were labelled with the serpina antibody. Lanes 1 and 2 represent 3-month-old normal wild type vs dystrophic *mdx flexor digitorum brevis* (FDB), respectively. The comparative blotting was statistically verified using an unpaired Student's *t*-test (n=4 replicates). Standard deviation represented by Error bars, (\*p<0.05).

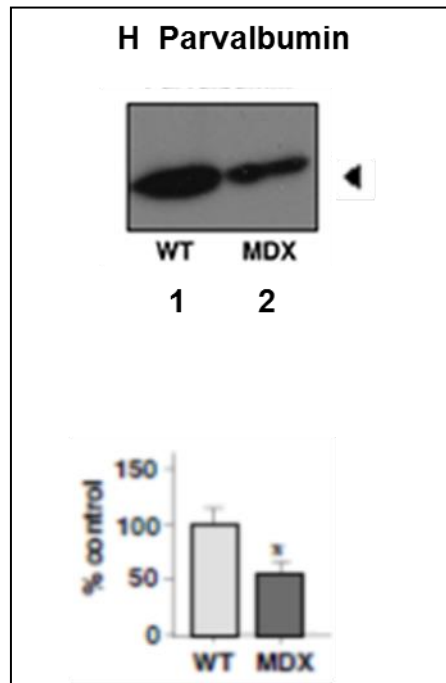


**Figure 5-6H Immunoblotting analysis of calcium-binding protein parvalbumin in *interosseus* muscle**

Shown are representative blots with expanded views of immuno-decorated protein bands indicated by the arrowhead, with graphical presentation of the statistical evaluation. Immunoblots were labelled with the parvalbumin antibody. Lanes 1 and 2 represent 3-month-old normal wild type vs dystrophic *mdx interosseus* (INT), respectively. The comparative blotting was statistically verified using an unpaired Student's *t*-test (n=4 replicates). Standard deviation represented by Error bars, (\*p<0.05).

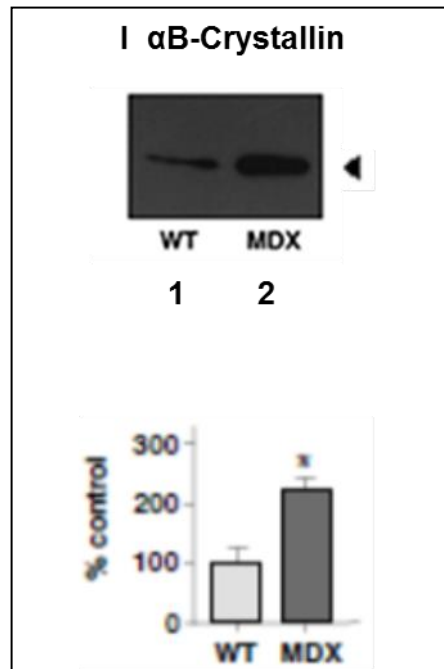


**Figure 5-6I Immunoblotting analysis of αB-crystallin in *interosseus* muscle**

Shown are representative blots with expanded views of immuno-decorated protein bands indicated by the arrowhead, with graphical presentation of the statistical evaluation. Immunoblots were labelled with the αB-crystallin antibody. Lanes 1 and 2 represent 3-month-old normal wild type vs dystrophic *mdx interosseus* (INT), respectively. The comparative blotting was statistically verified using an unpaired Student's *t*-test (n=4 replicates). Standard deviation represented by Error bars, (\*p<0.05).

### 5.2.8 Histological profiling of skeletal muscle tissue from *mdx* mice

In order to further characterise the various skeletal muscles, histological examination was performed using hematoxylin and eosin-stained muscle cross-sections from wild-type (WT; A, C, E and G) and *mdx* mice (B, D, F and H) seen in figure 5-7. The histological analysis of cross sections from the SOL, EDL, FDB and INT muscles observed central nucleation in all examined types of skeletal muscle from *mdx* mice (Fig 5-7B, D, F and H). In addition, the muscles exhibited variations in fiber size and the occurrence of small, rounded fibers. As expected, central nuclei were rarely detected in the muscle fibers from WT mice (Fig 5-7A, C, E and G). Quantitative evaluation of central nucleation showed a significantly lower degree of nucleation in the FDB and INT compared with the SOL and EDL muscles.

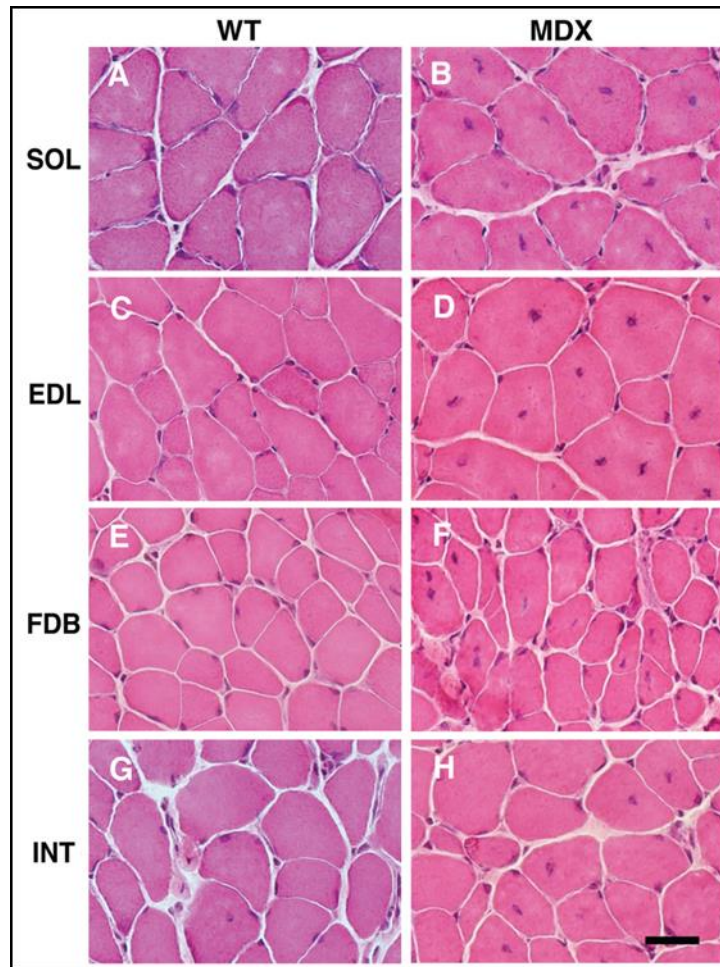


**Figure 5-7 Histological profiling of skeletal muscles from *mdx* mice**

Shown is a representative hematoxylin and eosin-stained muscle cross-sections from wild-type (WT; A, C, E and G) and dystrophic *mdx* mice (B, D, F and H). Note the lower degree of central nuclei in the *flexor digitorum brevis* (FDB; E and F) and *interosseus* (INT; G and H) muscles, compared with the *soleus* (SOL; B) and *extensor digitorum longus* (EDL; D) muscles from *mdx* mice. Muscles were prepared from 3-month-old dystrophin-deficient versus aged-matched wild type mice. Scale bar, 20  $\mu\text{m}$ .

### 5.3 Discussion

In this chapter, proteomic profiling of 4 skeletal muscle subtypes, SOL, EDL, FDB and INT muscle, has revealed considerable changes in the extent of protein perturbations in different muscles of the *mdx* dystrophic mouse model of Duchenne muscular dystrophy. While we observed 24, 17 and 19 altered protein species in *mdx* SOL, EDL and FDB muscles, respectively, dystrophin-deficient INT muscle preparations revealed only changes in fast troponin I,  $\alpha$ B-crystallin, the 40 kDa protein and the cytosolic Ca<sup>2+</sup>-binding protein parvalbumin.

This is an interesting discovery from a global profile of protein expression patterns in dystrophinopathy and supports the idea that the loss of dystrophin and resulting reduction of associated glycoproteins leads in considerably different secondary alterations and cellular adaptations in specific skeletal muscles, even though all contractile *mdx* muscle tissues exhibit the same primary genetic defect. Previous proteomic reports of *mdx* muscle tissues agree that the deficiency in the membrane cytoskeletal protein dystrophin leads to impaired protein expression patterns in contractile tissues (Lewis et al., 2009). While past studies on *mdx* muscle proteomics vary significantly on the listing of distinct proteins involved in the molecular pathogenesis of muscular dystrophy, the disintegration of sarcolemmal integrity clearly has severe impact for the overall function of the affected muscle fibers.

Interestingly, as shown in the previous chapter severely dystrophic *mdx* diaphragm muscle displays extensive alterations in a large number of muscle proteins (Doran et al., 2006a; Doran et al., 2006b; Doran et al., 2009b; Carberry., et al 2012a), while mildly affected phenotypes such as *mdx* extraocular muscle which exhibit much less changes in its proteome (Lewis and Ohlendieck, 2010). This establishes a link between the pathophysiological phenotype of individual *mdx* muscle tissues and the level of proteome-wide changes.

### 5.3.1 Moderate expression changes of RuBPs labelled skeletal muscle proteins

Muscle-associated proteins with an altered abundance in *mdx* muscle tissues are predominantly involved in the contraction-relaxation cycle, muscle metabolism, metabolite transportation, and the cellular stress response. While in the mildly affected *mdx* INT muscle phenotype, the most significantly increased protein was fast troponin I (Swartz et al., 2006) suggesting a certain level of remodeling of the regulatory elements in the contractile apparatus (Gordon et al., 2000). Other protein alterations in *mdx* INT muscle were minimal, as compared to the other skeletal muscles examined.

Two additional observations on the *mdx* INT muscle support the proteomic analyses. Firstly, the occurrence of central nucleation in the muscle fibers was lower in the INT and FDB compared with the SOL and EDL hind limb muscles (Fig 5-7). This is key, as central nucleation is considered as a reliable sign of recent muscle fiber regeneration. Secondly, there was no observed increase in muscle mass in INT and FDB, in contrast to that of the SOL and EDL muscles. Hypertrophy has been reported in dystrophin-deficient muscles in a number of models of DMD, including the *mdx* mouse (Kornegay et al., 2012) though the signaling pathways resulting in muscle growth have not yet been fully revealed (Andres-Mateos et al., 2013) (Gundersen, 2011). However, both central nucleation and the level of hypertrophy are in agreement with a less severe impairment of the *mdx* INT and FDB, compared with the SOL and EDL muscles (Carberry et al., 2013b).

In *mdx* SOL muscle, various myosin light chains consisting of MLC1/3, MLC2 and MLC3 isoforms (Gonzalez et al., 2002), were revealed to be increased in expression in the dystrophin-deficient fibers. The highly complex myosin molecule forms a hexameric structure containing 2 MHC heavy chains and various MLC light chains in the contractile apparatus (Bozzo et al., 2005; Clark et al., 2002). Various arrangements of myosin heavy and light chains form a wide array of fiber type-specific isoforms and the myosin complement of contractile fibers is very flexible (Pette and Staron, 2000; Holland and

Ohlendieck, 2013).

Previous proteomic studies have established that neuromuscular activity has an intense effect on the myosin isoform expression patterns (Donoghue et al., 2005; Donoghue et al., 2007). The drastic alterations in *mdx* SOL muscle suggest that the dystrophic phenotype is concomitant with considerable remodeling of the contractile apparatus, together with myosin, myosin binding proteins and troponin. Interestingly, the unique GPI-anchored cadherin-13 protein is elevated in *mdx* SOL muscle and may promote angiogenesis the process of new blood vessel formation from existing vessels (Philippova et al., 2006). Altered expression levels of the molecular chaperone  $\alpha$ B-crystallin, ferritin, glutathione S-transferase and peroxiredoxin indicate intensified demands for cellular stress response, iron storage, detoxification and anti-oxidant activity in dystrophic fibers, respectively.

Interestingly, specific isoforms of 14-3-3 proteins are altered in muscular dystrophy, which has been reported for various neurodegeneration processes (Steinacker et al., 2011). This indicates that interactions of 14-3-3 proteins with signaling receptors, phosphatases and kinases are disturbed in *mdx* SOL muscle. Reduced concentrations of ATP synthase, malate dehydrogenase and myoglobin suggest metabolic disturbances in *mdx* SOL muscle.

In the *mdx* EDL muscle, altered protein expression levels were shown for contractile elements such as myosin, troponin, actin and actinin, and in the actomyosin apparatus. Proteomic analysis also revealed a striking increase in levels of key glycolytic enzymes. The affected cytosolic proteins were also identified by mass spectrometry as glyceraldehyde-3-phosphate dehydrogenase, triosephosphate isomerase, phosphoglycerate mutase and phosphoglycerate kinase which are involved in the production of 1,3-bisphosphoglycerate and NADH, the reversible conversion of dihydroxyacetone phosphate and glyceraldehyde-3-phosphate, the reversible conversion of 3-phosphoglycerate into 2-phosphoglycerate and the generation of ATP and 3-phosphoglycerate from ADP and 1,3-bisphosphoglycerate, respectively

(Ohlendieck, 2010). The increased expression in several glycolytic enzymes indicates a shift to more anaerobic metabolism.

Interestingly, one of the chief regulatory enzymes for converting glycogen into glucose for utilisation in muscle, glycogen phosphorylase, was shown to be elevated in contractile *mdx* EDL tissue. Previous proteomic profiling of slow-twitching versus fast-twitching skeletal muscles has established that fast muscles reveal higher levels of enzymes involved in the glycolytic pathway and exhibit increase concentrations of glycogen phosphorylase (Gelfi et al., 2006).

In addition, the increased expression of lactate dehydrogenase, an enzyme that catalyses the interconversion of the final product of glycolysis, pyruvate, and lactate supports the idea of a glycolytic shift in *mdx* EDL muscle. During periods of high intensity such as exercise, skeletal muscles adopt this anaerobic glycolysis (Wells et al., 2009), thus a sharp increase of glycolytic enzymes suggest an increased demand on the glycolytic pathway in the bioenergetics of dystrophin-deficient *mdx* EDL muscle.

While in contrast to the *mdx* EDL muscle, the dystrophin-deficient *mdx* FDB muscle revealed a reduction in a crucial glycolytic enzyme. The skeletal muscle aldolase, an enzyme that catalyses the reversible biochemical breakdown of fructose-1,6-biphosphate into glyceraldehyde-3-phosphate and dihydroxyacetone phosphate (Ohlendieck, 2010). In the gluconeogenic pathway, muscle aldolase has been shown to form a supramolecular complex with alpha-actinin and fructose-1,6-biphosphatase on both sides of the Z-line in skeletal muscle fibers. It has been suggested that the tight association between aldolase and fructose-1,6-biphosphatase might enable efficient substrate channeling between these proteins (Rakus et al., 2004).

However, it is thought that many glycolytic enzymes have a multi-functional role in various cell types motility (Kim and Dang, 2005). Thus, alterations in these glycolytic enzymes may affect a number of biological systems other than the anaerobic breakdown

of glucose in skeletal muscles (Ohlendieck, 2010). For instance, enzymes with a key glycolytic function have also been shown to be involved in transcriptional regulation, metabolic integration, regulation of apoptosis and stimulation of cell motility (Kim and Dang, 2005). As a result it is difficult to determine from alterations in one key glycolytic enzyme whether this relates to distinct metabolic changes in *mdx* FDB or perhaps showing adaptations in a separate unrelated glycolysis biological system. Altered expression levels in tropomyosin and troponin and the cytosolic Ca<sup>2+</sup>-binding protein parvalbumin suggest abnormalities in the contractile apparatus and ion homeostasis, respectively.

In comparison with the *mdx* SOL muscle, the apparent increased abundance of the molecular chaperone  $\alpha$ B-crystallin in dystrophic FDB muscle agrees with the idea of an intensified cellular stress response in muscular dystrophy (Doran et al., 2006b). Interestingly, the cytoskeletal proteins desmin and vimentin were shown to be elevated in dystrophic *mdx* muscle suggesting a potential compensatory mechanism for the structural instabilities in the membrane cytoskeleton of the dystrophin-deficient fibers in the *mdx* FDB muscle.

## 5.4 Conclusion

In conclusion, the comparative proteomic analysis of 4 widely used skeletal muscles of the *mdx* mouse model of Duchenne muscular dystrophy, SOL, EDL, FDB and INT muscles, has revealed that high-resolution two-dimensional gel electrophoretic separation in combination with electrospray ionization mass spectrometry are highly suitable techniques for studying muscle subtype-specific changes in the *mdx* dystrophic skeletal muscle proteome. The variations in the number and degree of protein changes in the analysed *mdx* muscles suggest that the INT muscle is a protected phenotype, much less affected compared to that of the SOL, EDL and FDB muscles. These proteomic findings are in agreement with the lack of hypertrophy in FDB and INT

muscles and the lower levels of central nucleation compared with SOL and EDL muscle (Carberry et al., 2013b). Thus, the evaluation of experimental gene therapies for treating dystrophinopathy or future pharmacological studies should note that dystrophin-deficient skeletal muscle subtypes are not all affected in the same way. The individual physiological, biochemical and histological properties of specific muscles have to be taken into account when one wants to determine secondary abnormalities and adaptations in muscular dystrophy.

# **6 Comparative proteomic analysis of the contractile protein-depleted fraction of the *mdx* mouse model of dystrophinopathy**

## **6.1 Introduction**

In recent years extensive proteomic surveys have highlighted various skeletal muscle extracts. However, since the main proteins of the actomyosin apparatus and its supporting sarcomeric components frequently negate weak signals from minor muscle protein species during proteomic analyses, we have employed a pre-fractionation step to remove certain parts of this analytical problem. In order to eliminate a large portion of highly abundant contractile proteins, differential centrifugation of the crude skeletal muscle extracts was performed to reduce the samples complexity. The subsequent protein fraction was then separated by two-dimensional gel electrophoresis and landmark proteins identified by mass spectrometry. In order to better comprehend the complex alterations that occur during X-linked muscular dystrophy, this chapter focused on analyse of contractile protein-depleted fractions from 8-week-old normal versus dystrophic hind limb muscle preparations.

### **6.1.1 Duchenne muscular dystrophy and hind limb skeletal muscles**

Primary genetic abnormalities in the dystrophin gene result in the loss of a crucial 427kDa cytoskeletal membrane protein located in the subsarcolemmal region of the muscle fibers (Dalkilic and Kunkel, 2003). This loss causes secondary effects which lead to muscle weakness and damage due to sarcolemmal instability, disturbance of the

excitation-contraction coupling, metabolic pathways, alterations in ion homeostasis, and cellular signalling (Emery, 2002). As the dystrophin protein anchors large membrane glycoprotein complexes within the cell, membrane rupturing occurs due to its absence and results in the loss of membrane integrity. It is this reduction in the dystroglycan complex presence which is believed to be an important role in the degeneration of dystrophic muscles (Carlson and Makiejus, 1990; Williams and Bloch, 1999).

### 6.1.2 Experimental design

Comparative gel-based proteomic analysis of *mdx* hind limb muscles, subcellular fractionation was performed prior to gel electrophoretic separation of the contractile protein-depleted. Crude hind limb muscle extracts were separated by two-dimensional gel electrophoresis and labelled with the fluorescent dyes (RuBPs). This was followed by a detailed comparative DIGE analysis of subcellular hind limb fraction of 8-week-old dystrophin-deficient mice versus age-matched control mice across 3-11NL pH range. Then proteins with a significant change in their concentration were identified by mass spectrometry. Key proteomic findings were verified by immunoblot analysis. Proteomic profiling established a distinct change in abundance of 10 protein species in the dystrophic *mdx* hind limb muscles. Identified proteins were involved in various processes from the metabolite transport, ion handling and and the cellular stress response.

## 6.2 Results

### 6.2.1 Comparative proteomic analysis of *mdx* hind limb skeletal muscle

In order to analyse the minor muscle protein species and the extent of secondary changes in the *mdx* hind limb skeletal subproteome due to absence in the

membrane cytoskeletal dystrophin protein, a pre-fractionation step to remove the actomyosin apparatus and its supporting sarcomeric components was employed. The urea-soluble protein complement from the 8-week-old wild type versus age-matched dystrophic hind limb muscle was then investigated. Following fluorescent labelling of wild type or *mdx* samples with the CyDyes Cy3, as well as fluor tagging of the pooled standard using the CyDye Cy5, high-resolution two-dimensional gel electrophoresis was carried out to separate the subproteome from dystrophic *mdx* hind limb muscle. A pH-range of 3-11NL in the first dimension was employed to establish a global proteomic pattern.

Detailed densitometric analysis was carried out using a Typhoon Trio variable imager scanner and Samespot Progenesis 2-D analysis software was performed to establish differential expression patterns of the aged muscle. Figure 6-3 shows the 2-D DIGE analysis of 8-week-old dystrophic *mdx* versus aged-matched normal hind limb skeletal muscle. An altered concentration was revealed for 10 protein species, with 8 proteins being increased and 2 proteins showing decreased expression in the *mdx* contractile protein-depleted fractions. Mass spectrometry was then used to identify these significant muscle-associated proteins of interest and listed in Table 6-3.

### 6.2.2 RuBPs analysis of landmark proteins in total extract of normal hind limb skeletal muscle

Prior to the subcellular fractionation gel electrophoretic separation of the total crude extract were performed. A list of landmark 2D protein spots from the hind limb muscle are numbered 1 to 30 and marked by circles in the total muscle extract landmark master gel shown in Fig 6-1. The mass spectrometric identification of these unchanged landmark muscle proteins is listed in Table 6-1. This table contains the identified muscle-associated proteins names, international accession number,

relative molecular masses, *pI*-values, number of matched peptide sequences, Mascot scores, and percentage sequence coverage of major individual muscle protein species in dystrophic *mdx* hind limb muscles.

Identified protein species ranged from a molecular mass of 12 kDa (parvalbumin) to 57 kDa (ATP synthase) and with a *pI*-range from 3.9 *pI* (calsequestrin) to 9.0 *pI* (troponin TnT). Spots 1 to 30 represent major muscle-associated protein species from ATP synthase (spot 1), enolase (spots 2 and 3), actin (spot 4), creatine kinase (spots 5,6, 13, 15 and 18), fructose-bisphosphate aldolase A (spots 7 and 8), calsequestrin (spots 9 and 10), tropomyosin (spot 11), malate dehydrogenase (spot 12), phosphate dehydrogenase (spot 14), myozenin-1 (spot 16), carbonic anhydrase (spot 17), various myosin light chains consisting of MLC1/3, MLC2 (spots 19, 26-29), adenylate kinase (spot 20), triosephosphate (spot 21), troponin TnI (spot 22), troponin TnT (spots 23-25) and parvalbumin (spot 30). A significant number of the landmark proteins identified are part of the contractile apparatus.

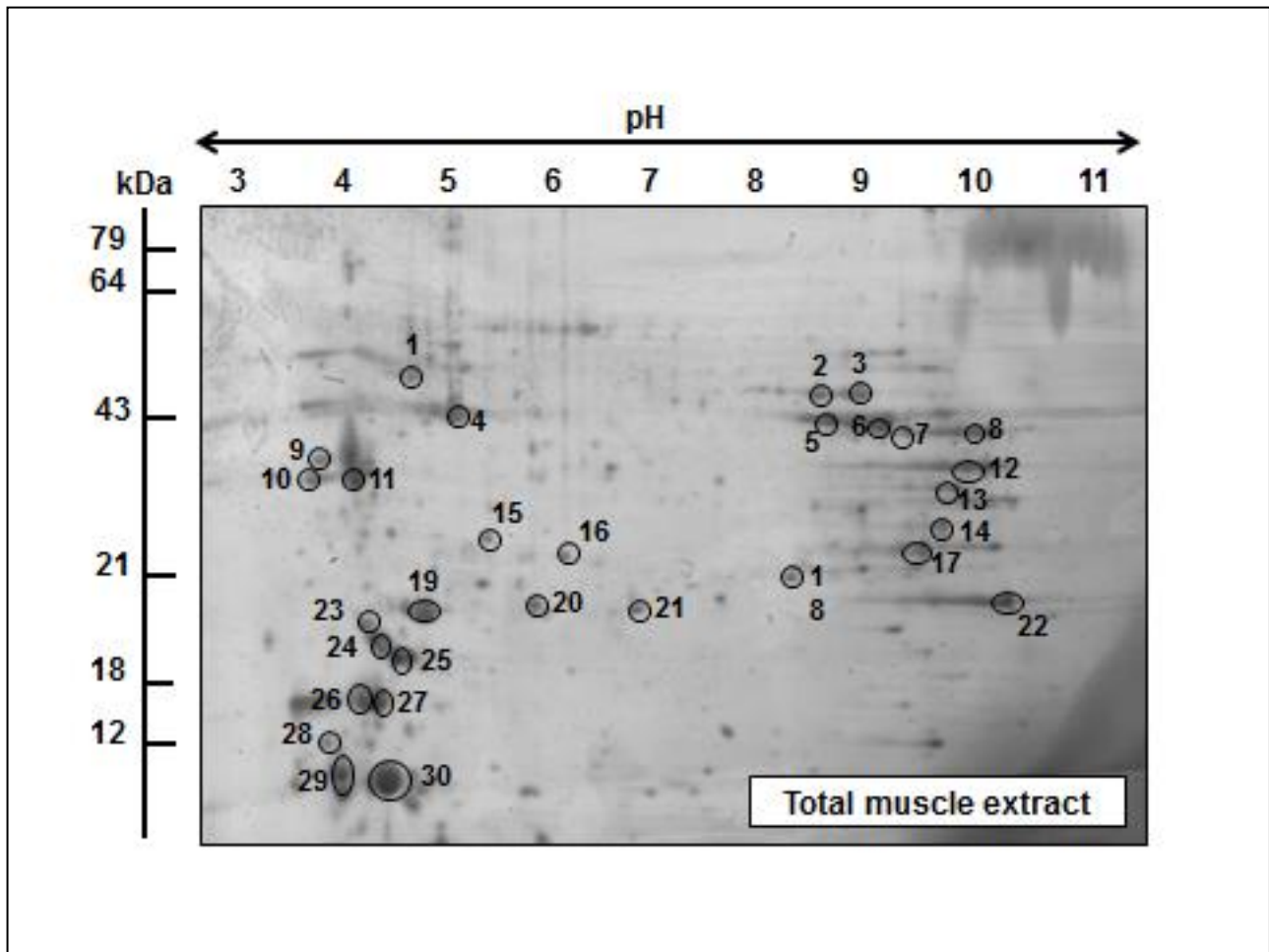


**Figure 6-1 landmark 2D gel of total mouse skeletal muscle extracts**

Figure 6-1 Two-dimensional gel electrophoretic analysis of total muscle extracts. Shown is a RuBPs-stained gel representing major protein species from crude 8-week-hind limb muscle extracts. Major protein spots are numbered 1 to 30 and marked by circles. See Table 6-1 for the mass spectrometric identification of the 2D landmark proteins. The pH-values of the first dimension and molecular mass standards of the second dimension are shown on the top and on the left of the panels, respectively

**Table 6.1 Mass spectrometry list of 2D-landmark proteins from crude tissue extracts**

<b>Spot No.</b>	<b>Protein Name</b>	<b>Accession No.</b>	<b>Isoelectric point (pI)</b>	<b>Molecular mass (Da)</b>	<b>Number of peptides</b>	<b>Coverage (%)</b>	<b>Mascot Score</b>
1	ATP synthase, Atp5b protein	AAH37127	5.24	56632	34	67	834
2	Enolase, beta	NP_031959	6.73	47343	27	63	1249
3	Enolase, beta	NP_031959	6.73	47343	28	61	693
4	Actin, beta	CAA27396	5.78	39451	15	27	481
5	Creatine kinase, M-type	NP_031736	6.58	43250	20	44	911
6	Creatine kinase, M-type	NP_031736	6.58	43250	21	46	949
7	Fructose-bisphosphate aldolase A isoform 2	NP_031464	8.31	39795	21	57	344
8	Fructose-bisphosphate aldolase A isoform 2	NP_031464	8.31	39795	22	66	1063
9	Calsequestrin, skeletal muscle	AAC63616	3.93	45619	12	28	219

10	Calsequestrin, skeletal muscle	AAC63616	3.93	45619	9	25	463
11	Tropomyosin, beta chain isoform 1	NP_033442	4.66	32933	12	30	232
12	Malate dehydrogenase, mitochondrial	NP_032643	8.93	36053	11	44	301
13	Creatine kinase, M-type	NP_031736	6.58	43250	15	34	551
14	Glyceraldehyde-3-phosphate dehydrogenase	AAH85315	7.59	36099	12	46	281
15	Creatine kinase, M-type	NP_031736	6.58	43250	19	43	879
16	Myozenin-1	NP_067483	8.57	31438	13	62	406
17	Carbonic anhydrase, CA3 isoform	NP_031632	6.89	29638	15	58	167
18	Creatine kinase, M-type	NP_031736	6.58	43250	13	23	267
19	Myosin light chain MLC1/3 muscle isoform 1f	NP_067260	4.98	20697	17	78	792
20	Adenylate kinase isoenzyme AK1	NP_067490	5.7	23334	20	74	497

21	Triosephosphate isomerase	AAB48543	5.62	22724	12	83	323
22	Troponin TnI, fast skeletal muscle	NP_033431	8.65	21518	12	31	191
23	Troponin TnT, fast muscle isoform	AAB39743	9.01	29358	6	13	237
24	Troponin TnT, fast muscle isoform	AAL77612	5.08	36537	14	351	8
25	Troponin TnT, fast muscle isoform	AAB39743	9.01	29358	18	378	10
26	Myosin light chain MLC2, skeletal muscle isoform	NP_058034	4.82	19059	92	883	22
27	Myosin light chain MLC2, skeletal muscle isoform	NP_058034	4.82	19059	92	463	21
28	Myosin light chain MLC2, skeletal muscle isoform	NP_058034	4.82	19059	52	162	7
29	Myosin light chain MLC1/3, muscle isoform 1f	NP_067260	4.98	20697	39	313	11
30	Parvalbumin, alpha	NP_038673	5.02	11923	71	659	12

### 6.2.3 DIGE analysis of landmark proteins in the contractile protein-depleted fraction from mouse skeletal muscle

A list of landmark 2D protein spots from the subcellular hind limb muscle fraction are numbered 1 to 39 and marked by circles in the subcellular fraction landmark master gel shown in Fig 6-2. The mass spectrometric identification of these landmark muscle proteins is listed in Table 6-2. This table contains the identified muscle-associated proteins names, international accession number, relative molecular masses, *pI*-values, number of matched peptide sequences, Mascot scores, and percentage sequence coverage of major individual muscle protein species in dystrophic *mdx* hind limb muscles.

Identified protein species ranged from a molecular mass of 12 kDa (parvalbumin) to 86 kDa (phosphofructokinase) and with a *pI*-range from 4.7 *pI* (tropomyosin) to 8.7 *pI* (phosphoglycerate mutase). Spots 1 to 39 represent most abundant subproteomic protein species from transferrin (spot 1), Phosphofructokinase (spot 2), various heat shock protein Hsp70 isoforms (spots 3-6), Pgm2 protein (spot 7), pyruvate kinase (spots 8 and 9), ATP synthase (spot 10), hippocalcin-like protein (spot 11), enolase (spots 12-15 and 22), actin (spot 16), beta-actin-like protein (spot 17), creatine kinase (spot 18), fructose-bisphosphate aldolase (spot 19), tropomyosin (spots 20 and 21), phosphate dehydrogenase (spot 23), malate dehydrogenase (spots 24 and 25), phosphoglycerate mutase (spots 27 and 28), DJ-1 protein (spot 30), peroxide reductase (spot 31), manganese superoxide dismutase (spot 32), phosphatidylethanolamine binding protein (spot 33), adenylate kinase (spot 34), ferritin (spot 35), peptidyl-prolyl isomerase (spot 36), parvalbumin (spots 37 and 38) and hemoglobin (spot 39). In contrast to the total extracts, a substantial number neutral-to-acidic protein species have been removed in the subcellular fraction with limited number of minor spots with contractile.

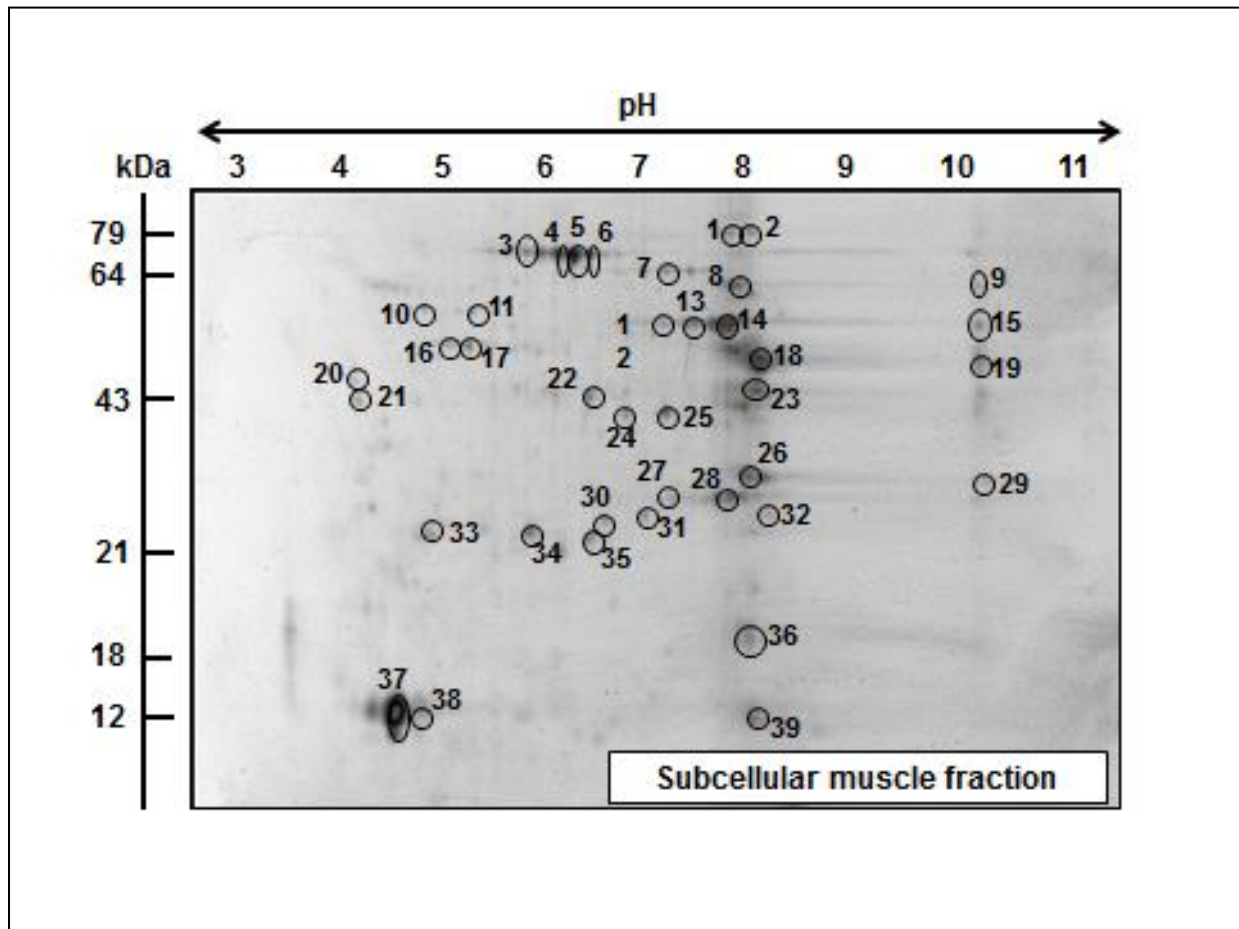


**Figure 6-2 landmark 2D gel of the subcellular mouse muscle fraction**

Figure 6-2 Two-dimensional gel electrophoretic analysis of the subcellular mouse muscle fraction. Shown is a DIGE-labelled gel representing major protein species from the contractile protein-depleted fraction. Major protein spots are numbered 1 to 39 and marked by circles. See Table 6-2 for the mass spectrometric identification of the 2D landmark proteins. The pH-values of the first dimension and molecular mass standards of the second dimension are shown on the top and on the left of the panels, respectively.

**Table 6.2 Mass spectrometry list of 2D-landmark proteins from the subcellular fraction**

<b>Spot No.</b>	<b>Protein Name</b>	<b>Accession No.</b>	<b>Isoelectric point (pI)</b>	<b>Molecular mass (Da)</b>	<b>Number of peptides</b>	<b>Coverage (%)</b>	<b>Mascot Score</b>
1	Transferrin	AAL34533	6.92	78832	4	6	41
2	Phosphofructokinase, muscle	GI:13529638	8.24	86119	8	10	53
3	Heat shock protein Hsp70, inducible	ABK96811	5.53	70378	5	11	136
4	Heat shock protein Hsp70, mitochondrial	BAA04493	5.91	73773	4	7	82
5	Heat shock protein Hsp70, mortalin	AAB28641	5.72	73403	4	6	99
6	Heat shock protein Hsp70, mitochondrial	BAA04493	5.91	73773	2	3	74
7	Pgm2 protein, partial	GI:33416468	6.02	63700	12	24	109
8	Pyruvate kinase, muscle isoform M1	GI:359807367	6.69	58470	11	22	182
9	Pyruvate kinase, muscle isoform M1	GI:359807367	6.69	58470	9	22	148

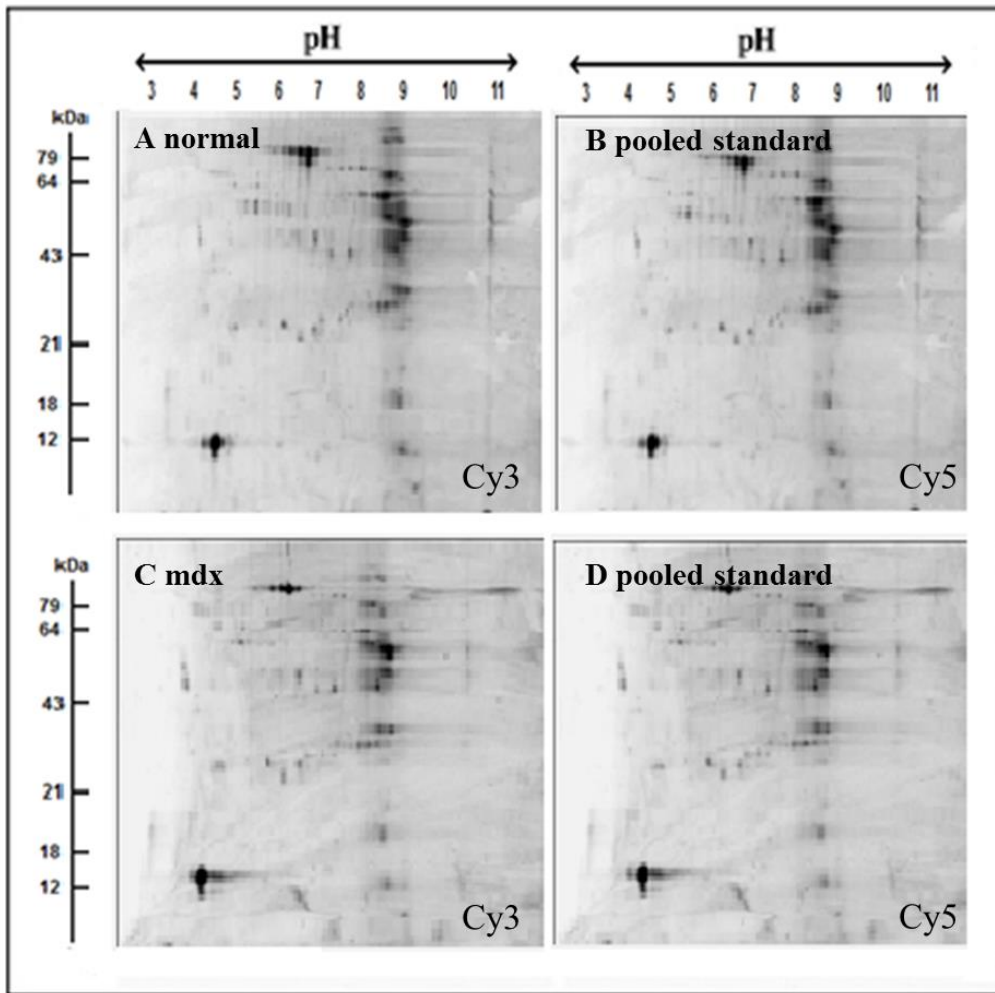
10	ATP synthase Atp5b protein	GI:23272966	5.24	56632	5	12	42
11	Hippocalcin-like protein 1	GI:407263738	5.54	22459	2	28	44
12	Enolase, beta	GI:6679651	6.73	47343	4	14	110
13	Enolase, beta	GI:6679651	6.73	47343	4	13	107
14	Enolase, beta	GI:6679651	6.73	47343	15	45	316
15	Enolase, beta	GI:6679651	6.73	47343	12	35	241
16	Actin, alpha, skeletal muscle	GI:4501881	5.23	42372	7	19	62
17	Beta-actin-like protein 2	GI:30425250	5.3	42325	2	4	44
18	Creatine kinase, M-type	GI:6671762	6.58	43250	6	22	181
19	Fructose-bisphosphate aldolase A isoform 2	GI:6671539	8.31	39795	10	30	71
20	Tropomyosin, beta chain	GI:11875203	4.66	32933	2	9	42
21	Tropomyosin, alpha-1 chain isoform 3	GI:31560030	4.71	32747	9	17	92
22	Enolase, beta	GI:6679651	6.73	47343	5	16	138

23	Glyceraldehyde-3-Phosphate dehydrogenase	GI:6679937	8.44	36077	6	20	83
24	Malate dehydrogenase, cytosolic	GI:387129	6.16	36628	4	16	108
25	Malate dehydrogenase, cytosolic	GI:387129	6.16	36628	4	16	113
26	Phosphoglycerate mutase 2	GI:9256624	8.65	28980	7	22	93
27	Triosephosphate isomerase	GI:54855	6.9	27021	4	20	116
28	Triosephosphate isomerase	GI:54855	6.9	27021	8	55	125
29	Phosphoglycerate mutase 2	GI:9256624	8.65	28980	4	17	60
30	DJ-1 protein	GI:55741460	6.32	20236	3	12	42
31	Thioredoxin-dependent peroxide reductase, mitochondrial	GI:6680690	7.15	28337	4	16	57
32	Manganese superoxide dismutase	GI:53450	8.8	24894	2	3	36

33	Phosphatidylethanol-amine binding protein	GI:1517864	5.19	21018	3	18	93
34	Adenylate kinase, isoenzyme AK1	GI:10946936	5.7	23330	5	33	87
35	Ferritin light chain 1	GI:120524	5.66	20847	4	32	81
36	Peptidyl-prolyl cis-trans isomerase A	NP_032933	7.74	18134	4	35	89
37	Parvalbumin	GI:53819	5.02	11937	3	26	80
38	Parvalbumin	GI:53819	5.02	11937	6	57	136
39	Hemoglobin beta	GI:229301	7.26	15767	5	40	98

#### 6.2.4 Proteomic analysis of dystrophic skeletal muscle

Following the optimisation and initial mass spectrometric identification of landmark muscle proteins in mouse skeletal muscle, comparative DIGE analysis was performed to determine potential differences protein expression patterns in *mdx* skeletal muscle subproteome. 4 biological replicates for each sample type were run using a two dye system. Each repeat contained a subcellular hind limb muscle fraction. Figure 6-3 shows the analytical 2-D gels of Cy3-labelled normal and dystrophic skeletal muscle and corresponding Cy5-labelled pooled standards. The overall 2D spot patterns of normal versus dystrophic mouse skeletal muscle were relatively comparable as a result a detailed denitometric analysis was performed in order to determine potential differences in individual protein species. Densitometric analysis was carried out using a Typhoon Trio variable imager scanner and Samespot Progenesis 2-D analysis software was performed to establish differential protein expression patterns. The detailed proteomic profiling of the contractile protein-depleted fraction revealed distinct changes in 10 muscle protein species in the *mdx* dystrophic muscle preparations.



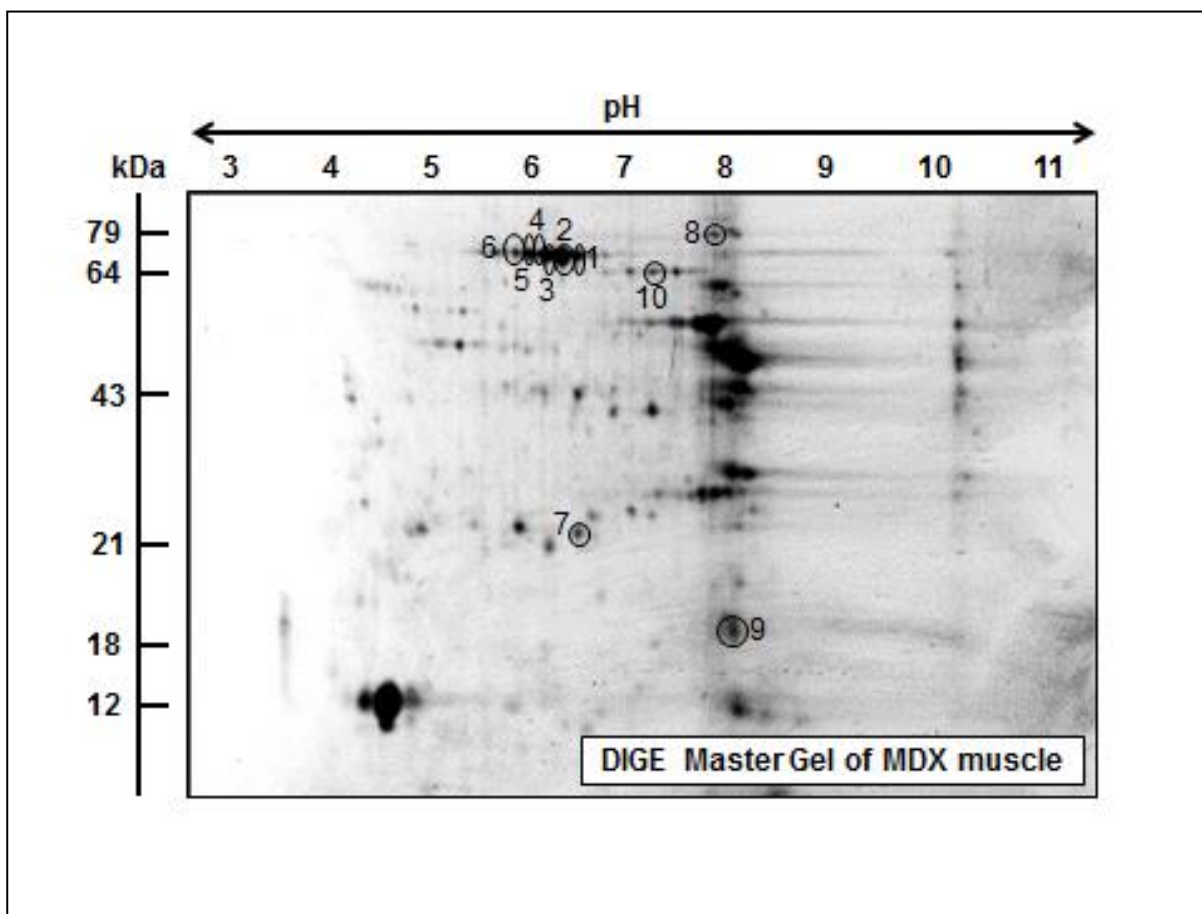
**Figure 6-3 Fluorescence 2D-DIGE analytical gel of normal versus *mdx* skeletal muscle fraction**

Figure 6-3 Two-dimensional gel electrophoretic analysis of the subcellular mouse muscle fraction. Shown are Cy3-labelled gels of the soluble fraction of contractile protein-depleted normal (A) and dystrophic *mdx* (C) skeletal muscle as well as Cy5-labelled gels with all the samples combined to form a pooled standard (B) and (D). Analytical DIGE gels with electrophoretically separated proteins are displayed across 3-11 NL pH range. The pH-values of the first dimension gel system and molecular mass standards (in kDa) of the second dimension are indicated on the top and the left of the panels, respectively.

## 6.2.5 DIGE analysis of dystrophic muscle proteins

The comparative proteomic analysis of normal vs dystrophic *mdx* hind limb muscle, performed with the contractile protein-depleted fraction, revealed altered expression patterns for 10 distinct protein spots. Proteins with significant changes are numbered 1 to 10 and marked by circles in the DIGE master gel Fig 6-4. The mass spectrometric identification of these altered muscle protein species are listed in Table 6-3. This table contains the identified muscle-associated proteins names, international accession number, relative molecular masses, *pI*-values, number of matched peptide sequences, Mascot scores, and percentage sequence coverage of major individual muscle protein species in dystrophic *mdx* hind limb muscles.

Identified protein species ranged from a molecular mass of 18 kDa (peptidyl-prolyl cis-trans isomerase) to 79 kDa (transferrin) and with a *pI*-range from 5.5 *pI* (Hsp70) to 7.7 *pI* (peptidyl-prolyl cis-trans isomerase). Altered proteins were shown to be various isoforms of the molecular chaperone Hsp70 (spots 1-3 and 6), an unnamed protein BAC34145 (spots 4 and 5), ferritin light chain (spot 7), the transferrin protein (spot 8), peptidyl-prolyl cis-trans isomerase (spot 9) and Pgm2 protein (spot 10). While the 2 enzymes were revealed to be decreased in abundance, the heat shock proteins and iron-binding proteins expression levels showed an increased abundance (Table 6-3).



**Figure 6-4 Fluorescence 2D-DIGE master gel of the subcellular mouse muscle fraction**

Figure 6-4 Two-dimensional gel electrophoretic analysis of the subcellular mouse muscle fraction. Shown is a DIGE-labelled gel representing the analysis of dystrophin-deficient hind limb muscles from the *mdx* mouse animal model of Duchenne muscular dystrophy. Protein species with a significantly altered abundance are numbered 1 to 10 and marked by circles. See Table 6-3 for the mass spectrometric identification of the changed muscle proteins in muscular dystrophy. The pH-values of the first dimension and molecular mass standards of the second dimension are shown on the top and on the left of the panels, respectively.

**Table 6.3 List of changed proteins in the subcellular fraction from *mdx* muscle as verified by fluorescent 2D-DIGE analysis**

Spot No.	Protein Name	Accession No.	Isoelectric point (pI)	Molecular mass (Da)	Number of peptides	Coverage (%)	Mascot Score	Fold Change WT v MDX
1	Heat shock protein Hsp70, mitochondrial	BAA04493	5.91	73773	2	3	74	1.9
2	Heat shock protein Hsp70, mortalin	AAB28641	5.72	73403	4	6	99	1.9
3	Heat shock protein Hsp70, mitochondrial	BAA04493	5.91	73773	4	7	82	1.9
4	Unnamed protein product	BAC34145	5.75	70730	11	22	238	1.8
5	Unnamed protein product	BAC34145	5.75	70730	9	18	305	1.8
6	Heat shock protein Hsp70, inducible	ABK96811	5.53	70378	5	11	136	1.7
7	Ferritin light chain 1	GI:120524	5.66	20847	4	32	81	1.6
8	Transferrin	AAL34533	6.92	78832	4	6	41	1.6
9	Peptidyl-prolyl cis-trans isomerase A	NP_032933	7.74	18134	4	35	89	-1.4
10	Pgm2 protein, partial	GI:33416468	6.02	63700	12	24	109	-1.7

## 6.2.6 Immunoblot analysis of dystrophic hind limb muscle

In order to further characterise the *mdx* hind limb muscle, comparative immunoblotting was carried out following the mass spectrometric identification of key changes in the *mdx* skeletal muscle subproteome. Immunoblotting was performed to verify the altered concentration in Hsp70, transferrin, and ferritin light chain protein in normal versus dystrophic muscle preparations (Figure 6-5E, F, H), respectively.

Prior to investigating the novel candidates with distinct changes in expression in the *mdx* hind limb muscle, established biomarker proteins with unchanged concentration, increased expression and decreased expression were blotted. This included Immunolabelling of myosin MLC2, laminin and parvalbumin which exhibited comparable expression levels in normal versus *mdx* preparations (Figure 6-5A, B, G), respectively. In contrast, the dystrophin-associated glycoprotein  $\beta$ -dystroglycan and the extracellular matrix protein collagen revealed significantly altered concentrations in dystrophin-deficient muscle (Figure 6-5C, D), respectively.

Immunoblotting of the novel marker candidates of x-linked muscular dystrophy, as shown here by subcellular proteomics analysis, clearly confirmed their changed expression in dystrophic *mdx* muscle. Immuno-labelled transferrin, Hsp70 and ferritin light chain blots revealed statistically significant reduced levels in *mdx* hind limb muscle (figure 6-5E, F, H), respectively. Immunoblots in Figure 6-5A-F were prepared with crude tissue extracts to establish changes in abundance on the global muscle protein level. However, immune decoration of ferritin light chain did not produce a sufficient signal. Thus ferritin analysis, in combination with the unchanged marker protein parvalbumin, was carried out with the contractile protein-depleted fraction (Figure 6-5G, H) respectively.

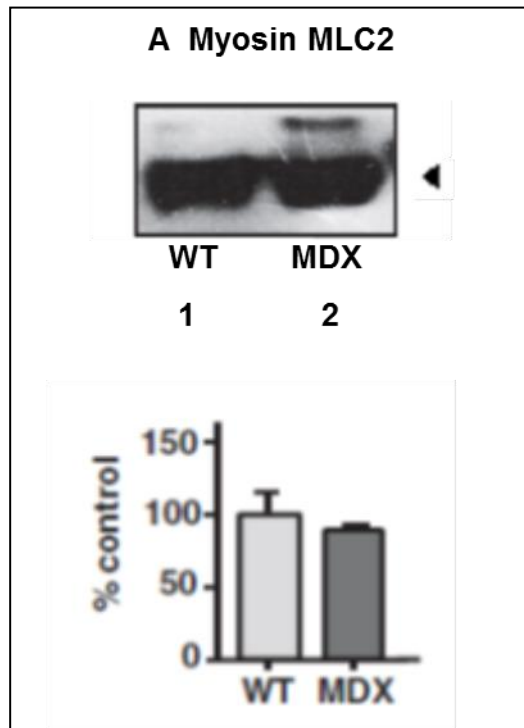


**Figure 6-5A Immunoblotting analysis of unchanged MLC2**

Shown are representative blots with expanded views of immuno-decorated protein bands indicated by the arrowhead, with graphical presentation of the statistical evaluation. Immunoblots were labelled with the myosin MLC2 antibody. Lanes 1, 2 represent normal wild type versus dystrophic muscle from total tissue extracts, respectively. The comparative blotting was statistically verified using an unpaired Student's *t*-test (n=4 replicates).

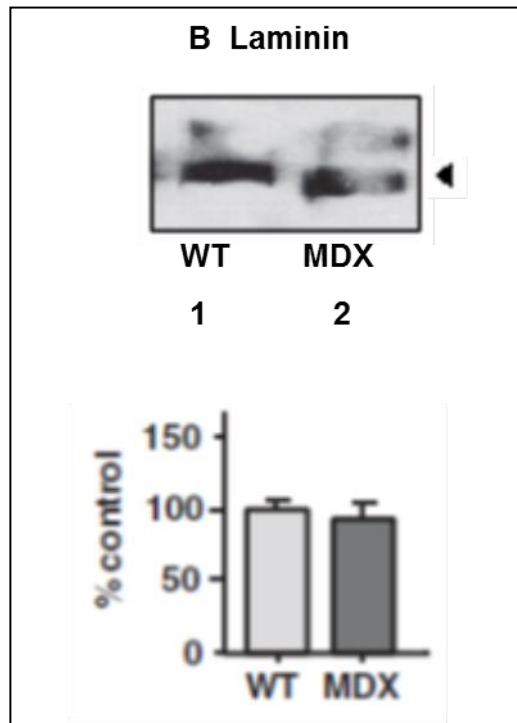


**Figure 6-5B Immunoblotting analysis of equally loaded extracellular matrix protein laminin**

Shown are representative blots with expanded views of immuno-decorated protein bands indicated by the arrowhead, with graphical presentation of the statistical evaluation. Immunoblots were labelled with the laminin antibody, an unchanged protein in dystrophic myofibres. Lanes 1, 2 represent normal wild type versus dystrophic muscle from total tissue extracts, respectively. The comparative blotting was statistically verified using an unpaired Student's *t*-test (n=4 replicates).

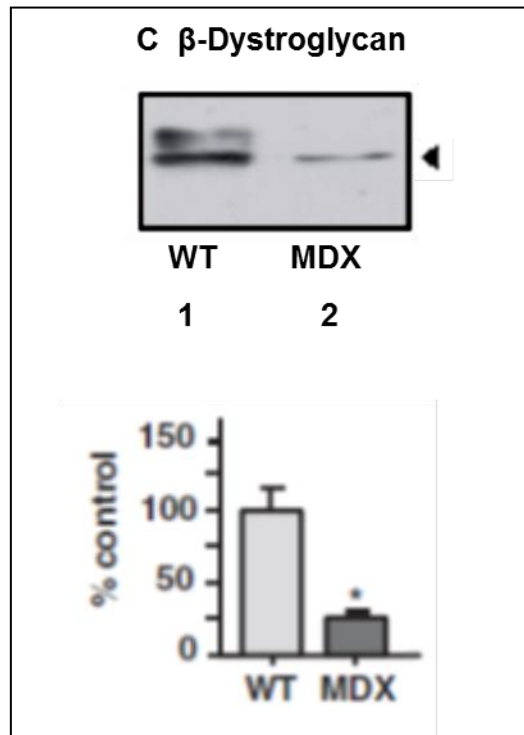


**Figure 6-5C Immunoblotting analysis of dystrophin-associated glycoprotein  $\beta$ -dystroglycan**

Shown are representative blots with expanded views of immuno-decorated protein bands indicated by the arrowhead, with graphical presentation of the statistical evaluation. Immunoblots were labelled with the  $\beta$ -dystroglycan Novocastra antibody. Lanes 1, 2 represent normal wild type versus dystrophic muscle from total tissue extracts, respectively. The comparative blotting was statistically verified using an unpaired Student's *t*-test (n=4 replicates). Standard deviation represented by Error bars, (\* $p < 0.05$ ).

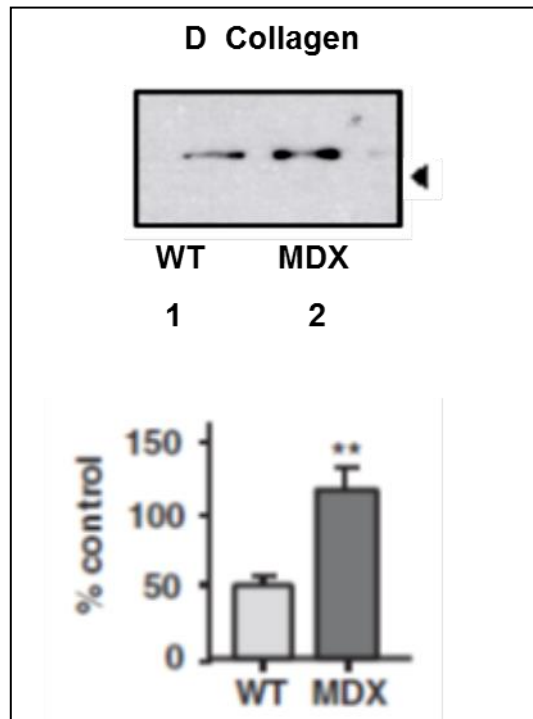


**Figure 6-5D Immunoblotting analysis of extracellular matrix protein collagen**

Shown are representative blots with expanded views of immuno-decorated protein bands indicated by the arrowhead, with graphical presentation of the statistical evaluation. Immunoblot analysis of novel biomarker proteins in hind limb muscle normal versus *mdx*. Immunoblots were labelled with the collagen antibody. Lanes 1, 2 represent normal wild type versus dystrophic muscle from total tissue extracts, respectively. The comparative blotting was statistically verified using an unpaired Student's *t*-test ( $n=4$  replicates). Standard deviation represented by Error bars, (\*\* $p<0.005$ ).

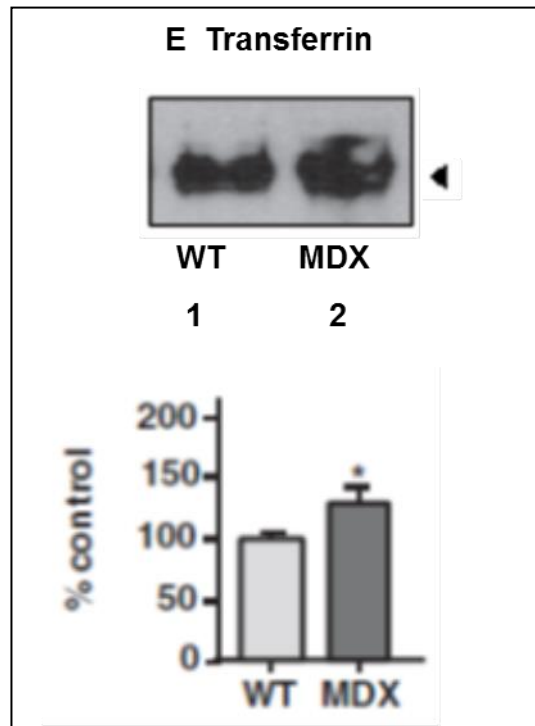


**Figure 6-5E Immunoblotting analysis of iron transporter protein transferrin**

Shown are representative blots with expanded views of immuno-decorated protein bands indicated by the arrowhead, with graphical presentation of the statistical evaluation. Immunoblot analysis of novel biomarker proteins in hind limb muscle normal versus *mdx*. Immunoblots were labelled with the transferrin antibody. Lanes 1, 2 represent normal wild type versus dystrophic muscle from total tissue extracts, respectively. The comparative blotting was statistically verified using an unpaired Student's *t*-test (n=4 replicates). Standard deviation represented by Error bars, (\**p*<0.05).

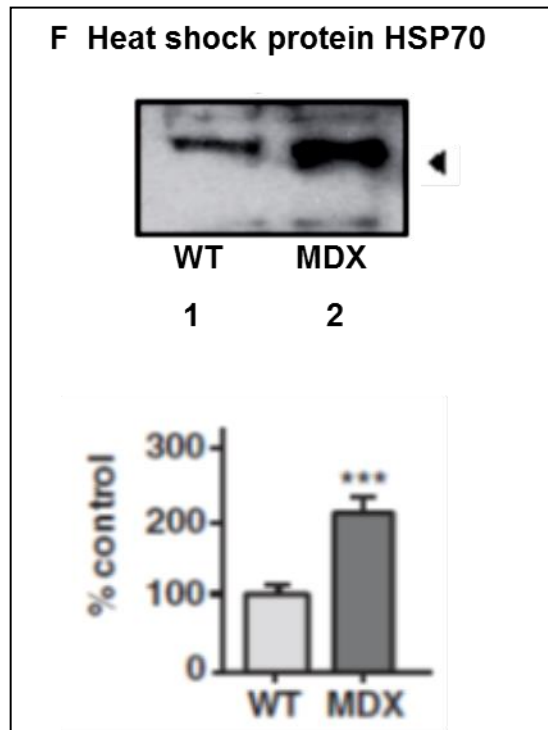


**Figure 6-5F Immunoblotting analysis of large heat shock protein 70**

Shown are representative blots with expanded views of immuno-decorated protein bands indicated by the arrowhead, with graphical presentation of the statistical evaluation. Immunoblot analysis of novel biomarker proteins in hind limb muscle normal versus *mdx*. Immunoblots were labelled with the Hsp70 antibody. Lanes 1, 2 represent normal wild type versus dystrophic muscle from total tissue extracts, respectively. The comparative blotting was statistically verified using an unpaired Student's *t*-test ( $n=4$  replicates). Standard deviation represented by Error bars, (\*\*\*) $p<0.001$ ).

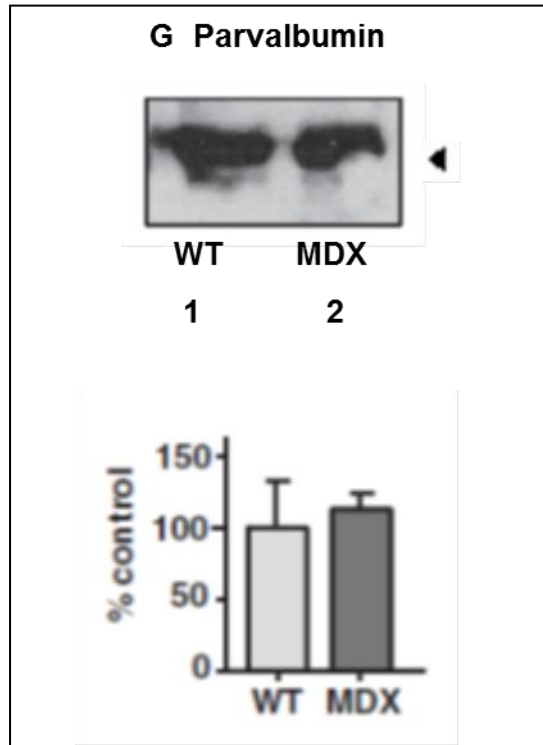


**Figure 6-5G Immunoblotting analysis of unchanged calcium-binding protein parvalbumin**

Shown are representative blots with expanded views of immuno-decorated protein bands indicated by the arrowhead, with graphical presentation of the statistical evaluation. Immunoblots were labelled with the parvalbumin antibody. Lanes 1, 2 represent normal wild type versus dystrophic muscle from the contractile protein-depleted subcellular fraction, respectively. The comparative blotting was statistically verified using an unpaired Student's *t*-test (n=4 replicates).

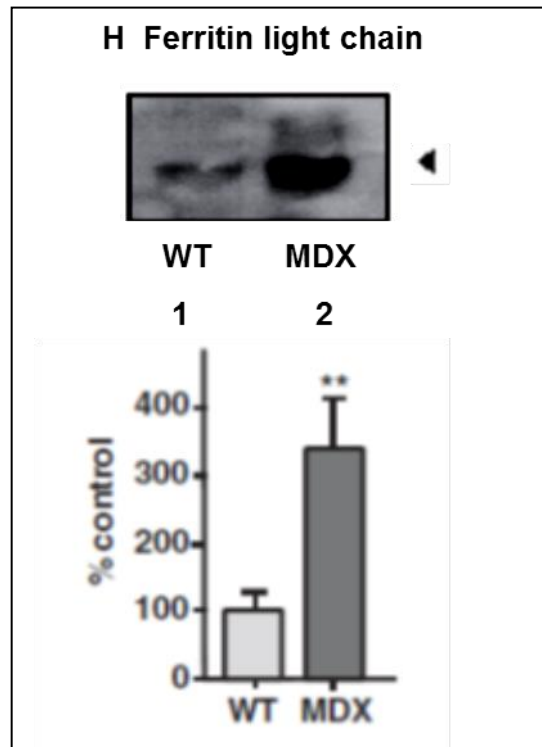


**Figure 6-5H Immunoblotting analysis of iron storage protein ferritin**

Shown are representative blots with expanded views of immuno-decorated protein bands indicated by the arrowhead, with graphical presentation of the statistical evaluation. Immunoblot analysis of novel biomarker proteins in hind limb muscle normal versus *mdx*. Immunoblots were labelled with the ferritin light chain antibody. Lanes 1, 2 represent normal wild type versus dystrophic muscle from the contractile protein-depleted subcellular fraction, respectively. The comparative blotting was statistically verified using an unpaired Student's *t*-test (n=4 replicates). Standard deviation represented by Error bars, (\*\*p<0.005).

## 6.3 Discussion

Duchenne muscular dystrophy is one of the most crippling childhood neuromuscular disorders, therefore meriting comprehensive large-scale studies into the establishment of detailed biomarker signatures of dystrophinopathy (Lewis et al., 2009; Griffin and Rosiers, 2009). Subproteomic surveys have clearly revealed that organelle proteomics is well suited for evaluating global alterations in distinct subcellular fractions from skeletal muscles during pathological or physiological adaptations (Ohlendieck, 2012). Although the primary defects causing X-linked muscular dystrophy are well-known and the resulting absence in the membrane cytoskeletal dystrophin protein is well documented, little is established about the complexity of secondary alterations leading to dystrophinopathy.

In this chapter as outlined in Figure 6-6 below, an investigation into the suitability of introducing a simple subcellular fractionation step to swiftly eliminate a large part of the actomyosin apparatus from muscle homogenates was performed. Subsequently, allowing for the comparative analysis of low level protein species by MS-based subproteomics. The flowchart of Figure 6-6 clearly verifies the different protein expression patterns in the fluorescent 2-D gel images, with the separation of the abundant contractile protein fraction from the pellet representing less frequent muscle proteins.

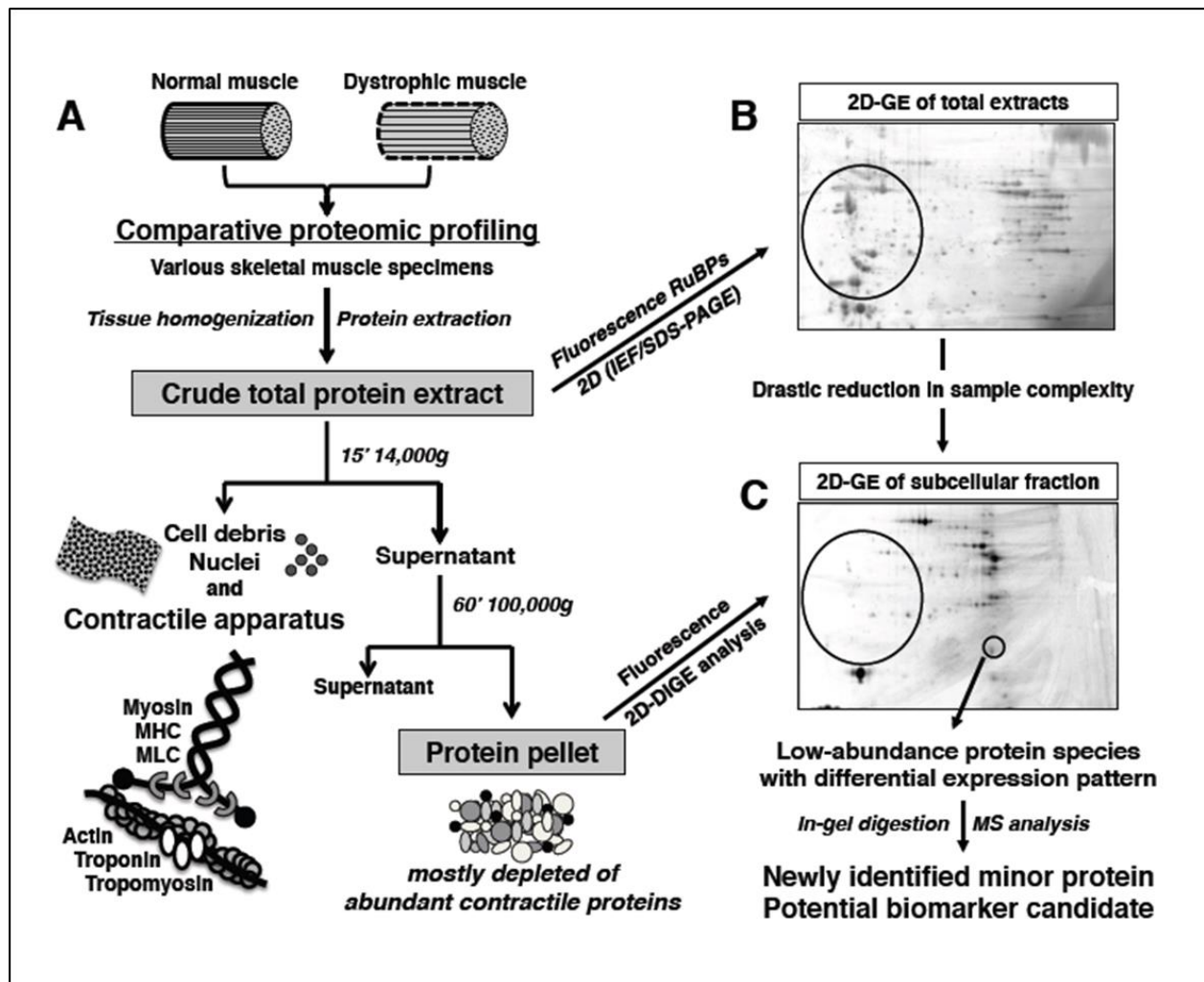


**Figure 6-6 Differential centrifugation of muscle homogenates to obtain a contractile protein-depleted fraction for comparative subproteomic analysis**

Shown is a flowchart of the subcellular fractionation protocol used to swiftly isolate low abundant protein fractions in normal versus dystrophic skeletal muscle homogenates (A). The separation of the abundant contractile protein fraction from the pellet representing less frequent muscle proteins is shown by the considerably different protein expression patterns in the fluorescent 2-D gel images of crude tissue extracts (B) vs the protein pellet following differential centrifugation (C). An open circle represents the contractile protein-containing area of 2D gels in the acidic-to-neutral pI range.

The drastic reduction in protein abundance in the acidic-to-neutral area of the gel image in Figure 6-6C, as compared to the crude extract shown in Figure 6-6B, suggests the successful elimination of a substantial portion of contractile elements, like the actins, troponins, myosins and tropomyosins (Holland and Ohlendieck 2013; Gannon et al., 2009). To confirm the depletion of the actomyosin apparatus, mass spectrometry analysis was performed on the 2-D gels before and after differential centrifugation to clearly identify abundant landmark protein spots.

Table 6-1 lists their identity as actin (spot 4), tropomyosin (spot 11), myosin light chains MLC1f (spots 19, 29), MLC2 (spots 26-28), troponin I (spot 22) and troponin T (spots 23-25). In contrast, many of the contractile muscle proteins have subsequently been eliminated by differential centrifugation. Table 6-2 shows a limited number of proteins with contractile elements, like actin (spots 16, 17) and tropomyosin (spots 20, 21). A number of the other 2D-landmark protein species in both the crude extracts and subcellular fraction of the skeletal muscle homogenates were identified as involved in various processes from the metabolite transport, ion handling and and the cellular stress response.

### 6.3.1 Proteomic expression changes of skeletal muscle analysis

Previous proteomic surveys have predominantly concentrated on total tissue extracts and as a result have identified mainly abundant muscle-associated proteins, such as components involved in various processes from metabolism, ion handling, stabilization of the cytoskeleton and extracellular matrix, excitation-contraction coupling and the cellular stress response (Lewis et al., 2009; Guevel et al., 2011; Gardan-Salmon et al., 2011; Rayavarapu et al., 2013; Carberry et al., 2012a; Carberry et al., 2012b; Carberry et al., 2013b).

In contrast, this chapter as shown that the depletion of the contractile apparatus by differential centrifugation, results in the comparative proteomic profiling of minor low

abundant protein species in normal vs dystrophic preparations. Changes in expression of these minor muscle-associated proteins were identified as various isoforms of the heat shock protein Hsp70, transferrin, ferritin light chain and the enzymes phosphoglucomutase and peptidyl-prolyl cis-trans isomerase in the *mdx* muscle.

### 6.3.2 Increased expression of Iron handling proteins

Transferrin (Szöke and Panteghini, 2012) and ferritin light chain (Crichton and Declercq, 2010) are essential iron-transporting proteins and key elements of iron metabolism (Wang and Pantopoulos, 2011). Elevated levels of transferrin and ferritin proteins in dystrophic muscle support recent findings from the proteomic profiling of the aged *mdx* heart (Holland et al., 2013a) and the aged *mdx* diaphragm, shown in chapter 4.

During the aging dystrophic diaphragm study which investigated 8-week to 22-month range (Carberry et al., 2012a), we also examined the 8-week to 12-month range and recorded a drastic increase in ferritin light chain levels in *mdx* muscle. Deficiency in dystrophin seems to impair iron homeostasis and the elevated iron transporter and binding-protein concentrations possibly suggest a compensatory mechanism to help prevent harmful iron overloading in muscle tissues. The 2-fold increase in concentration of transferrin indicates disruptions in iron absorption and consumption in muscular dystrophy, as circulating transferrin functions as an iron transporter providing iron requirements to tissue proteins (Wang and Pantopoulos, 2011).

### 6.3.3 Perturbed stress response in *mdx* tissue

Elevated levels of molecular chaperones are indicative of intensified cellular stress in dystrophic muscle tissue. One of these key molecular chaperones is Heat shock protein Hsp70 which exists as several different isoforms (Young, 2010). The various isoforms of Hsp70 play a main role in skeletal muscle stress in response to injury, oxidative conditions, reperfusion-induced ischemia, excessive exercise and neuromuscular disorders (Liu et al., 2006). In the aging dystrophic diaphragm study (Carberry et al., 2012a) which examined the 8-week to 12-month range also recorded a significant increase in heat shock protein Hsp70-cognate levels in *mdx* muscle.

During periods of muscle stress molecular chaperone regulation has been shown to be crucial in protecting muscle from damage (Maglara et al., 2003). In general, stress proteins facilitate in protein-protein interactions by helping to stabilise misfolded proteins or peptide clusters as well as regulating their degradation and elimination in order to prevent harmful unwanted accumulation of non-functional protein aggregates (Boluyt et al., 2006). Hence, the observed increase in expression of mitochondrial Hsp70 isoforms can be seen as a compensatory mechanism to protect dystrophic fibers from excessive oxidative stress and supporting previous reports on elevated levels of the small heat shock protein  $\alpha$ Hsp in dystrophic skeletal muscle (Doran et al., 2006a).

### 6.3.4 Other proteins

Besides the molecular chaperone Hsp70, two other protein spots were identified with an increased concentration displaying similar molecular mass and somewhat different isoelectric points. These protein spots relate to an unnamed protein (BAC34145 protein product, gi|26340966|) with unknown function. The reduction in expression of the enzymes phosphoglucomutase and peptidyl-prolyl-isomerase indicates abnormal

glycogen utilisation and impaired protein folding processes in *mdx* muscle, respectively. Phosphoglucomutase facilitates the interconversion of glucose-1-phosphate and glucose 6-phosphate during glycogenesis and glycogenolysis, making it a key protein of glycogen and glucose metabolism in muscle (Ohlendieck, 2011).

Reduced levels of this enzyme indicate impaired glucose utilisation in dystrophic muscle fibers. Peptidyl-prolyl-isomerase facilitates in protein folding by accelerating the process. In oligopeptides, this enzyme mediates the cis-trans isomerisation of proline imidic peptide bonds (Quintá et al., 2011). Therefore, its decreased concentration might reduce the capability of dystrophic muscles to correctly refold certain classes of muscle proteins.

## 6.4 Conclusion

In conclusion, the systematic depletion of abundant contractile proteins from muscle preparations before gel electrophoretic protein separation has resulted in improved access to minor low level protein species from dystrophic muscle. The comparative proteomic profiling of subcellular hind limb fraction of 8-week-old dystrophin-deficient mice versus age-matched control mice has revealed changes in expression levels in a number of interesting proteins and highlighted potential novel biomarker candidates for Duchenne muscular dystrophy.

This chapter demonstrates that the employment of organelle proteomics can overcome particular technical limitations of whole tissue proteomics and should be used to complement these proteomic findings. Since skeletal muscle tissues are characterised by a mainly diverse range of minor low level protein species and a large dynamic range of protein expression patterns, the employment of pre-fractionation procedures significantly reduces sample complexity and thus enables for a more comprehensive coverage of complex muscle protein mixtures and the skeletal

proteome.

## 7 General Discussion

X-linked Duchenne muscular dystrophy is an extremely progressive childhood neuromuscular disorder and can be characterised by primary genetic abnormalities in the dystrophin gene. Defects in the dystrophin gene result in the loss of a crucial 427kDa cytoskeletal membrane protein (Dalkilic and Kunkel, 2003).

The optimisation of animal models is a vital area in biomedical proteomics and proteomic biomarker discovery. The application of gel-based proteomics is routinely employed to establish muscle-associated biomarkers and in recent years been used with the *mdx* animal model of muscular dystrophy for the biochemical evaluation of novel experimental therapies, such as exon skipping for a potential treatment for DMD (Doran et al., 2009b).

The overall goal of this report was to establish a detailed proteomic signature for the *mdx* animal model across various age groups and muscle types. It is important to stress that the muscles in *mdx* mouse exhibit varying degrees of degeneration. This report focused on moderately affected *mdx* hind limb muscles, the mildly affected phenotype of the *mdx interossious* muscle which was shown to be even less necrotic than the *mdx soleus*, *extensor digitorum longus* or *tibialis anterior* muscles. In contrast, the *mdx* diaphragm muscle was shown to be severely affected (Stedman et al., 1991) and aging of the diaphragm exacerbate the dystrophic phenotype (Carberry et al., 2012a). Thus, the aged *mdx* diaphragm muscle more closely resembles that of the neuromuscular pathology exhibited in Duchenne patients (Lefaucheur et al., 1995).

Skeletal muscle proteomics is concerned with the global identification, comprehensive cataloguing and biochemical analysis of the entire protein complement of contractile fibers in normal and pathological specimens (Isfort, 2002). Previous proteomic reports have revealed that MS-based technologies are suitable for studying a representative proportion of muscle-associated proteins involved in regulation, contraction, structure,

metabolism and cellular stress response (Doran et al., 2008; O'Connell et al., 2008; Lewis et al., 2009). Figure 7-1 represents an overview of the past usage of MS-based proteomics employed to characterise the dystrophin-glycoprotein complex and secondary alterations in the dystrophic *mdx* mouse (Holland et al., 2013b). Figure 7-1 includes the various age groups and muscle types evaluated by proteomics and also highlights the comparative proteomic approaches discussed in this report.

Mass spectrometry in combination with fluorescence labelling techniques can detect several thousand muscle-associated proteins in high-resolution 2D gel electrophoresis (Doran et al., 2006b). However, there are limitations to this technique with respect to analysing the entire cellular proteome (Rabilloud et al., 2009). Membrane proteins, high molecular mass proteins and low-level abundance proteins can be challenging to detect in polyacrylamide gels due to the hydrophobic nature, pore size and dynamic range, respectively.

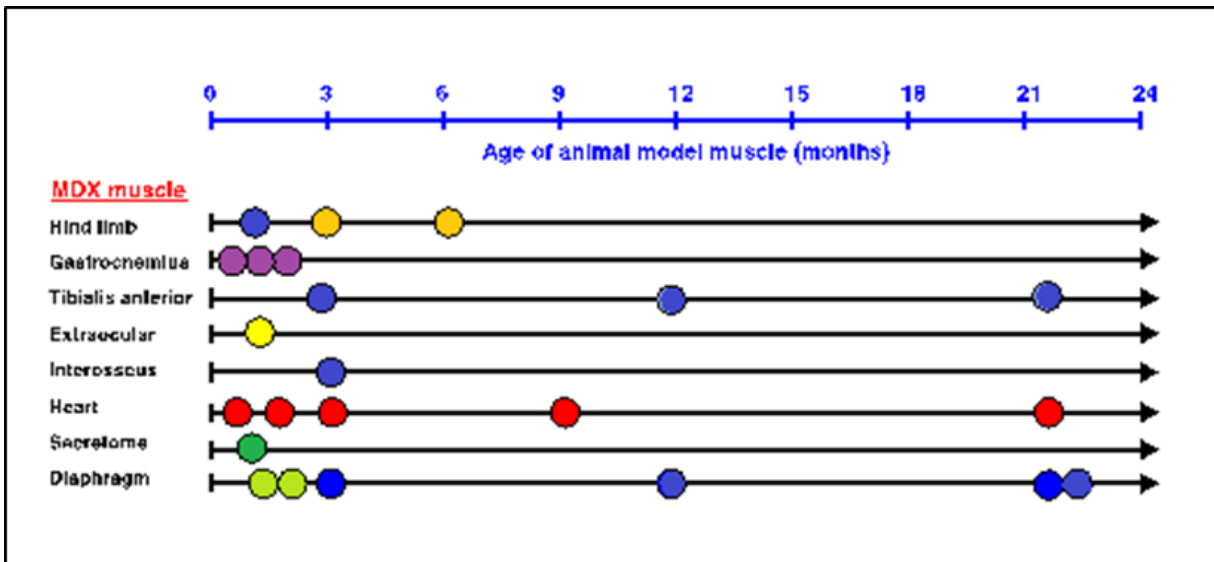


**Figure 7-1 MS-based proteomic profiling of the *mdx* mouse model of Duchenne muscular dystrophy**

Figure 7-1 represents the various types of muscle and age groups of the *mdx* mouse that have been analysed over the recent years to establish global changes in the dystrophic muscle proteome. All highlighted proteomic studies have been discussed in a detailed review of the proteomics of the dystrophin-glycoprotein complex and dystrophinopathy (Staunton et al., 2011). While, the blue circles represent the muscle types covered in this thesis.

Thus, since the main proteins of the actomyosin apparatus and its supporting sarcomeric components frequently negate weak signals from minor muscle protein species during proteomic analyses, we have employed a pre-fractionation step to remove certain parts of this analytical problem (Carberry et al., 2014). In order to eliminate a large portion of highly abundant contractile proteins, differential centrifugation of the crude skeletal muscle extracts were performed to reduce the samples complexity as shown in Chapter 6.

In the *mdx* animal model of dystrophinopathy, different skeletal muscle subtypes are affected to varying degrees resulting from the same single base substitution of the dystrophin gene. Thus, to establish potential muscle subtype-specific alterations in secondary changes due to dystrophin-deficiency, we have performed a comparative proteomic survey of multiple *mdx* muscles. Highlighting alterations in naturally protected and moderately affected phenotypes as shown in Chapter 5.

Furthermore, the established *mdx* mouse model of dystrophinopathy exhibits progressive muscle tissue deterioration with age and more closely resembles the human pathology as a result aged *mdx* muscle specimens were analysed on a large-scale survey of potential age-related changes in the dystrophic phenotype as shown in Chapters 3 and 4. This established senescent *mdx* mouse diaphragm muscle as a more suitable dystrophic phenotype. Thus, we investigated this particular tissue further to determine the global changes in the protein complement during the natural aging process of the *mdx* muscle.

Figure 7-2 illustrates an overview of the proteomic results from the senescent *mdx* mouse model survey for Duchenne muscular dystrophy. Global changes in structural proteins, extracellular proteins, contractile proteins, molecular chaperones, calcium-binding proteins, glycolytic enzymes, mitochondrial enzymes and metabolite transporters suggest changes in the cytoskeletal complex and its indirect linkage to the extracellular matrix, reorganisations within the actomyosin apparatus, an intensified cellular stress response, compromised ion handling and metabolic disturbances.

Overall, this analysis revealed that protein expression patterns are severely changed in dystrophin-deficient *mdx* diaphragm muscle and that these pathobiochemical alterations are more intense compared to that of the different *mdx* skeletal muscles examined in this thesis (Rayavarapu et al., 2013; Ge et al., 2003; Carberry et al., 2012a; Carberry et al., 2013a). Additionally, it was revealed that isoforms of the same protein exhibit differential expression patterns suggesting possible post-translational modifications such as glycosylation demonstrating the complexity of the disease. These features display the benefits of 2-D gel electrophoresis in its ability to present crude soluble protein complement of the muscle fibers.

Elevated levels of dermatopontin and the resulting increase in collagen supports the progressive accumulation of connective tissue in the dystrophic *mdx* diaphragm (et al Carberry). ATP production appears severely disturbed in diaphragm tissue whereas we saw only moderate alterations in ATP production in the moderately affected hind limb muscles and the milder phenotype of the fingers and toes exhibited spared mitochondrial function. This bioenergetic dysfunction of mitochondria in the senescent *mdx* diaphragm indicates that aged mitochondria are incapable of meeting the ATP demand of the dystrophic muscle fibers. In addition, the proteomic findings of a decreased concentration of the vital and rate-limiting metabolite transporters for the utilisation of oxygen and fatty acids, intracellular oxygen transporter myoglobin and the fatty acid binding protein FABP3, suggest the idea of impaired mitochondrial metabolism.

The contractile apparatus degeneration and/or remodeling of the skeletal muscles were indicated here with actin, troponins, tropomyosin and myosin light chains to varying degrees. All the muscle types exhibited an intensified cellular stress response with the up-regulation of various heat shock proteins due to the lack of dystrophin. Increased iron transporter and binding-protein concentrations indicate disruptions in iron absorption and consumption in muscular dystrophy, the elevated abundance suggests impaired iron homeostasis in the degenerating *mdx* diaphragm and hind limb

muscles.

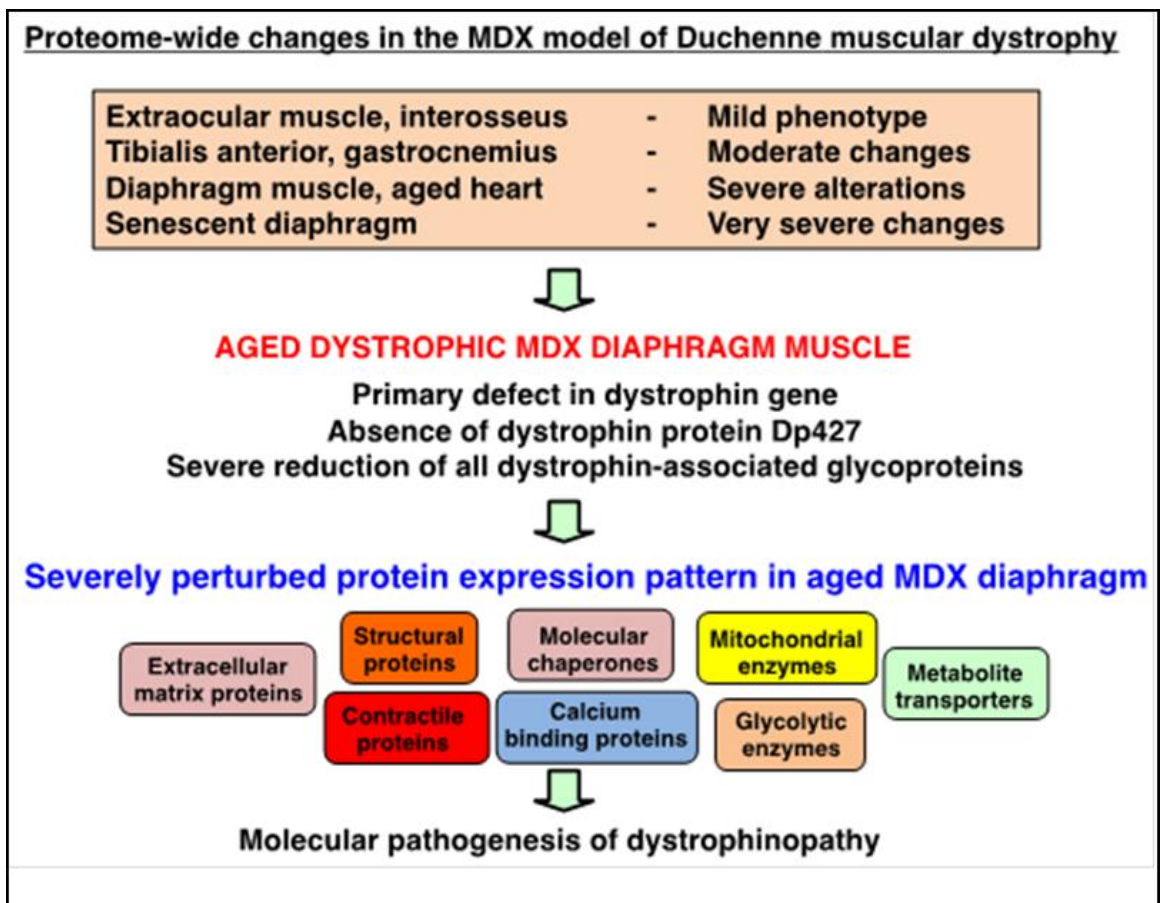


**Figure 7-2 Proteomic survey of the *mdx* animal model for Duchenne muscular dystrophy**

The diagram summarises the key classes of diaphragm proteins identified by the proteomic analysis of the aged and *mdx* dystrophin-deficient mouse model of X-linked muscular dystrophy. The severely affected protein expression pattern of *mdx* dystrophic muscle includes extracellular matrix proteins, structural proteins, contractile proteins, molecular chaperones, calcium-binding proteins, mitochondrial enzymes, glycolytic enzymes and metabolite transporters. Thus, the absence of the dystrophin isoform Dp427 and resulting reduction in dystrophin-associated glycoproteins in the dystrophic sarcolemma seems to trigger a variety of secondary abnormalities in muscular dystrophy.

Sarcolemma disruption is high in *mdx* diaphragm tissue. As the dystrophin protein anchors large membrane glycoprotein complexes within the cell, membrane rupturing occurs due to its absence and results in the loss of membrane integrity. One of these glycoproteins,  $\beta$ -dystroglycan is rescued in the finger and toe muscles of Chapter 5 (Dowling et al., 2004). The rescue of  $\beta$ -dystroglycan reduces the contraction-induced micro-rupturing normally observed in dystrophic tissue. The dystrophic diaphragm revealed progressive accumulation of connective tissue with elevated levels of dermatopontin and the resulting increase in collagen, while the fingers and toes appear naturally protected.

Interestingly, the number of fibers containing central nuclei was lower in the fingers and toes compared to that of the *mdx* hind limb muscles (Fig 5-7). This is vital, since central nucleation is considered as a sign of recent muscle fiber regeneration. The fingers and toes also observed no increase in muscle mass, in contrast to the hind limb muscles. Both central nucleation and the level of hypertrophy of the finger and toe muscles are in line with a less severe impairment (Carberry et al., 2013b).

From our studies we have demonstrated that the INT and FDB muscle are under less stress than the severely dystrophic diaphragm tissue. This is apparent from the stress response possible due to the rescue of the dystroglycan protein and evident from lack of central nucleation and hypertrophy. The smaller diameter of the muscle fibers may facilitate the replacement of utrophin and offer mechanical stability to the cell membrane.

Over the last decade major advances have been made in both the understanding of the molecular genetics and pathogenesis of Duchenne muscular dystrophy. This has raised expectations of a curative treatment with gene therapy. Exon skipping therapy is a form of non-viral gene therapy, were it was hypothesized that one could change the severe DMD phenotype into a milder BMD phenotype, simply if one was able to change the splicing of the DMD gene to produce a smaller in-frame transcript.

A comparative proteomic analysis was performed to evaluate exon skipping as a potential therapeutic approach and revealed a restoration of key muscle-associated proteins after the dystrophin isoform was restored in the dystrophic diaphragm (Doran et al., 2009b). Reversal of differential proteins involved in dystroglycan complex, energy production and calcium handling were significantly expressed. Although this therapy appears promising one of the challenges is the need for personalised therapies. Skipping over a single exon in such a large size gene will only target a small number of suitable candidates to treat (Rando, 2007) (Lim and Rando, 2008) and offer a milder form of the disease and personalised therapies would prove costly at this initial stage of the development.

While the large size and complexity of dystrophin is problematic, it does carry a silver lining as the vast majority of the gene remains unchanged (Menhart, 2003). Thus this major challenge of personalised therapy is partly obviated by the fact some deletions are very common in DMD and that a vast majority of DMD cases are represented by a relatively small number of deletions. This means, theoretically a limited number of antisense oligonucleotides will be effective in a majority of DMD patients (Aartsma-Rus et al., 2003).

Over the years, many pharmacological interventions have been proposed as likely treatments for DMD/BMD. Glucocorticoids offer the only method of preserving muscle function. Though their mechanism(s) of action is unknown, glucocorticoids such as prednisone and prednisone-derivative deflazacort are effective in slowing the progression of DMD. Side effects are associated with both drugs, which include excessive weight gain which can negatively impact muscle function (Biggar et al., 2006). Treatment of DMD boys carried out by using Deflazacort resulted in improved pulmonary function, suggested an improvement in the respiratory muscles (Biggar et al., 2001). There is universal agreement that boys with DMD benefit from corticosteroid treatment.

A number of neuromuscular disorders are characterised by this membrane-spanning complex that a detailed analysis is warranted into its assembly, interactions and maintenance in healthy fibers versus its dysfunction in dystrophic muscle tissue. The comprehensive proteomic study of the high-molecular mass proteins excluded from traditional 2D gels with subsequent MS identification may provide insight into the fate of protein species over the progression of muscular dystrophies. A detailed label-free analysis into severely dystrophic aged diaphragm, mildly affected hind limb and spared extraocular and *interosseus* fibers may provide new insights into the compensatory mechanisms that counteract dystrophic abnormalities. Since the approximately 30,000 protein-coding genes in the human genome are predicted to produce several 100,000 protein species, it is assumed that the number of muscle-associated protein isoforms far exceeds that of the skeletal muscle-specific genes. Therefore, future studies into the analysis of post-translational modifications and the classification of protein isoforms in healthy and diseased muscle is warranted.

In recent years, comparative proteomic studies with *mdx* muscle tissue extracts have shown significant alterations in the enzyme adenylate kinase AK1 (Marouga et al., 2005; Ng et al., 2012; Theodoridis et al., 2012), the actin binding protein profilin, the fatty acid binding protein FABP3 (Okamoto and Fujiwara, 2006), the cytosolic Ca<sup>2+</sup>-binding protein parvalbumin (Stastna and van Eyk, 2012), the Ca<sup>2+</sup>-binding protein calsequestrin CSQf (Cox and Mann 2011), the enzyme carbonic anhydrase CA3 (Carberry et al., 2012b), the molecular chaperone cvHsp/HspB7 (Marouga et al., 2005; Kato et al., 2011), the oxygen carrier myoglobin (Stastna and van Eyk, 2012), different isoforms of annexin (Okamoto and Fujiwara, 2006), the ion transporter transferrin (Forbes et al., 1994; Graham et al., 2010), the mitochondrial enzyme isocitrate dehydrogenase (Kornegay et al., 2012; Stastna and van Eyk, 2012; Mallick and Kuster, 2010) and the extracellular matrix protein dermatopontin (Mouisel et al., 2010).

These proteomic profiles of the *mdx* mouse were performed with multiple muscle

subtypes, variety of tissue extracts or subcellular fractions, various protein separation techniques, opposing labelling methods and different mass spectrometric techniques. The proteomic results in this report has established that the abundance of annexin, carbonic anhydrase, cvHsp, profiling, transferrin and dermatopontin is severely increased and that the concentration of adenylate kinase, calsequestrin, isocitrate dehydrogenase, myoglobin, and parvalbumin is drastically reduced in dystrophic model of Duchenne muscular dystrophy. This makes these proteins suitable biomarker candidates of dystrophinopathy, which might be helpful to evaluate diagnostic, prognostic or therapeutic approaches. With a number of potential blood-based biomarkers present such as transferrin they could offer a simpler, cheaper and less invasive means for obtaining and analysing samples.

In conclusion, the proteomic results presented here indicate that the aged *mdx* diaphragm, which shows severe respiratory impairment following fibrosis (Ishizaki et al., 2008), is a suitable model system to study the molecular pathogenesis of Duchenne muscular dystrophy. Although the cure for DMD remains elusive gene therapies such as exon skipping does provide hope. While supportive care remains vital until a curative treatment has been developed, with the use of corticosteroids, physiotherapy and orthoses shown to increase life expectancy and quality of life DMD patients considerably.

## **Bibliography**

Aartsma-Rus, A., A. A. Janson, W. E. Kaman, M. Bremmer-Bout, J. T. den Dunnen, and F. Baas. 2003. Therapeutic antisense-induced exon skipping in cultured muscle cells from six different DMD patients. *Hum Mol Genet* 12: 907–914.

Adams, M. E., M. H. Butler, T. M. Dwyer, M. F. Peters, A. A. Murnane, and S. C. Froehner. 1993. Two forms of mouse syntrophin, a 58 kD dystrophin-associated protein, differ in primary structure and tissue distribution. *Neuron* 11 (3): 531-40.

Agbulut, O., P. Noirez, G. Butler-Browne, and H. Jockusch. 2004. Specific isomyosin proportions in hyperexcitable and physiologically denervated mouse muscle. *FEBS Lett.* 561(1-3): 191-194.

Ahn, A. H., C. A. Freener, E. Gussoni, M. Yoshida, E. Ozawa, and L. M. Kunkel. 1996. The three human syntrophin genes are expressed in diverse tissues, have distinct chromosomal locations, and each bind to dystrophin and its relatives. *J Biol Chem* 271 (5): 2724-30.

Ahn, A. H., M. Yoshida, M. S. Anderson, C. A. Feener, S. Selig, Y. Hagiwara, E. Ozawa, and L. M. Kunkel. 1994. Cloning of human basic A1, a distinct 59-kDa dystrophin-associated protein encoded on chromosome 8q23-24. *Proc Natl Acad Sci USA* 91 (10): 4446-50.

Alderton, J. M., and R. A. Steinhardt. 2000. Calcium influx through calcium leak channels is responsible for the elevated levels of calcium-dependent proteolysis in dystrophic myotubes. *J Biol Chem* 275: 9452-9460.

Anderson, L., and J. Seilhamer. 1997. A comparison of selected mRNA and protein abundances in human liver. *Electrophoresis* 18 (3-4): 533-7.

Andres-Mateos, E., H. Brinkmeier, T. N. Burks, R. Mejias, D. C. Files, M. Steinberger, A. Soleimani, R. Marx, J. L. Simmers, B. Lin, E. Finanger Hedderick, T. G. Marr, B. M. Lin, C. Hourde, L. A. Leinwand, D. Kuhl, M. Foller, S. Vogelsang, I. Hernandez-Diaz, D. K. Vaughan, D. Alvarez de la Rosa, F. Lang, and R. D. Cohn. 2013. Activation of serum/glucocorticoid-induced kinase 1 (SGK1) is important to maintain skeletal muscle homeostasis and prevent atrophy. *EMBO Mol Med* 5: 80-91.

- Barresi, R., S. A. Moore, C. A. Stolle, J. R. Mendell, and K. P. Campbell. 2000. Expression of gamma-sarcoglycan in smooth muscle and its interaction with the smooth muscle sarcoglycan-sarcospan complex. *J Biol Chem* 275 (49): 38554-60.
- Biggar, W.D., M. Gingras, D. L. Fehlings, V. A. Harris, and C. A. Steele. 2001. Deflazacort treatment of Duchenne muscular dystrophy. *J Pediatr* 138: 45-50.
- Biggar, W.D., V. A. Harris, L. Eliasoph, and B. Alman. 2006. Long-term benefits of deflazacort treatment for boys with Duchenne muscular dystrophy in their second decade. *Neuromuscular Disorders* 16: 249-255.
- Blake, D. J., A. Weir, S. E. Newey, and K. E. Davies. 2002. Function and genetics of dystrophin and dystrophin-related proteins in muscle. *Physiol Rev* 82 (2): 291-329.
- Boittin, F. X., G. Shapovalov, C. Hirn, and U. T. Rüegg. 2010. Phospholipase A2 derived lysophosphatidylcholine triggers Ca<sup>2+</sup> entry in dystrophic skeletal muscle fibers. *Biochem Biophys Res Commun* 391: 401-406.
- Bottinelli, R., R. Betto, S. Schiaffino, and C. Reggiani. 1994. Maximum shortening velocity and coexistence of myosin heavy chain isoforms in single skinned fast fibers of rat skeletal muscle. *J Muscle Res Cell Motil.* 15(4): 413-419.
- Boyce, F. M., A. H. Beggs, C. Feener, and L. M. Kunkel. 1991. Dystrophin is transcribed in brain from a distant upstream promoter. *Proc Natl Acad Sci USA* 88 (4): 1276-80.
- Bozzo, C., B. Spolaore, L. Toniolo, L. Stevens, B. Bastide, C. Cieniewski-Bernard, A. Fontana, Y. Mounier and C. Reggiani. 2005. Nerve influence on myosin light chain phosphorylation in slow and fast skeletal muscles. *FEBS J* 272: 5771-5785.
- Bradford, M. M. 1976. A rapid and sensitive method for the quantitation of microgram quantities of protein utilizing the principle of protein-dye binding. *Anal Biochem* 72: 248-254.
- Brownson, C., and P. Loughna. 1996. Alterations in the mRNA levels of two metabolic enzymes in rat skeletal muscle during stretch-induced hypertrophy and disuse atrophy. *Pflügers Archiv-European Journal of Physiology* 431 (6): 990-992.

- Brownson, C., H. Isenberg, W. Brown, S. Salmons, and Y. Edwards. 1988. Changes in skeletal muscle gene transcription induced by chronic stimulation. *Muscle & Nerve* 11 (11): 1183-1189.
- Burniston, J. G., and E. P. Hoffman. 2011. Proteomic responses of skeletal and cardiac muscle to exercise. *Expert Rev Proteomics* 8 (3): 361-377.
- Byers, T. J., H. G. Lidov, and L. M. Kunkel. 1993. An alternative dystrophin transcript specific to peripheral nerve. *Nat Genet* 4 (1): 77-81.
- Campbell, K. P. 1995. Three muscular dystrophies: loss of cytoskeleton extracellular matrix linkage. *Cell* 80 (5): 675-9.
- Campbell, K. P., and S. D. Kahl. 1989. Association of dystrophin and an integral membrane glycoprotein. *Nature London* 338 (6212): 259-62.
- Carberry, S., H. Brinkmeier, Y. Zhang, C. K. Winkler, and K. Ohlendieck. 2013b. Comparative proteomic profiling of soleus, extensor digitorum longus, flexor digitorum brevis and interosseus muscle from the *mdx* mouse model of Duchenne muscular dystrophy. *Int J Mol Med* 32: 544–556.
- Carberry, S., M. Zweyer, D. Swandulla, and K. Ohlendieck. 2012b. Profiling of age-related changes in the tibialis anterior muscle proteome of the *mdx* mouse model of dystrophinopathy. *J. Biomed Biotechnol* 2012: 691641.
- Carberry, S., M. Zweyer, D. Swandulla, and K. Ohlendieck. 2013a. Application of Fluorescence Two-Dimensional Difference In-Gel Electrophoresis as a Proteomic Biomarker Discovery Tool in Muscular Dystrophy Research. *BIOLOGY* 2: 1438-1464.
- Carberry, S., M. Zweyer, D. Swandulla, and K. Ohlendieck. 2014. Comparative proteomic analysis of the contractile-protein-depleted fraction from normal versus dystrophic skeletal muscle. *Anal Biochem* 446: 108-115.
- Carberry, S., M. Zweyer, D. Swandulla, K. Ohlendieck. 2012a. Proteomics reveals drastic increase of extracellular matrix proteins collagen and dermatopontin in the aged *mdx* diaphragm model of Duchenne muscular dystrophy. *Int J Mol Med* 30: 229-234.

Carlson, C. G., and R. V. Makiejus. 1990. A noninvasive procedure to detect muscle weakness in the *mdx* mouse. *Muscle Nerve* 13 (6):480-4.

Chamberlain, J. S., J. Metzger, M. Reyes, D. Townsend, and J.A. Faulkner. 2007. Dystrophin-deficient *mdx* mice display a reduced life span and are susceptible to spontaneous rhabdomyosarcoma. *Federation of American Societies for Experimental Biology Journal* 21 (9): 2195-2204.

Clark, K. A., A. S. McElhinn, M. C. Beckerle, and C. C. Gregorio. 2002. Striated muscle cytoarchitecture: an intricate web of form and function. *Annu Rev Cell Dev Biol* 18: 637-706.

Conjard, A., M. Peuker, and D. Pette. 1998. Energy state and myosin heavy chain isoforms in single fibers of normal and transforming rabbit muscles. *Pflugers Arch.* 436(6): 962-969.

Conte, G, Gioja L. 1836. Scrofola del sistema muscolare. *Ann Clin Osp Incurabili Napoli* 2: 66-79.

Cooke, R. 1986. The mechanism of muscle contraction. *CRC Crit Rev Biochem* 21 (1): 53-118.

Cote, C. H., F. Ambrosio, and G. Perreault. 1999. Metabolic and contractile influence of carbonic anhydrase III in skeletal muscle is age dependent. *American Journal of Physiology* 276 (2): R559-R565.

Cox, J., and M. Mann. 2011. Quantitative, high-resolution proteomics for data-driven systems biology. *Annu Rev Biochem* 80: 273–299.

Crichton, R. R., and J. P. Declercq. 2010. X-ray structures of ferritins and related proteins. *Biochim Biophys Acta* 1800: 706-718.

Crosbie, R. H., J. Heighway, D. P. Venzke, J. C. Lee, and K. P. Campbell. 1997. Sarcospan, the 25-kDa transmembrane component of the dystrophin-glycoprotein complex. *J Biol Chem* 272 (50): 31221-4.

Culligan, K., L. Glover, P. Dowling, and K. Ohlendieck. 2001. Brain dystrophin-glycoprotein complex: persistent expression of  $\beta$ -dystroglycan, impaired

oligomerization of Dp71 and up-regulation of utrophins in animal models of muscular dystrophy. *BMC Cell Biol* 2:2.

Dalkilic, I., and L. M. Kunkel. 2003. Muscular dystrophies: genes to pathogenesis. *Curr Opin Genet Dev* 13 (3): 231-238.

Deconinck, A. E., J. A. Rafael, J. A. Skinner, S. C. Brown, A. C. Potter, L. Metzinger, D. J. Watt, J. G. Dickson, J. M. Tinsley, and K. E. Davies. 1997. Utrophin-dystrophin deficient mice as a model for Duchenne muscular dystrophy. *Cell* 90 (4): 717-27.

Dellefave, M. L., and E. M. McNally. 2007. Cardiomyopathy in neuromuscular disorders. *Progress in Pediatric Cardiology* 24: 35-46.

Donoghue, P., P. Doran, P. Dowling, and K. Ohlendieck. 2005. Differential expression of the fast skeletal muscle proteome following chronic low-frequency stimulation. *Biochim Biophys Acta* 1752: 166-176.

Donoghue, P., P. Doran, K. Wynne, K. Pedersen, M. J. Dunn and K. Ohlendieck. 2007. Proteomic profiling of chronic low-frequency stimulated fast muscle. *Proteomics* 7: 3417-3430.

Doran, P., G. Martin, P. Dowling, H. Jockusch, and K. Ohlendieck. 2006a. Proteome analysis of the dystrophin-deficient *MDX* diaphragm reveals a drastic increase in the heat shock protein  $\alpha$ HSP. *Proteomics* 6 (16): 4610-21.

Doran, P., K. O'Connell, J. Gannon, M. Kavanagh, and K. Ohlendieck. 2008. Opposite pathobiochemical fate of pyruvate kinase and adenylate kinase in aged rat skeletal muscle as revealed by proteomic DIGE analysis. *Proteomics* 8 (2): 364-77.

Doran, P., P. Dowling, P. Donoghue, M. Buffini, and K. Ohlendieck. 2006b. Reduced expression of regucalcin in young and aged *mdx* diaphragm indicates abnormal cytosolic calcium handling in dystrophin-deficient muscle. *Biochim Biophys Acta* 1764 (4): 773-85.

Doran, P., P. Donoghue, K. O'Connell, J. Gannon, and K. Ohlendieck. 2009a. Proteomics of skeletal muscle aging. *Proteomics* 9 (4): 989-1003.

Doran, P., S. D. Wilton, S. Fletcher, and K. Ohlendieck. 2009b. Proteomic profiling of antisense-induced exon skipping reveals reversal of pathobiochemical abnormalities in dystrophic *mdx* diaphragm. *Proteomics* 9 (3): 671-85.

Dowling, P., P. Doran, J. Lohan, K. Culligan, and K. Ohlendieck. 2004. Naturally protected muscle phenotypes: Development of Novel Treatment Strategies for Duchenne Muscular Dystrophy. *Basic Appl Myol* 14 (3): 169-177.

D'Souza, V. N., T. M. Nguyen, G. E. Morris, W. Karges, D. A. Pillers, and P. N. Ray. 1995. A novel dystrophin isoform is required for normal retinal electrophysiology. *Hum Mol Genet* 4 (5): 837-42.

Duchenne, G. B. A. 1868. Recherches sur la paralysie musculaire pseudohypertrophique. *Arch Gen Med* 11: 552-588.

Egan, B., P. Dowling, P. L. O' Connor, M. Henry, P. Meleady, J. R. Zierath, and D. J. O'Gorman. 2011. 2-D DIGE analysis of the mitochondrial proteome from human skeletal muscle reveals time course-dependent remodelling in response to 14 consecutive days of endurance exercise training. *Proteomics* 11(8): 1413-28.

Emery, A. E. 2002. The muscular dystrophies. *Lancet* 359 (9307): 687-695.

Farley, J. M., and P. R. Miles. 1977. Role of depolarization in acetylcholine-induced contractions of dog trachealis muscle. *J Pharmacol Exp Ther* 201 (1): 199-205.

Fenn, J. B., M. Mann, C. K. Meng, S. F. Wong, and C. M. Whitehouse. 1989. Electrospray ionization for mass spectrometry of large biomolecules. *Science* 246 (4926): 64-71.

Forbes, E. G., A. D. Cronshaw, J. R. MacBeath, and D. J. Hulmes. 1994. Tyrosine-rich acidic matrix protein (TRAMP) is a tyrosine-sulphated and widely distributed protein of the extracellular matrix. *FEBS Lett* 351: 433-436.

Fremont, P., P. M. Charest, C. Cote C, and P. A. Rogers. 1988. Carbonic anhydrase III in skeletal muscle fibers: an immunocytochemical and biochemical study. *Journal of Histochemistry & Cytochemistry* 36 (7): 775-782.

- Franceschini, A., D. Szklarczyk, S. Frankild, M. Kuhn, et al. 2013. STRING v9.1: protein-protein interaction networks, with increased coverage and integration. *Nucleic Acids Res* 41(Database issue): D808-D815.
- Gannon, J., P. Doran, A. Kirwan, and K. Ohlendieck. 2009. Drastic increase of myosin light chain MLC-2 in senescent skeletal muscle indicates fast-to-slow fibre transition in sarcopenia of old age. *Eur J Cell Biol* 88: 685-700.
- Gardan-Salmon, D., J. M. Dixon, S. M. Lonergan, and J. T. Selsby. 2011. Proteomic assessment of the acute phase of dystrophin deficiency in *mdx* mice. *Eur J Appl Physiol* 111: 2763-2773.
- Ge, Y., M. P. Molloy, J. S. Chamberlain, and P. C. Andrews. 2003. Proteomic analysis of *mdx* skeletal muscle: Great reduction of adenylate kinase 1 expression and enzymatic activity. *Proteomics* 3: 1895–1903.
- Geers, C., and G. Gros. 2000. Carbon dioxide transport and carbonic anhydrase in blood and muscle. *Physiological Reviews* 80 (2): 681-715.
- Gelfi, C., A. Vigano, S. D. Palma, M. Ripamonti, S. Begum, P. Cerretelli, and R. Wait. 2006. 2-D protein maps of rat gastrocnemius and soleus muscles: a tool for muscle plasticity assessment. *Proteomics* 6: 321-340.
- Goldspink, G., K. Fernandes, P. E. Williams, and D. J. Wells. 1994. Age-related changes in collagen gene expression in the muscles of *mdx* dystrophic and normal mice. *Neuromuscul Disord* 4: 183-191.
- Gonzalez, B., P. Negredo, R. Hernando, and R. Manso. 2002. Protein variants of skeletal muscle regulatory myosin light chain isoforms: prevalence in mammals, generation and transitions during muscle remodelling. *Pflügers Arch* 443: 377-386.
- Gordon, A. M., E. Homsher, and M. Regnier. 2000. Regulation of contraction in striated muscle. *Physiol Rev* 80: 853-924.
- Gorecki, D. C., A. P. Monaco, J. M. Derry, A. P. Walker, E. A. Barnard, and P. J. Barnard. 1992. Expression of four alternative dystrophin transcripts in brain regions regulated by different promoters. *Hum Mol Genet* 1 (7): 505-10.

Graham, K. M., R. Singh, G. Millman, G. Malnassy, F. Gatti, K. Bruemmer, C. Stefanski, H. Curtis, J. Sesti and C. G. Carlson. 2010. Excessive collagen accumulation in dystrophic (*mdx*) respiratory musculature is independent of enhanced activation of the NF-kappaB pathway. *J Neurol Sci* 294: 43-50.

Griffin, J. L., and C. Des Rosiers. 2009. Applications of metabolomics and proteomics to the *mdx* mouse model of Duchenne muscular dystrophy: lessons from downstream of the transcriptome. *Genome Medicine* 1 (3): 32.

Guenet, J. L. 2011. Animal models of human genetic diseases: do they need to be faithful to be useful? *Mol Genet Genomics* 286: 1-20.

Guevel, L., J. R. Lavoie, C. Perez-Iratxeta, K. Rouger, L. Dubreil, M. Feron, S. Talon, M. Brand, and L. A. Megeney. 2011. Quantitative proteomic analysis of dystrophic dog muscle. *Journal of Proteome Research* 10 (5): 2465-2478.

Gundersen, K. 2011. Excitation-transcription coupling in skeletal muscle: the molecular pathways of exercise. *Biol Rev Camb Philos Soc* 86: 564-600.

Head, S. I. 2010. Branched fibres in old dystrophic *mdx* muscle are associated with mechanical weakening of the sarcolemma, abnormal Ca<sup>2+</sup> transients and a breakdown of Ca<sup>2+</sup> homeostasis during fatigue. *Experimental Physiology* 95 (5): 641-656.

Hohenester, E., D. Tisi, J. F. Talts, and R. Timpl. 1999. The crystal structure of a laminin G-like module reveals the molecular basis of alpha-dystroglycan binding to laminins, perlecan and agrin. *Mol Cell* 4 (5): 783-92.

Holland, A., and K. Ohlendieck. 2013. Proteomic profiling of the contractile apparatus from skeletal muscle. *Expert Rev Proteomics* 10: 239–257.

Holland, A., P. Dowling, M. Zweyer, D. Swandulla, M. Henry, M. Clynes, and K. Ohlendieck. 2013a. Proteomic profiling of cardiomyopathic tissue from the aged *mdx* model of Duchenne muscular dystrophy reveals a drastic decrease in laminin, nidogen and annexin. *Proteomics* 13: 2312–2323.

Holland, A., S. Carberry, and K. Ohlendieck. 2013b. Proteomics of the dystrophin-glycoprotein complex and dystrophinopathy. *Curr. Protein Pep Sci* 14 (8): 680-97.

Holmes, K. C. 1997. The swinging lever-arm hypothesis of muscle contraction. *Curr Biol* 7: R112–R118.

Huxley H. 2004. Fifty years of muscle and the sliding filament hypothesis. *Eur J Biochem* 271: 1403–1415.

Huxley, A. F. 2000. Cross-bridge action: present views, prospects, and unknowns. *J Biomechan* 33: 1189–1195.

Ibraghimov-Beskrovnaya, O., J. M. Ervasti, C. J. Leveille, C. A. Slaughter, S. W. Sernett, and K. P. Campbell. 1992. Primary structure of dystrophin-associated glycoproteins linking dystrophin to the extracellular matrix. *Nature London* 355 (6362): 696-702.

Irintchev, A., M. Zweyer, and A. Wernig. 1997. Impaired functional and structural recovery after muscle injury in dystrophic *mdx* mice. *Neuromuscular Disorders* 7 (2): 117-125.

Isfort, R. J. 2002. Proteomic analysis of striated muscle. *J Chromatogr B Analyt Technol Biomed Life Sci* 771 (1-2): 155-65.

Ishizaki, M., T. Suga, E. Kimura, T. Shiota, R. Kawano, Y. Uchida, K. Uchino, S. Yamashita, Y. Maeda, and M. Uchino. 2008. *Mdx* respiratory impairment following fibrosis of the diaphragm. *Neuromuscul Disord* 18: 342-348.

Jarmey, C. 2006. *The Atlas of Musculo-skeletal Anatomy*. Lotus Publishing, Chichester.

Jean, K. M., L. Kornguta, J. Dykema, L. Daya, T. Pringsheima, and N. Jettea. 2014. A systematic review and meta-analysis on the epidemiology of Duchenne and Becker muscular dystrophy. *Neuromuscular Disorders* (in press).

Jones, D. A., D. L. Turner, D. B. McIntyre, and D. J. Newham. 2009. Energy turnover in relation to slowing of contractile properties during fatiguing contractions of the human anterior tibialis muscle. *Journal of Physiology* 587 (17): 4329-4338.

Jung, D., F. Duclos, B. Apostol, V. Straub, J. C. Lee, V. Allamand, D. P. Venzke, Y. Sunada, C. R. Moomaw, C. J. Leveille, C. A. Slaughter, T. O. Crawford, J. D. McPherson, and K. P. Campbell. 1996. Characterization of delta sarcoglycan, a

novel component of the oligomeric sarcoglycan complex involved in limb-girdle muscular dystrophy. *J Biol Chem* 271 (50): 32321-9.

Karp, N. A., and K. S. Lilley. 2005. Maximising sensitivity for detecting changes in protein expression: experimental design using minimal CyDyes. *Proteomics* 5 (12): 3105-15.

Kato, A., O. Okamoto, K. Ishikawa, H. Sumiyoshi, N. Matsuo, H. Yoshioka, M. Nomizu, T. Shimada, and S. Fujiwara. 2011. Dermatopontin interacts with fibronectin, promotes fibronectin fibril formation, and enhances cell adhesion. *J Biol Chem* 286: 14861-14869.

Kim, J. W., and C. V. Dang. 2005. Multifaceted roles of glycolytic enzymes. *Trends Biochem Sci* 30: 142-150.

Kinali, M., Y. A. Manzur, and F. Muntoni. 2007. Recent developments in the management of Duchenne Muscular Dystrophy. *Paediatrics and child health* 18: 22-26.

Klose, J. 2009. From 2-D electrophoresis to proteomics. *Electrophoresis*, 30 (S1): S142-S149.

Koenig, M., A. P. Monaco, and L. M. Kunkel. 1988. The complete sequence of dystrophin predicts a rod-shaped cytoskeletal protein. *Cell* 53 (2): 219-28.

Kornegay, J. N., J. R. Bogan, D. J. Bogan, M. K. Childers, J. Li, P. Nghiem, D. A. Detwiler, C. A. Larsen, R. W. Grange, R. K. Bhavaraju-Sanka, S. Tou, B. P. Keene, J. F. Howard, J. Wang, Z. Fan, S. J. Schatzberg, M. A. Styner, K. M. Flanigan, X. Xiao, and E. P. Hoffman. 2012. Canine models of Duchenne muscular dystrophy and their use in therapeutic strategies. *Mamm Genome* 23: 85–108.

Kornegay, J. N., M. K. Childers, D. J. Bogan, J. R. Bogan, P. Nghiem, J. Wang, Z. Fan, J. F. Howard, S. J. Schatzberg, J. L. Dow, R. W. Grange, M. A. Styner, E. P. Hoffman, and K. R. Wagner. 2012. The paradox of muscle hypertrophy in muscular dystrophy. *Phys Med Rehabil Clin N Am* 23: 149-172.

- Kragstrup, T. W., M. Kjaer, and A. L. Mackey. 2011. Structural, biochemical, cellular, and functional changes in skeletal muscle extracellular matrix with aging. *Scand J Med Sci Sports* 21: 749-757.
- Kuznetsov, A. V., K. Winkler, F. R. Wiedemann, P. von Bossanyi, K. Dietzmann and W. S. Kunz. 1998. Impaired mitochondrial oxidative phosphorylation in skeletal muscle of the dystrophin-deficient *mdx* mouse. *Mol. Cell. Biochem* 183, 87–96.
- Laemmli, U. K. 1970. Cleavage of structural proteins during the assembly of the head of bacteriophage T4. *Nature London* 227 (5259): 680-5.
- Lefaucheur, J. P., C. Pastoret, and A. Sebillé. 1995. Phenotype of dystrophinopathy in old *mdx* mice. *Anatomical Record* 242(1): 70-76.
- Lewis, C., H. Jockusch, and K. Ohlendieck. 2010. Proteomic profiling of the dystrophin-deficient *MDX* heart reveals drastically altered levels of key metabolic and contractile proteins. *J Biomed Biotechnol*.
- Lewis, C., S. Carberry, and K. Ohlendieck. 2009. Proteomic profiling of X-linked muscular dystrophy. *J Muscle Res Cell Motil* 30: 267-269, 2009.
- Lidov, H. G., S. Selig, and L. M. Kunkel. 1995. Dp140: a novel 140 kDa CNS transcript from the dystrophin locus. *Hum Mol Genet* 4 (3): 329-35.
- Lieber, R. L. 2010. *Skeletal muscle Structure, Function, and Plasticity*. 3rd edition, Lippincott Williams & Wilkins, Baltimore, MD.
- Lim, L. E., and K. P. Campbell. 1998. The sarcoglycan complex in limb-girdle muscular dystrophy. *Curr Opin Neurol* 11 (5): 443-52.
- Lim, L. E., F. Duclos, O. Broux, N. Bourg, Y. Sunada, V. Allamand, J. Meyer, I. Richard, C. Moomaw, C. Slaughter, M. S. Tomé, M. Fardeau, C. E. Jackson, J. S. Beckmann, and K. P. Campbell. 1995. Beta sarcoglycan: characterization and role in limb-girdle muscular dystrophy linked to 4q12. *Nat Genet* 11 (3): 257-65.
- Lim, L. E., and T. A. Rando. 2008. Therapy for Duchenne muscular dystrophy- an opportunity for personalized medicine?. *Nat Clin Pract Neurol* 4, 149-58.

Liu, Y., L. Gampert, K. Nething, and J. M. Steinacker. 2006. Response and function of skeletal muscle heat shock protein 70. *Front Biosci* 11: 2802-2827.

Lynch, G. S., R. T. Hinkle, J. S. Chamberlain, S. V. Brooks, and J. A. Faulkner. 2001. Force and power output of fast and slow skeletal muscles from *mdx* mice 6-28 months old. *Journal of Physiology* 535(2): 591-600.

Maglara, A. A., A. Vasilaki, M. J. Jackson, and A. McArdle. 2003. Damage to developing mouse skeletal muscle myotubes in culture: protective effect of heat shock proteins. *J Physiol* 548: 837-846.

Mallick, P., and B. Kuster. 2010. Proteomics: A pragmatic perspective. *Nat Biotechnol* 28: 695–709.

Mallouk N., V. Jacquemond, and B. Allard. 2000. Elevated subsarcolemmal Ca<sup>2+</sup> in *mdx* mouse skeletal muscle fibers detected with Ca<sup>2+</sup>-activated K<sup>+</sup> channels. *Proc Natl Acad Sci USA* 97: 4950-4955.

Marouga, R., S. David, and E. Hawkins. 2005. The development of the DIGE system: 2D fluorescence difference gel analysis technology. *Anal. Bioanal. Chem* 382: 669–678.

Meissner, G., and X. Lu. 1995. Dihydropyridine receptor-ryanodine receptor interactions in skeletal muscle excitation-contraction coupling. *Biosci Rep* 15 (5): 399-408.

Menhart, N. 2006. Hybrid spectrin type repeats produced by exon-skipping in dystrophin. *BBA* 1764: 993-999.

Meryon, E. 1852. On Granular and Fatty Degeneration of the Voluntary Muscles. *Med Chir Trans* 35: 73–84.

Mesin, L., E. Merlo, R. Merletti, and C. Orizio. 2010. Investigation of motor unit recruitment during stimulated contractions of tibialis anterior muscle. *Journal of Electromyography and Kinesiology* 20(4): 580-589.

Minden, J. S., S. R. Dowd, H. E. Meyer, and K. Stühler. 2009. Difference gel electrophoresis. *Electrophoresis* 30 (S1): S156-S161.

- Minetti, C., M. Bado, G. Morreale, M. Pedemonte, and G. Cordone. 1996. Disruption of muscle basal lamina in congenital muscular dystrophy with merosin deficiency. *Neurology* 46(5): 1354-8.
- Monaco, A.P., C. J. Bertelson, S. Liecht-Gallati, H. Moser, and L. M. Kunkel. 1988. An explanation for the phenotypic differences between patients bearing partial deletions of the DMD locus. *Genomics* 2: 90-95.
- Mouisel, E., A. Vignaud, C. Hourde, G. Butler-Browne, and A. Ferry. 2010. Muscle weakness and atrophy are associated with decreased regenerative capacity and changes in mTOR signaling in skeletal muscles of venerable (18-24-month-old) dystrophic *mdx* mice. *Muscle & Nerve* 41(6): 809-818.
- Muntoni, F., S. Torelli, and A. Ferlini. 2003. Dystrophin and mutations: one gene, several proteins, multiple phenotypes. *Lancet Neurol* 2: 731-40.
- Neuhoff, V, R Stamm, and H Eibl. 1985. Clear background and highly sensitive protein staining with Coomassie Blue dyes in polyacrylamide gels: A systemic analysis. *Electrophoresis* 6: 427-448.
- Ng, R., G. B. Banks, J. K. Hall, L. A. Muir, J. N. Ramos, J. Wicki, G. L. Odom, P. Konieczny, J. Seto, J. R. Chamberlain, and J. S. Chamberlain. 2012. Animal models of muscular dystrophy. *Prog Mol Biol Transl Sci* 105: 83-111.
- O'Connell, K., J. Gannon, P. Doran, and K. Ohlendieck. 2008. Reduced expression of sarcalumenin and related Ca<sup>2+</sup> -regulatory proteins in aged rat skeletal muscle. *Exp Gerontol* 43(10): 958-61.
- O'Farrell, P. H. 1975. High resolution two-dimensional electrophoresis of proteins. *J Biol Chem* 250(10): 4007-21.
- Ohlendieck, K. 2010. Proteomics of skeletal muscle glycolysis. *Biochim Biophys Acta* 1804(11): 2089-2101.
- Ohlendieck, K. 2012. Organelle proteomics in skeletal muscle biology. *J Integr Omics* 2: 27-38.
- Okamoto, O., and S. Fujiwara. 2006. Dermatopectin, a novel player in the biology of the extracellular matrix. *Connect Tissue Res* 47: 177-189.

- Pastoret, C., and A. Seville. 1995a. *MDX* mice show progressive weakness and muscle deterioration with age. *Journal of the Neurological Sciences* 129(2): 97-105.
- Pastoret, C., and A. Seville. 1995b. Age-related differences in regeneration of dystrophic (*mdx*) and normal muscle in the mouse. *Muscle & Nerve* 18(10) 1147-1154.
- Percival, J. M., M. P. Siegel, G. Knowels, and D. J. Marcinek. 2013. Defects in mitochondrial localization and ATP synthesis in the *mdx* mouse model of Duchenne muscular dystrophy are not alleviated by PDE5 inhibition. *Hum Mol Genet* 22: 153–167.
- Pette, D., and R. S. Staron. 2000. Myosin isoforms, muscle fiber types, and transitions. *Microsc Res Tech* 50: 500-509.
- Philippova, M., A. Banfi, D. Ivanov, R. Gianni-Barrera, R. Allenspach, P. Erne, and T. Resink. 2006. Atypical GPI-anchored T-cadherin stimulates angiogenesis in vitro and in vivo. *Arterioscler Thromb Vasc Biol* 26: 2222-2230.
- Piluso, G., M. Mirabella, E. Ricci, A. Belsito, C. Abbondanza, S. Servidei, A. A. Puca, P. Tonali, G. A. Puca, and V. Nigro. 2000. Gamma1- and gamma2-syntrophins, two novel dystrophin-binding proteins localized in neuronal cells. *J Biol Chem* 275 (21): 15851-60.
- Porter, J. D., J. A. Rafael, R. J. Ragusa, J. K. Brueckner, J. I. Trickett, and K. E. Davies. 1998. The sparing of extraocular muscle in dystrophinopathy is lost in mice lacking utrophin and dystrophin. *J Cell Sci* 111(13): 1801-11.
- Pritschow, B. W., T. Lange, J. Kasch, C. Kunert-Keil, W. Liedtke and H. Brinkmeier. 2011. Functional TRPV4 channels are expressed in mouse skeletal muscle and can modulate resting Ca<sup>2+</sup> influx and muscle fatigue. *Pflügers Arch* 461: 115-122.
- Quintá, H. R., N. M. Galigniana, A. G. Erlejman, M. Lagadari, G. Piwien-Pilipuk, and M. D. Galigniana. 2011. Management of cytoskeleton architecture by molecular chaperones and immunophilins. *Cell Signal* 23: 1907-1920.
- Rabilloud, T. 1998. Use of thiourea to increase the solubility of membrane proteins in two-dimensional electrophoresis. *Electrophoresis* 19(5): 758-760.

- Rabilloud, T., A. R. Vaezzadeh, N. Potier, C. Lelong, E. Leize-Wagner, and M. Chevallet. 2009. Power and limitations of electrophoretic separations in proteomics strategies. *Mass Spectrom Rev* 28(5): 816-43.
- Rabilloud, T., J. M. Strub, S. Luche, A. Dorsselaer, and J. Lunardi. 2001. A comparison between Sypro Ruby and ruthenium II tris(bathophenanthroline disulfonate) as fluorescent stains for protein detection in gels. *Proteomics* 1(5): 699-704.
- Rabilloud, T., L. Vuillard, C. Gilly, and J. J. Lawrence. 1994. Silver-staining of proteins in polyacrylamide gels: a general overview. *Cell Mol Biol (Noisy-le-grand)* 40(1): 57-75.
- Rafael, J. A., J. I. Trickett, A. C. Potter, and K. E. Davies. 1999. Dystrophin and utrophin do not play crucial roles in nonmuscle tissues in mice. *Muscle Nerve* 22(4): 517-9.
- Rakus, D., M. Pasek, H. Krotkiewski and A. Dzugaj. 2004. Interaction between muscle aldolase and muscle fructose 1,6-bisphosphatase results in the substrate channeling. *Biochemistry* 43: 14948-14957.
- Rando, T. A. 2006. Non-viral gene therapy for Duchenne Muscular Dystrophy: Progress and challenges. *Biochimica et Biophysica Acta* 1772: 263–271.
- Rayavarapu, S., W. Coley, E. Cakir, V. Jahnke, S. Takeda, Y. Aoki, H. Grodish-Dressman, J. K. Jaiswal, E. P. Hoffman, K. J. Brown, Y. Hathout, and K. Nagaraju. 2013. Identification of disease specific pathways using in vivo SILAC proteomics in dystrophin deficient *mdx* mouse. *Mol Cell Proteomics* 12: 1061–1073.
- Reedy, M. C. 2000. Visualizing myosin's power stroke in muscle contraction. *J Cell Sci* 113(20): 3551-62.
- Rentschler, S., H. Linn, K. Deininger, M. T. Bedford, X. Espanel, and M. Sudol. 1999. The WW domain of dystrophin requires EF-hands region to interact with beta-dystroglycan. *Biol Chem* 380(4): 431-42.

Shevchenko, A., H. Tomas, J. Havlis, J. V. Olsen, and M. Mann. 2006. In-gel digestion for mass spectrometric characterization of proteins and proteomes. *Nat Protoc* 1(6): 2856-60.

Sicinski, P., Y. Geng, A. S. Ryder-Cook, E. A. Barnard, M. G. Darlison, and P. J. Barnard. 1989. The molecular basis of muscular dystrophy in the *mdx* mouse: a point mutation. *Science* 244(4912): 1578-80.

Stal, P., P. O. Eriksson, A. Eriksson, and L. E. Thornell. 1987. Enzyme-histochemical differences in fibre-type between the human major and minor zygomatic and the first dorsal interosseus muscles. *Arch Oral Biol* 32: 833-841.

Staron, R. S. 1997. Human skeletal muscle fiber types: delineation, development, and distribution. *Can J Appl Physiol* 22: 307-327.

Stastna, M., and J. E. van Eyk. 2012. Secreted proteins as a fundamental source for biomarker discovery. *Proteomics* 12: 722–735.

Staunton, L., H. Jockusch, C. Wiegand, T. Albrecht, and K. Ohlendieck. 2011. Identification of secondary effects of hyperexcitability by proteomic profiling of myotonic mouse muscle. *Mol Biosyst* 7: 2480–2489.

Stedman, H. H., H. L. Sweeney, J. B. Shrager, H. C. Maguire, R. A. Panettieri, B. Petrof, M. Narusawa, J. M. Leferovich, J. T. Sladky, and A. M. Kell. 1991. The *mdx* mouse diaphragm reproduces the degenerative changes of Duchenne muscular dystrophy. *Nature* 352: 536–539.

Steinacker, P., A. Aitken, and M. OttO. 2011. 14-3-3 proteins in neurodegeneration. *Semin Cell Dev Biol* 22: 696-704.

Swartz, D. R., Z. Yang, A. Sen, S. B. Tikunova and J. P. Davis. 2006. Myofibrillar troponin exists in three states and there is signal transduction along skeletal myofibrillar thin filaments. *J Mol Biol* 361: 420-435.

Szöke, D., and M. Panteghini. 2012. Diagnostic value of transferrin. *Clin Chim Acta* 413: 1184-1189.

- Tanabe, T., K. G. Beam, B. A. Adams, T. Niidome, and S. Numa. 1990. Regions of the skeletal muscle dihydropyridine receptor critical for excitation-contraction coupling. *Nature London* 346(6284): 567-9.
- Teichmann, M. D., F. V. Wegner, R. H. Fink, J. S. Chamberlain, B. S. Launikonis, B. Martinac, and O. Friedrich. 2008. Inhibitory control over Ca<sup>2+</sup> sparks via mechanosensitive channels is disrupted in dystrophin deficient muscle but restored by mini-dystrophin expression. *PLoS One* 3: e3644.
- Theodoridis, G. A., H. G. Gika, E. J. Want, and I. D. Wilson. 2012. Liquid chromatography-mass spectrometry based global metabolite profiling: A review. *Anal Chim Acta* 711: 7–16.
- Tinsley, J. M., D. J. Blake, A. Roche, U. Fairbrother, J. Riss, B. C. Byth, A. E. Knight, J. Kendrick-Jones, G. K. Suthers, D. R. Love, Y. H. Edwards, and K. E. Davies. 1992. Primary structure of dystrophin-related protein. *Nature* 360(6404): 591-3.
- Toogood, H. S., D. Leys, and N. S. Scrutton. 2007. Dynamics driving function: new insights from electron transferring flavoproteins and partner complexes. *Federation of European Biochemical Societies Journal* 274(21): 5481-5504.
- Towbin, J. A., J. F. Hejtmancik, P. Brink, B. Gelb, X. M. Zhu, J. S. Chamberlain, E. R. McCabe, and M. Swift. 1993. X-linked dilated cardiomyopathy. Molecular genetic evidence of linkage to the Duchenne muscular dystrophy (dystrophin) gene at the Xp21 locus. *Circulation* 87(6): 1854-65.
- Trensz, F., S. Haroun, A. Cloutier, M. V. Richter, and G. Grenier. 2010. A muscle resident cell population promotes fibrosis in hindlimb skeletal muscles of *mdx* mice through the Wnt canonical pathway. *Am J Physiol Cell Physiol* 299: C939-C947.
- Tutdibi, O., H. Brinkmeier, R. Rüdél, and K. J. Föhr. 1999. Increased calcium entry into dystrophin-deficient muscle fibres of *MDX* and *ADR-MDX* mice is reduced by ion channel blockers. *J Physiol* 515: 859-868.
- Vainzof, M., D. Ayub-Guerrieri, P. C. Onofre, P. C. Martins, V. F. Lopes, D. Zilberztajn, L. S. Maia, K. Sell, and L. U. Yamamoto. 2008. Animal models for genetic neuromuscular diseases. *J Mol Neurosci* 34: 241-248.

- Vidal, B., A. L. Serrano, M. Tjwa, M. Suelves, E. Ardite, R. De Mori, B. Baeza-Raja, M. Martinez de Lagran, P. Lafuste, V. Ruiz-Bonilla, et al. 2008. Fibrinogen drives dystrophic muscle fibrosis via a TGFbeta/alternative macrophage activation pathway. *Genes Dev* 22: 1747-1752.
- Viswanathan, S., M. Unlu, and J. S. Minden. 2006. Two-dimensional difference gel electrophoresis. *Nat Protoc* 1(3): 1351-8.
- Wagner, K. R., J. B. Cohen, and R. L. Huganir. 1993. The 87K postsynaptic membrane protein from Torpedo is a protein-tyrosine kinase substrate homologous to dystrophin. *Neuron* 10(3): 511-22.
- Wang, J., and K. Pantopoulos. 2011. Regulation of cellular iron metabolism. *Biochem. J* 434: 365–381.
- Wells, D. J. 2006. Therapeutic restoration of dystrophin expression in Duchenne muscular dystrophy. *J Muscle Res Cell Motil* 27: 387–398.
- Wells, G. D., H. Selvadurai, and I. Tein. 2009. Bioenergetic provision of energy for muscular activity. *Paediatr Respir Rev* 10: 83-90.
- Williams, M. W., and R. J. Bloch. 1999. Extensive but coordinated reorganization of the membrane skeleton in myofibers of dystrophic (*mdx*) mice. *J Cell Biol* 144(6): 1259-70.
- Wineinger, M. A., R. T. Abresch, S. A. Walsh, and G. T. Carter. 1998. Effects of aging and voluntary exercise on the function of dystrophic muscle from *mdx* mice. *American Journal of Physical Medicine & Rehabilitation* 77(1): 20-27.
- Yaffe, D., A. Makover, D. Lederfein, D. Rapaport, S. Bar, E. Barnea, and U. Nudel. 1992. Multiple products of the Duchenne muscular dystrophy gene. *Symp Soc Exp Biol* 46:179-88.
- Yamashita, M., and J. B Fenn. 1984. Electrospray Ion Source. Another Variation on the Free-Jet Theme. *J Phys Chem* 88(20): 4451-4459.
- Yiu, E. M., and A. J. Kornberg. 2008. Duchenne muscular dystrophy. *Neurology India* 56: 236-247.

Young, J. C. 2010. Mechanisms of the Hsp70 chaperone system. *Biochem Cell Biol* 88: 291-300.

Zubrzycka-Gaarn, E. E., D. E. Bulman, G. Karpati, A. H. Burghes, B. Belfall, H. J. Klamut, J. Talbot, R. S. Hodges, P. N. Ray, and R. G. Worton. 1988. The Duchenne muscular dystrophy gene product is localized in sarcolemma of human skeletal muscle. *Nature London* 333(6172): 466-9.